2019

LEACHING CHARACTERISTICS OF RARE EARTH ELEMENTS FROM BITUMINOUS COAL-BASED SOURCES

Xinbo Yang
University of Kentucky, xinboyang1217@gmail.com
Author ORCID Identifier:
https://orcid.org/0000-0002-5306-7597
Digital Object Identifier: https://doi.org/10.13023/etd.2019.229

STUDENT AGREEMENT:

I represent that my thesis or dissertation and abstract are my original work. Proper attribution has been given to all outside sources. I understand that I am solely responsible for obtaining any needed copyright permissions. I have obtained needed written permission statement(s) from the owner(s) of each third-party copyrighted matter to be included in my work, allowing electronic distribution (if such use is not permitted by the fair use doctrine) which will be submitted to UKnowledge as Additional File.

I hereby grant to The University of Kentucky and its agents the irrevocable, non-exclusive, and royalty-free license to archive and make accessible my work in whole or in part in all forms of media, now or hereafter known. I agree that the document mentioned above may be made available immediately for worldwide access unless an embargo applies.

I retain all other ownership rights to the copyright of my work. I also retain the right to use in future works (such as articles or books) all or part of my work. I understand that I am free to register the copyright to my work.

REVIEW, APPROVAL AND ACCEPTANCE

The document mentioned above has been reviewed and accepted by the student's advisor, on behalf of the advisory committee, and by the Director of Graduate Studies (DGS), on behalf of the program; we verify that this is the final, approved version of the student's thesis including all changes required by the advisory committee. The undersigned agree to abide by the statements above.

<div align="right">

Xinbo Yang, Student

Dr. Rick Q. Honaker, Major Professor

Dr. Zacharias Agioutantis, Director of Graduate Studies

</div>

LEACHING CHARACTERISTICS OF RARE EARTH ELEMENTS FROM
BITUMINOUS COAL-BASED SOURCES

DISSERTATION

A dissertation submitted in partial fulfillment of
the requirements for the degree of Doctor of Philosophy
in the College of Engineering at the University of Kentucky

By

Xinbo Yang

Lexington, Kentucky

Director: Dr. Rick Q. Honaker, Professor of Mining Engineering

Lexington, Kentucky

2019

ABSTRACT OF DISSERTATION

LEACHING CHARACTERISTICS OF RARE EARTH ELEMENTS FROM
BITUMINOUS COAL-BASED SOURCES

The demand for rare earth elements (REEs) has increased over the last decade due to applications in high technology devices including those in the defense industry. The recovery of REEs from primary sources such as rare earth minerals are viable using physical separations followed by chemical processing. However, weak market values and environmental concerns have limited the viability of such operations. On the other hand, REE recovery from secondary sources such as apatite ore, bauxite waste, and waste recycling, provides an opportunity to take advantage of a resource that does not require mining costs as well as other associated costs given that these expenses are covered by the revenue generated from the production of the primary material. Coal-based materials represent a potential source for REEs which may be extracted and concentrated by the use of physical and/or chemical processes.

The current study focused on developing a leaching process to extract REEs from the pre-combustion coal sources including coarse and fine refuse and low-valued material obtained from coal preparation plants. Materials collected for leaching characteristic studies were found to have average total REE concentrations in the range of 200-350 ppm on a whole sample basis. Mineralogy studies performed on Fire Clay seam coal refuse using SEM-EDS detected micro-dispersed rare earth phosphate mineral particles which are generally difficult to dissolve in strong acid solutions. On the other hand, XRD analysis results from a high REE content segment of the West Kentucky No. 13 coal seam indicated the presence of fluorapatite which

is soluble in weak acid solutions. The mineral associations of REEs were studied by extracting REEs using different types of acids under various pH conditions. Differential extraction of the REEs was examined along with the associated impurity elements such as iron, aluminum, and calcium among others. The findings showed that the light REEs were primarily associated in a phosphate mineral form, whereas the heavy REEs were mostly present in an ion substitution form associated with clay minerals.

Relatively high concentrations of REEs were discovered in mixed-phase particles consisting of both coal and mineral matter. By reducing the particle size, more leachable forms of REEs were liberated and recovered along with the associated mineral matter embedded in the coal structure. The type of lixiviant played an important role during the initial stage of leaching but was found to be insignificant as the system reached equilibrium. Solids concentration in the leaching medium has an important role in establishing the throughput capacity of the leaching system. Test results found that an increase in solids concentration had a significant negative effect on rare earth recovery. This finding may be explained by higher concentrations of soluble calcium-based minerals such as calcite which provided localized pH increases near and within the pores of the solids. The result was precipitation of $CaSO_4$ within the pores which blocked access for the lixiviants. This hypothesis was supported by the findings from BET and XPS analyses which found lower pore volume in high solid concentration systems and the existence of $CaSO_4$ on the surface of the solids.

Leaching test results obtained using sulfuric acid over a range of temperatures showed that the leaching process was mainly driven by a diffusion control process. The activation energy determined for an Illinois No. 6 coal source was 14.6 kJ/mol at the beginning of the reaction and 35.9 kJ/mol for the rest of the leaching process up to 2 hours. For material collected from

the Fire Clay coal seam, the apparent activation energy was 36 kJ/mol at the start of the leaching reaction and decreased to 27 kJ/mol over the remaining period of the test. The activation energy values were nearly equivalent to the upper-level values that generally define a diffusion control process and the lower values of a chemical reaction control process. The lack of clarity in defining a clear control mechanism is likely associated with the variability in associated mineralogy, various modes of occurrence of the REEs and the interfacial transfer of product through the porous structure of the coal-based particles which requires relatively high activation energy. As such, both diffusion control and chemical reaction control mechanisms are likely occurring simultaneously during the leaching process with diffusion control being more dominant.

KEYWORDS: rare earth elements, coal, mode of occurrence, leaching, kinetics

Xinbo Yang
(Author's Name)

04/22/2019
(Date)

LEACHING CHARACTERISTICS OF RARE EARTH ELEMENTS FROM
BITUMINOUS COAL-BASED SOURCES

By

Xinbo Yang

Dr. Rick Honaker
(Director of Dissertation)

Dr. Zacharias Agioutantis
(Director of Graduate Studies)

04/22/2019
(Date)

TABLE OF CONTENTS

LIST OF TABLES

LIST OF FIGURES

CHAPTER 1. INTRODUCTION

1.1. BACKGROUND

The increasing demand of rare earth elements (REEs) in advanced technology development such as electric vehicles and a variety of applications in material sciences have fueled the urgency to produce large amounts of refined rare earth elements economically. Recently, coal sources were found to contain low concentrations of REEs with the amounts of high-density, highly-valued REEs being particularly attractive. Given that the worldwide production of coal has exceeded 5 billion tons annually, the amount of REEs in the source far exceeds the production needs for the world. This investigation focused on recovering REEs from pre-combustion coal sources including coarse and fine refuse as well as the mixed-phase (middlings) material that is discarded at a typical coal preparation plant operation.

The value of REEs existing in coal deposits worldwide has been well recognized; however, efforts to develop technologies and circuits needed to economically extract the REEs from coal has been inadequate. The REEs in pre-combustion coal sources are associated with many different forms of minerals such as crystallized structure or ion substitution forms (Seredin & Dai, 2012). The ability to concentrate the crystallized mineral forms using physical separation technologies is limited due to a grain size of less than 10 microns, which requires an excessive amount of energy to liberate, and the lack of separation technologies that are capable of achieving effective performance at and below the liberation size (Zhang *et al*, 2015). Therefore, the most promising avenue for the economic extraction of the REEs is the use of acid leaching followed by appropriate hydrometallurgical processes to concentrate the REEs from pregnant leach solution (PLS).

The potential of developing a leaching process to extract REEs from coal refuse required further investigation regarding:

(1) The determination of the mineral association of REEs in coal (Qualitative information was generally known but quantitative data was not available);

(2) The complexity of mineral composition in coal refuse from which the knowledge would allow the development of strategies to enhance the selectivity of REE recovery;

(3) The dissolution characteristics and rates of various impurity minerals such as calcite, pyrite, etc. which affect leaching efficiency including leaching rate and speciation stability of the REEs;

(4) The dissolution characteristics of individual REEs including the quantification of the activation energy to be used to develop separation strategies leading to the selective recovery of critical REEs from less critical elements.

1.2. OBJECTIVES

The goal of this study was to obtain the fundamental and empirical data needed to develop a leaching process and circuit that will economically recover REEs from pre-combustion coal-based sources, particularly the waste streams from coal preparation plants. The specific objectives of the investigation included:

(1) Determining the mineral association of REEs in coal through mineralogy characterization (i.e. XRD, XRF, SEM-EDS, etc.), and by sequential extraction to determine element rare earth release from carbonates, sulfides, organic association,

2

dissolution under various conditions and the correlation results from mineralogical characterization;

(2) Assessing the ion exchange ability of various cation agents (i.e. H^+, NH^+, etc.) that could be used to recover soluble/exchangeable REEs from coal refuse. The study focused on the efficiency achievable over a range of solution temperatures and pH values to analyze the effect of the dominant reaction mechanism;

(3) Evaluating the effect of different lixiviates on leaching efficiency of the REEs considering the existence of anions (i.e. SO_4^{2-}, HSO_4^-, NO_3^-, Cl^-, etc.);

(4) Quantifying the effect of process variables on the efficiency of REE leaching including equilibrium time, acid concentration, solid concentration, temperature, etc;

(5) Using the data obtained from experimental tests to determine the activation energy of the leaching of each REE and assessing the mechanisms that control the leaching rate;

(6) Determining the effect of major solution species (i.e. Ca^{2+}, Fe^{3+}, etc.) on REE^{3+} stability in solution;

(7) To assess the effect of impurities resulting from the dissolution of various minerals such as calcite and pyrite to better understand the coal refuse leaching system.

(8) Integrating the information and developing an optimal leaching process that is efficient and selective.

1.3. ORGANIZATION

The dissertation is organized into eight chapters. The first chapter consists of a brief introduction of the background and objectives of the current study. The second chapter gives a comprehensive review of the occurrences of REEs in coal, the existing

hydrometallurgical process of REEs from other REEs deposits, and the basic understanding of leaching process including the solid-liquid reaction and process rate analysis.

The third chapter introduces experimental details including material preparation, leaching apparatus and experimental procedures that were developed to conduct the leaching tests. It includes the characterization studies and the instrumentations for quantitative elemental analysis, surface characterization, and mineralogy characterization, etc. The results and discussions on the experiments are provided in chapter four, five, and six. Chapter four includes the studies on different mode of occurrence of REEs in coal. Chapter five focuses on the leaching kinetics of REEs in coal. Chapter six further explained the complication of the leaching system interpreting the kinetic models applied in chapter five. The conclusions of the dissertation are listed in chapter seven, followed by the suggestions for future study in chapter eight.

CHAPTER 2. LITERATURE REVIEW AND THEORETICAL PRINCIPLES

2.1. OCCURRENCES OF REES

Rare earth elements (REEs) are in fact not rare in the natural occurrence. However, REEs are rarely concentrated in a form that is easily extractable. The abundance of rare earth elements in the Earth's crust is larger than the silver, gold or platinum group metals and are components in over 200 rock-forming minerals. (Cotton, 2006; Moldoveanu & Papangelakis, 2012)

The rare-earth elements are normally referred to "Lanthanides" (atomic number 57-71) on the periodic table except Promethium (atom number 61) being unstable in nature. Yttrium (atomic number 39) and Scandium (atomic number 21) are included in the category of REEs due to their similar physical and chemical properties as Lanthanoids and the affiliated footprint. Due to their similarities in their ionic radii, the REEs are interchangeable in most minerals that are difficult to separate and concentrate (Jordens, Cheng and Waters, 2013; Jha *et al*, 2016).

The U.S. Department of Energy listed five REEs as being in critical supply (CREEs) within the next 5-15 years which include neodymium, terbium, yttrium, dysprosium, and europium (Chu, S., 2011). Another common classification method for REEs is to divide the elements into two groups by atomic numbers. The light REEs (LREEs) include: La, Ce, Pr, Nd, Sm, Sc; and the heavy REEs (HREEs): Eu, Gd, Tb, Dy, Ho, Er, Tm Yb, Lu, Y. (Moldoveanu & Papangelakis, 2013) The heavy REEs are in greater demand and less commonly found naturally in concentrated forms (Xiao, Liu, *et al*, 2015).

The natural occurrences of REEs are not as metallic element but as mineral compounds, that are typically grouped into halides, carbonates, oxides, phosphates and silicates, etc. due to the geochemistry of the environment (Hedrick, 1994; Kanazawa and Kamitani, 2006; Walters and Lusty, 2011; Kumari *et al*, 2015). Over 200 types of rare earth minerals (Walters & Lusty, 2011) have been identified of which only a few are commercially significant based on their REE content. A list of various REEs containing minerals are summarized in Table 1 (Jha et al., 2016; Jordens et al., 2013; Krishnamurth & Gupta, 2005).

Other than the REEs bearing minerals, clay-adsorbed REE ions were recognized as a valuable type of REE deposit also known as the weathered crust elution-deposited REE, of which low grade RE ions are adsorbed onto permanently negative charged alumina-silicate minerals (Ruan *et al*, 2005). A typical deposit was discovered in southern China over the past decade, which contained low REE concentrations in the range of 0.03-0.3% by weight. Clay-adsorbed REEs have the potential of being more economic since the ions are easier to extract and most of the ion substituted REEs are heavy REEs which have higher market value (Kanazawa & Kamitani, 2006).

The type of REE sources was differentiated based on their REE contents and economical feasibilities. The primary sources (Jha *et al* 88, 2016) include: 1) Bastnaesite: contains LREE oxides and provides more than 70% of rare earth oxides, used to be produced in Mountain Pass, California, U.S.A. and some other mines in China primarily for iron ore and REE as byproduct; 2) Monazite: contains light REE phosphate, mostly extracted from heavy sand, which production has been depressed due to its radioactive property; 3) Xenotime: carries heavy REE and is mainly recovered as a heavy mineral byproduct; 4) Clay adsorbed REEs: known as the weathered crust elution-deposited REE,

6

of which low grade RE ions are adsorbed onto permanently negative charged alumina-silicate minerals due to naturally heating and weathering. A secondary source of REEs is a co-product through other industries, such as REE recovery in the phosphoric acid industry from apatite mineral (Brahim et al. 2008), recycling of lamp phosphor, and recycling of magnet scrap, etc. (Peelman, Sun, Sietsma, & Yang, 2014)

Table 1.REEs containing minerals (Jha et al., 2016); REO = rare earth oxide.

REEs containing minerals	Chemical Formula	Weight Percentage		
		REOs	ThO$_2$	UO$_2$
Phosphates				
Britholite	$(Ce,Ca)_5(SiO_4,PO_4)_3(OH,F)$	56	1.5	–
Brockite	$(Ca,Th,Ce)(PO_4)\cdot H_2O$	–	–	–
Chevkinite	$(Ca,Ce,Th)_4(Fe^{2+},Mg)_2(Ti,Fe^{3+})_3Si_4O_{22}$	–	–	–
Churchite	$YPO_4\cdot H_2O$	–	–	–
Crandallite	$CaAl_3(PO_4)_2(OH)_5\cdot H_2O$	–	–	–
Florencite	$CeAl_3(PO_4)_2(OH)_6$	–	1.4	–
Fluorapatite	$(Ca,Ce)_5(PO_4)_3F$	–	–	–
Gorceixite	$(Ba,REE)Al_3[(PO_4)_2(OH)_5]\cdot H_2O$	–	–	–
Goyazite	$SrAl_3(PO_4)_2(OH)_5\cdot H_2O$	–	–	–
Monazite	$(Ce,La,Nd,Th)PO_4$	35–71	0–20	0–16
Rhabdophane	$(Ce,La,Nd)PO_4\cdot H_2O$	–	–	–
Vitusite	$Na_3(Ce,La,Nd)(PO_4)_2$	–	–	–
Xenotime	YPO_4	52–67	–	0–5
Halides				
Fluocerite	$(Ce,La)F_3$	–	–	–
Fluorite	$(Ca,REE)F_2$	–	–	–
Gagarinite	$NaCaY(F,Cl)_6$	–	–	–
Pyrochlore	$(Ca,Na,REE)_2Nb_2O_6(OH,F)$	–	–	–
Yttrofluorite	$(Ca,Y)F_2$	–	–	–
Carbonates				
Ancylite	$Sr(Ce,La)(CO3)2OH\cdot H2O$	46–53	0–0.4	0.1
Bastnasite	$(Ce,La)(CO3)F$	70–74	0–0.3	0.09
Calcio-ancylite	$(Ca,Sr)Ce3(CO3)4(OH)_3\cdot H2O$	60	–	–
Doverite	$YCaF(CO3)2$	–	–	
Parisite	$Ca(Ce,La)2(CO3)3F2$	59	0–0.5	0–0.3
Parisite	$Ca(Nd,Ce)2(CO3)3F2$	–	–	–
Synchysite	$Ca(Ce,La, Nd)(CO3)2F$	49–52	1.6	–
Oxides				
Anatase	$(Ti,REE)O2$	–	–	–
Brannerite	$(U,Ca,Y,Ce)(Ti,Fe)2O6$	–	–	–
Cerianite	$(Ce^{4+},Th)O_2$	–	–	–
Euxenite	$(Y,Ca,Ce,U,Th)(Nb,Ta,Ti)_2O_6$	–	–	–
Fergusonite	$(Ce,La,Nd,Y)(Nb,T)O_4$	–	–	–

Loparite	$(Ce,Na,Ca)(Ti,Nb)O_3$	–	–	–
Perovskite	$(Ca,REE)TiO_3$	<37	0–2	0–0.05
Samarskite	$(REE,Fe^{2+},Fe^{3+},U,Th,Ca)(Nb,Ta,Ti)O_4$	–	–	–
Uraninite	$(U,Th,Ce)O_2$	–	–	–
Silicates				
Allanite	$(Ce,Ca,Y)_2(Al,Fe^{2+},Fe^{3+})_3(SiO_4)_3(OH)$	3–51	0–3	–
Cerite	$Ce_9Fe^{3+}(SiO_2)_6[(SiO_3)(OH)](OH)_3$	–	–	–
Cheralite	$(Ca,Ce,Th)(P,Si)O_4$	–	<30	–
Eudialyte	$Na_4(Ca,Ce)_2(Fe^{2+},Mn^{2+},Y)ZrSi_8O_{22}(OH,Cl)_2$	1–10	–	–
Gadolinite	$(Ce,La,Nd,Y)_2Fe^{2+}Be_2Si_2O_{10}$	–	–	–
Gerenite	$(Ca,Na)_2(Y,REE)_3Si_6O_{18} \cdot 2H_2O$	–	–	–
Hingganite	$(Ce,Y,Yb,Er)_2Be_2Si_2O_8(OH)_2$	–	–	–
Iimoriite	$Y_2(SiO_4)(CO_3)$	–	–	–
Kainosite	$Ca_2(Y,Ce)_2Si_4O_{12}(CO_3)H_2O$	–	–	–
Rinkite	$(Ca,Ce)_4Na(Na,Ca)_2Ti(Si_2O_7)_2F_2(O,F)_2$	–	–	–
Sphene	$(Ca,REE)TiSiO_5$	<3	–	–
Steenstrupine	$Na_{14}Ce_6Mn_2Fe_2(Zr,Th)(Si_6O_{18})_2(PO_4)_7 \cdot 3H_2O$	–	–	–
Thalenite	$Y_3Si_3O_{10}(F,OH)$	–	–	–
Thorite	$(Th,U)SiO_4$	<3	–	10–16
Zircon	$(Zr,REE)SiO_4$	–	0.1–0.8	–

2.2. REES IN COAL

Coal sources were found to contain low concentrations of REEs. Their occurrences, mineralogy, and geochemical composition have been well studied (Hower, Ruppert and Eble, 1999; Seredin and Dai, 2012; Zhang *et al*., 2015; Dai, Graham and Ward, 2016). The average REE concentration in coal deposits worldwide was estimated to be 68.5 ppm, while the average value in the U.S. was 62.1 ppm (Seredin & Dai, 2012). However, the REE distribution in coal was found to be associated with the incombustible material in coal rather than the combustible carbon material (R. Honaker, Groppo, Bhagavatula, Rezaee, & Zhang, 2016). The average REEs concentration in the incombustible material is around 404 ppm in the world and 517 ppm in the US, which is comparable to the ion-adsorbed clay deposit in terms of rare earth oxide (REO) contents (Seredin & Dai, 2012). Despite the relatively low concentrations in coal-based sources, the reserve of coal worldwide is tremendous. The estimated total amount of REEs in coal in terms of metric tons was 50

million metric tons which is nearly 50% of the traditional REE bearing mineral reserves (W. Zhang et al., 2015).

Many studies were conducted in the effort to recover REEs from coal combustion byproducts, particularly coal fly ash material. However, leaching efficiency was not economically favorable primarily due to the REEs being fused into Al-Si glassy (amorphous) matrix. (Blissett, Smalley, & Rowson, 2014; Tiwari, Bajpai, Dewangan, & Tamrakar, 2015) Kolker et al. (2017) utilized a SHRIMP-RG ion microprobe analysis to characterize the grain scale distribution of REE in coal fly ash and confirmed that REE are chemically bound in an aluminosilicate glassy matrix due to the high boiler temperatures. The study showed that a significant portion of the REEs are present in iron oxide magnetospheres and are highly depleted in quartz (Kolker et al., 2017). Based on the difficult leaching characteristics associated with combustion byproducts from pulverized coal boilers, the most promising opportunity for economically recovering REEs from coal-based sources is from the treatment of pre-combustion feedstocks.

In pre-combustion coal sources, previous research found elevated REE concentrations in mixed-phase particles containing nearly equal proportions of coal and mineral matter. Figure 1 shows that REE concentrations exceeding 500 ppm existed with in the fraction of Fire Clay seam coal having an ash content between 50% and 80%. Recovering this fraction from the coarse refuse stream of a coal preparation plant would provide an excellent feedstock for a REE recovery circuit. Similar trends was observed from the analysis of samples collected from 20 coal processing operations located in the Central and Northern Appalachia coalfields (Honaker *et al*., 2015). The study found that a large majority of the

REEs in the feed coal reporting to coal preparation plants report to the coarse and fine refuse streams which was the basis for selecting the feedstocks used in this study.

The potential of extracting REEs from the refuse of coal production and the forms of REEs present in coal were studied for years by numerous investigators since 1960s. Dai et al. summarized the presence of REEs plus Yttrium in coal in primarily three forms, i.e. (Dai *et al.*, 2012; Seredin and Dai, 2012):

(1) Syngeneic clastic and pyroclastic minerals such as monazite and small amount of xenotime, or as an isomorphic admixture in minerals such as zircon, apatite, etc.;

(2) Diagenetic and epigenetic minerals of authigenic origin: associate with aluminum phosphates and sulfates, water-bearing phosphates, oxides, carbonates or fluorocarbonates;

(3) Organic compounds: Authigenic, and organically-bound REEs.

The concentration process for conventional REE minerals usually consists of physical concentration (e.g. gravity separation, magnetic separation, flotation, etc.) followed by metallurgical extraction (e.g. pyro-metallurgical, hydrometallurgical, etc.) (J. Zhang & Zhao, 2016). Extensive studies have been conducted at the University of Kentucky on the physical concentration of REE minerals from Fire Clay seam coal which is a resource found within the Central Appalachian coal basin of the eastern Kentucky coalfields. The research group characterized decarbonized coal specimens using Scanning Electron Microscopy with energy dispersive X-ray analyzer (SEM-EDX). The scanning profiles detected high Phosphorus (P) content particles embedded in other minerals which contained significant amount of La, Ce, Th and Nd Figures 2(a) and (b). With the use of a

Focus Ion Beam system, a five-micron particle was extracted and confirmed to be pure monazite using a Transmission Electron Microscope (TEM).

The study evaluated REE enrichment from coal using currently commercialized physical separation techniques: riffle shaking table, Wet High Intensity Magnetic Separator (WHIMS), electrostatic drum separation, and froth flotation etc. Froth flotation recovered 20% of the total REEs while upgrading the content from around 300 ppm to 400 ppm (Honaker *et al*, 2016). The obstacle in physical concentration of the REE bearing mineral from coal refuse system is mineral liberation and the subsequent size limitation of current separation technologies.
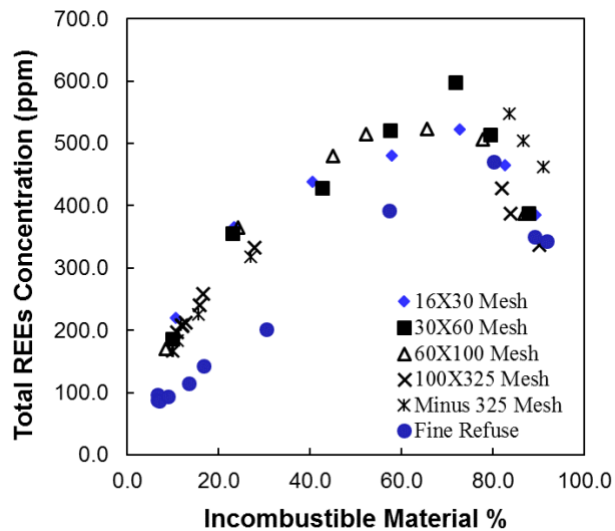
Figure 1. REEs distribution and correlation with incombustible material in coal. Sample collected from the coal processing plant operating Fireclay coal seam (Honaker *et al*, 2016).
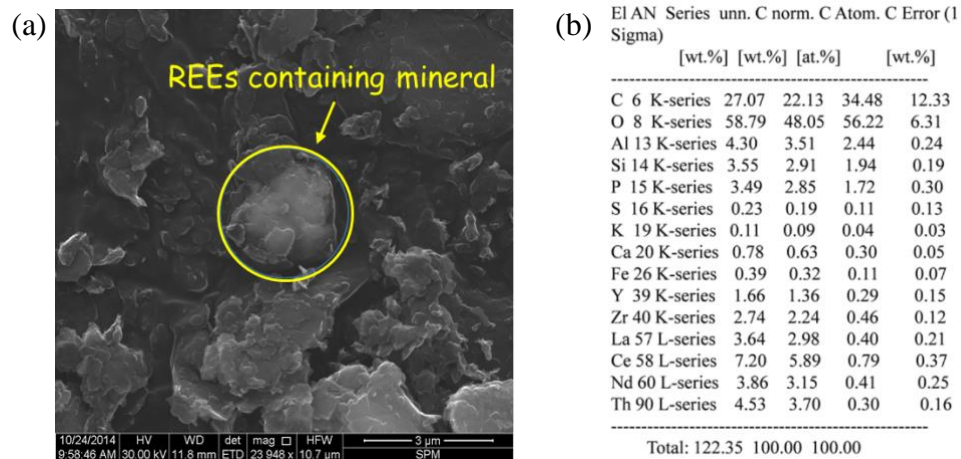
Figure 2. (a) SEM images of low- temperature plasma treated Fire Clay seam coal specimen, (b) The elemental concentration from SEM-EDS spectra.

The REE forms in coal was categorized into five different associations: water soluble, ion exchangeable and association with carbonates, organic matter, and aluminum-silicates (Dai *et al*., 2012). An analytical procedure was developed by Tessler et al. and has been

adopted by many researchers to sequentially extract trace metals in partitioning based on these five categories (Tessier, Campbell, & Bisson, 1979). The method utilizes different reagents to identify the following groups of association of elements:

(1) Ion Exchangeable: mix 1 grams of sample with 8ml of $MgCl_2$ (1 M) at pH 7, or NaOAc (1 M) at pH 8.2 for 1 hour at room temperature with continuous agitation;

(2) Carbonates Association: collect the residue from step 1 and leach with 8 ml of NaOAc (1 M) at pH 5 maintained using $C_2H_3O_2$ at room temperature with continuous agitation. Time required for extraction equilibrium needs to be recorded (~5 hours);

(3) Fe-Mn Oxide Association: collect the residue from step 2 and leach with 20 ml of $NH_2OH \cdot HCl$ in 25% CH_3COOH (v/v) at 100 °C with occasional agitation. Time required for extraction equilibrium (dissolution of free iron oxide) needs to be recorded (~5 hours);

(4) Organic Affinity: the residue of step 3 is leached in 30% hydrogen peroxide (H_2O_2) at pH 2 maintained by HNO_3 (5 ml) for 2 hours at 85°C, for two times to ensure completion. After cooling, add 5 ml of 3.2 M NH_4OAc with 20% HNO_3 (v/v) to prevent metal ion adsorption onto the oxidized material;

(5) Insoluble Residue (in crystal structure): digest with HF-HCLO4 mixture.

Several studies were conducted to investigate the REE mode of occurrences and distributions in different matrix in peat, low rank coal, high rank coal, and fly ash (Arbuzov et al., 2018; Dai et al., 2016; Riley, French, Farrell, Wood, & Huggins, 2012). The sequential extraction method was utilized to analyze the peat sample from western Siberia and the study concluded that not more than 25% of REEs in peat are in mineral association,

such as monazite, xenotime, and zircon, etc.; 10-30% of REEs is in humic substances, and 40-80% is in water-soluble form. (Arbuzov et al., 2018) However, studies conducted on post-combustion coal material showed that 70% of the light REEs and 50% of the heavy REEs in bituminous coals are predominantly associated with phosphate minerals, and 50-60% of the REEs in low ranks coals are associated with clays (Finkelman, Palmer, & Wang, 2018). Zhang et. al. discovered that the liberation of inorganic material from matrix of a high volatile bituminous coal contains a high concentration of REEs that are finely dispersed throughout the coal matrix. (Wencai Zhang, Yang, & Honaker, 2018a). In summary, the studies found that the REEs in low rank coals (i.e., lignite and subbituminous) are primarily associated with the organic matter whereas the association with higher rank coals are with the association mineral matter including grains of rare earth phosphate minerals that are smaller than 10 microns. As such, liberation of the REEs through extensive grinding is an essential step prior to chemical extraction process.

2.3. HYDROMETALLURGICAL PROCESSING OF RARE EARTH ELEMENTS

2.3.1. REE minerals

2.3.1.1. Bastnaesite

Bastnaesite $(Ce,La)(CO_3)F$, contains the highest amount of REEs compared to all the other rare earth minerals, corresponding to 70%~74% REOs (Chi *et al*, 2004; Jha *et al*, 2016). Significant deposits were discovered and mined in Mountain Pass, California, U.S., and the world largest deposit of mine was developed in China, which is well known as the Bayan Obo mine in Inner Mongolia (Krishnamurth & Gupta, 2005). Based on the analytical

data from the above-mentioned two deposits, bastnaesite contains preferentially light REEs (LREEs) including 50% Ce, 25-35% La, 15-20% Nd, 5-10% Pr, and small amounts of the other REEs (Jha et al., 2016).

As a fluorocarbonate mineral, bastnaesite is chemically vulnerable to heat which leads to a slow decomposition to RE oxides and combine with more stable anionic radicals such as phosphate (Jha *et al.*, 2016). Many physical separation processes were applicable for bastnaesite ore beneficiation, of which froth flotation using fatty acid or hydroxamate based collector was applied in both of the aforementioned deposits (Jordens et al., 2013) One of the outdated process steps was to roast the concentrated ore at 620-800 °C to decompose the carbonate and then leached in a HCl solution (Krishnamurth & Gupta, 2005). Considering 50% of the REEs in bastnaesite is Ce, the removal of Ca significantly shortens the steps needed in the downstream solvent extraction process to separate individual REEs. Also, carbonate was acid consuming (Jha et al., 2016). The current process achieves 98% REE recovery by using alkaline conversion to eliminate fluoride followed by HCl leaching, or roasting with sulfuric acid followed by NaCl salt leaching (Peelman, Sun, Sietsma, & Yang, 2016). The alkaline conversion process starts with the addition of concentrated HCl (~31%) to convert $RE_2(CO_3)_3$ to $RECl_3$ (Eq. 1) followed by the addition of NaOH at 90-100 °C to convert REF_3 to $RE(OH)_3$ (Eq. 2), and finalized by HCl leaching (Eq. 3), i.e.,

$$REF_3 - RE_2(CO_3)_3 + 9HCl \rightarrow REF_3 + 2RECl_3 + 3HCl + 3H_2O + 3CO_2 \quad \text{(Eq. 1)}$$

$$REF_3 + 3NaOH \rightarrow RE(OH)_3 + 3NaF \quad \text{(Eq. 2)}$$

$$RE(OH)_3 + 3HCl \rightarrow RECl_3 + 3H_2O \quad \text{(Eq. 3)}$$
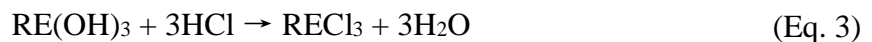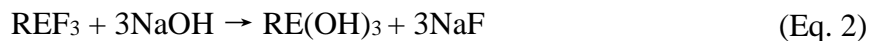
The abovementioned processes were able to achieve >90% REE recovery. However, the process created two problems: (1) the Ce_2O_3 is oxidized to CeO_2 during the roasting

process and the latter is difficult to leach; and (2) the release of HF gas produced from the leaching process which is strictly subject to environmental regulation (Q. W. Zhang & Saito, 1998).

Zhang & Saito developed a non-thermal process involving a grinding mill to provide the binding energy of NaOH powder and bastnaesite ore. The mechanochemical process converted bastnaesite to RE(OH)3 and Na compounds that can be washed off with water (Q. W. Zhang & Saito, 1998). Another newly developed method for bastnaesite leaching is to leach at room temperature with diluted sulfuric acid plus the addition of thiourea (CH4N2S) to enhance leaching performance (Yörükoğlu, Obut, & Girgin, 2003). This method increased Ce recovery from 22.8% to 93.0% by reducing Ce^{4+} to Ce^{3+}.

2.3.1.2. Monazite

Monazite is a REE phosphate ore containing 40~50% REO before treatment and up to 71% REO after physical beneficiation (Kanazawa & Kamitani, 2006). Monazite deposits are common throughout the world in placer deposits, beach sands and a component of the Bayan Obo mine in China. However, the major source of monazite is from heavy mineral sand processing as a byproduct of ilmenite, rutile and zircon production. The production of REEs from monazite ore is limited due to its high content of radioactive elements including 4~12% thorium and varying amounts of uranium (Gupta & Krishnamurthy, 2015). The high content of thorium is problematic in monazite processing and waste disposal, and requires an extra step to be separated from other REEs (J*ha et al*, 2016).

Hydrometallurgical processing methods for monazite leaching has been well established which fall into two categories: concentrated H2SO4 treatment and NaOH

decomposition. Both methods involve high temperature to activate the reactions (Gupta & Krishnamurthy, 2015). The temperature required to decompose monazite is around 1950 °C to break the orthophosphate lattice structure (Zhang *et al*, 2015).

The acid baking process digests monazite in 98% sulfuric acid with a solid-liquid ratio of 1:1 (w/w) under 200-230 °C to convert the phosphate crystal to REE sulfate as described in Eq. 4 and Eq. 5. The sulfate solid paste is then leached in water. The leachate solution is collected by filtration and neutralized to obtain the $RE(OH)_3$ and $Th(OH)_4$ precipitation. REEs are re-bleached through selective dissolution during which $Th(OH)_4$ remains in a solid state due their different aqueous stability (E. Kim & Osseo-Asare, 2012), i.e.:

$$2REPO_{4(s)} + 3H_2SO_4 \rightarrow RE_2(SO_4)_{3(s)} + 6H^+ + 2PO_4^{3-} \qquad \text{(Eq. 4)}$$

$$Th_3(PO_4)_{4(s)} + 6H_2SO_4 \rightarrow 3Th(SO_4)_{2(s)} + 12H^+ + 4PO_4^{3-} \qquad \text{(Eq. 5)}$$
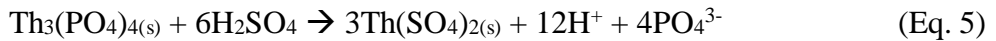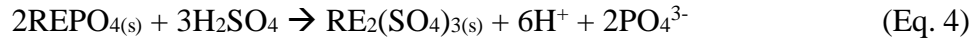
The acid baking process achieves high recovery of REEs but with poor selectivity because of high solids dissolution (Peelm*an et al*, 2014). Alkaline decomposition of rare earth phosphates is more selective and efficient. The RE phosphate is mixed with concentrated NaOH solution (50–75%) and heated under 120-150°C with or without pressure depends on the experimented efficiency (Eq. 6) and (Eq. 7) (Habashi, 1999).

$$REPO_{4(s)} + 3NaOH \rightarrow RE(OH)_{3(s)} + 3Na^+ + PO_4^{3-} \qquad \text{(Eq. 6)}$$

$$Th_3(PO_4)_{4(s)} + 12NaOH \rightarrow 3Th(OH)_{4(s)} + 12Na^+ + 4PO_4^{3-} \qquad \text{(Eq. 7)}$$
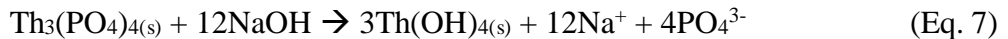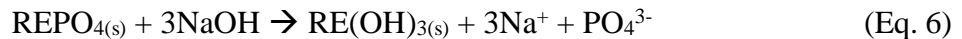
The Na_3PO_4 generated in this process is a marketable by-product which can be used as a fertilizer. The $RE(OH)_3$ and $Th(OH)_4$ are then dissolved in a mineral acid of choice followed by a Th scrubbing process which is the same as the abovementioned precipitation/selective dissolution process (E. Kim & Osseo-Asare, 2012). Leaching of $RE(OH)_3$ and $Th(OH)_4$ using 6M HCl at 80 °C for 2 h results in >90% REMs recovery at

a solid concentration of 30 g/L (Kuma*ri et al*, 2015). Na_2CO_3 as a roasting binder was evaluated but the efficiency is not comparable to NaOH roasting (Kumari et al., 2015)

Another alternative way of pretreating monazite is to convert REE phosphates to REE oxysulfides (RE_2O_2S) and oxychlorides (REOCl) by heating with $CaCl_2$ and $CaCO_3$ in a reducing and sulfurizing environment (Merritt, 1990). The converted product is dissolvable in dilute HCl (3%) which is very selective, thus no Th is present in the pregnant leach solution (PLS). Furthermore, this approach eliminates the presence of Mn as well, which depresses Ce leaching because the Mn^{4+} oxidizes Ce^{3+} to Ce^{4+} which is difficult to leach (Peelman *et al*, 2016).

2.3.2. REE Ion-adsorbed Clays

A unique type of REE deposit is the weathered crust elution-deposited rare earth ore which has REEs, particularly heavy element, adsorbed on clay surfaces (Tian, Chi, & Yin, 2010). The ore deposit was mostly discovered in tropical climate regions such as southern China (Bao & Zhao, 2008). Clay adsorbed REE ions are recognized to have a low average concentration of about 0.03-0.3% by weight. The REE deposit is highly valued due to the relatively high heavy REE content and the ease of extraction (Kanazawa & Kamitani, 2006). In fact, the clay adsorbed REEs account for 35% of the REE production in China (Yang *et al*, 2013). A portion of the REEs in coal are in the form of ion-adsorbed REEs with the amount depending on the depositional characteristics of the coal source.

2.3.2.1. Characterization of ion-exchangeable REEs

The ion-exchangeable REEs can be extracted using a salt cationic solution adjusted to a pH of 4 to 8 (Ruan *et al*, 2005). To estimate the amount of REEs that is ion-exchangeable,

a column leaching experiment is usually used to ensure maximum exchange efficiency. He, et al. (2016) used 250 grams of RE ore sample treated with 0.4 mol/L $(NH_4)_2SO_4$ solution at pH 5.5 to 6. The sample was collected continuously until the RE concentration in leachate was below the detection limit of Induced Coupled Plasma- Mass Spectrometry (ICP-MS) (He et al., 2016). Xiao et al. (2015) examined the effect of different key factors in REE ion exchange/leaching process using a typical leaching column laboratory reactor of 40 mm inner diameter with a heating jacket for temperature control (Xiao, Chen, *et al*, 2015). Their study indicated that the leaching efficiency of REEs was not sensitive to the acidity of the leaching agent as shown in Figure 3, which is a unique property of ion adsorbed REE clays. The results from the characterization studies also indicated that there are many other exchangeable metal ions, such as Al, Mg, Ca, Fe, K, Mn, and Zn etc., coexisting with REs which can have a negative effect on REE ion exchange, as well as the downstream processes (He et al., 2016; Xiao, Feng, et al., 2015).
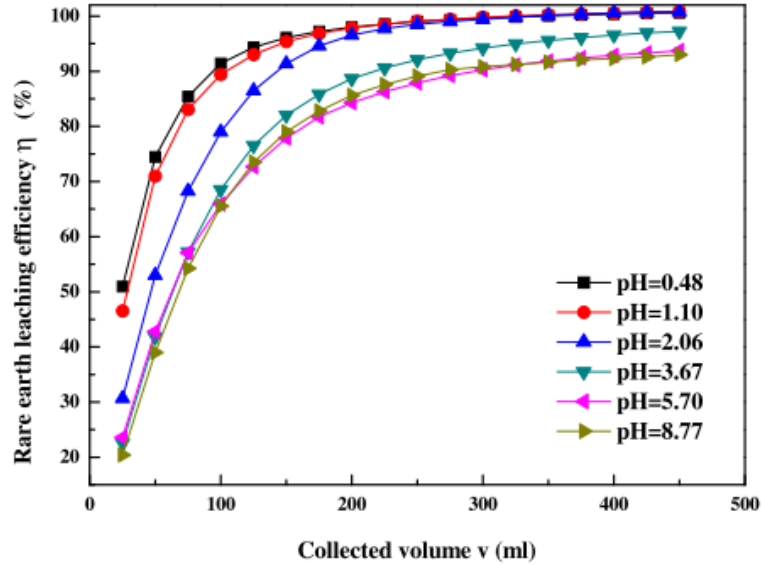
Figure 3. Effect of the pH on rare earth leaching from weathered crust elution-deposited (Initial radius of particle=1.0 mm, T= 25 ºC, Agent concentration =0.20 mol/L, Feed flow rate =0.60 ml/min) (Xiao, Chen, *et al*, 2015).

2.3.2.2. Recovery of REE using Ion Exchange Lixiviation

The most commonly used method for exchanging REE ions is to use salt leaching with ammonium sulfate $(NH_4)_2SO_4$ or equivalent ammonium salt. The process provides an 80-90% extraction rate (Moldoveanu and Papangelakis, 2013; Peelman *et al*, 2014). A common reaction for ion exchange to take place is (Moldoveanu & Papangelakis, 2013):

$$Al_2Si_2O_5(OH)_4 \cdot RE^{3+} + 3NH_4^+ = Al_2Si_2O_5(OH)_4 \cdot (NH_4^+)_3 + RE^{3+} \qquad \text{(Eq. 8)}$$
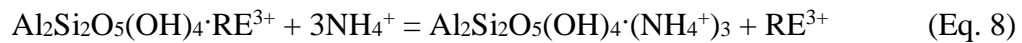
Using a strong acid was also evaluated which dissolved the entire structure; however, the process was determined to be impractical at large scale applications.

Researchers in Canada obtained clay samples from various geographical locations in Asia, Africa, and South America and conducted multiple tests on REE extraction using ion exchange technology. Their study concluded that the hydration energy of the exchange

cations determines the leaching power of monovalent ions for REE extraction in an order of $Cs^+>NH_4^+>Na^+>Li^+$, in both sulfate and chloride forms (Papangelakis & Moldoveanu, 2014). The industrial process in China also uses combined salt leachate of 7% NaCl and 1-2% Ammonium Sulfate at a pH of 4 to achieve a 95% REO recovery with a feed grade of 0.08% to 0.8% by weight (Fu, 2009). Researchers in Madagascar have tried to leaching ion substituted REE through ion exchange using seawater as a leachate; however, these trials yielded only 40% recovery (Peelman *et al*, 2014).

Magnesium sulfate was considered as an lixiviate agent to recover REE from clays to reduce the impact of ammonia-nitrogen pollution in the current ion exchange process (Xiao, et al., 2015). The research findings concluded that magnesium sulfate can provide a 93% leaching efficiency of REE in a column leaching reactor using 0.20 mol/L magnesium sulfate solution and a pH of around 5.70 at 25 Celsius degrees. The researchers also concluded that the use of magnesium sulfate in REE ion exchange could be able to lower the leaching efficiency of Al to about 50%, which is one of the major contaminations in REE extraction. Xiao et al. (2016) compared five different leaching agents at concentration of 0.20mol/L, the results indicated that REEs leaching efficiency achieved the highest and fastest with $(NH_4)_2SO_4$, followed by $(NH_4Cl)_2> MgSO_4>CaCl_2>MgCl_2$. (Xiao *et al*, 2016)

The effect of acidity in REE ion exchange/leaching tests were systematically studied by many researchers. Work conducted in Germany (Vobenkaul, Stoltz, Meyer, & Friedrich, 2015) extracted REEs from non-Chinese ion adsorbed clays using 0.5 mol/L ammonium sulfate, nitrate and chloride with and without sulfuric, nitric, and chloric acid at 0.1 mol/L respectively. The results showed that the highest recovery of about 90% achieved using a combination of 0.5 mol/L $(NH_4)_2SO_4$ and 0.1 mol/L H_2SO_4. However,

the study conducted using ion adsorbed clays in China (He, et al., 2016) showed that the pH variation in REE ion exchange using a column reactor was negligible ranging from pH 2 to 8 using ammonium salt solutions. The disagreement of the results indicates that resources react differently in leaching. The acidity of salt solution is preferred to be low with the concern of leachate contaminations by active metal ions; however, low pH values may favor the ion exchange solution by partially dissolving RE oxides that were formed during weathering and heat. (Vobenkaul, Stoltz, Meyer, & Friedrich, 2015) The reactor also impacts the role of pH optimization. A column leaching reactor prevents the precipitation of REEs whereas lower pH resists such reaction from happening in vessel reactors.

2.3.3. Secondary REE resources

Secondary resources are defined as materials that contain significant REE concentrations that are byproducts from the production of a primary product such as the tailings of a refining process or recycled materials (e.g., car batteries). The advantages of producing REE concentrates as a secondary product are that mining costs and a portion of processing costs are assigned to the production of the primary product. In some cases, the processing of the secondary resource provides environmental benefits by neutralizing acid producing components and reducing the volume of waste storage.

Many secondary resources have been identified as having elevated REE concentrations and their recovery has been the focus of a number of research projects (Binnemans *et al*, 2013; Wu, Li and Xu, 2013; Jha *et al*, 2016; Peelman *et al*, 2016; Lin *et al*, 2017). The potential REE containing resources associated with industrial wastes or byproducts include: apatite rock, phosphogypsum waste, bauxite waste (red mud), RE mineral mine tailings,

metallurgical slags, coal ash, incinerator ash and waste water streams. From the recycling industry, the sources may include: fluorescent lamp phosphors, Fe-Nd-B magnets, Sm-Co magnets, voice coil motors and computer monitors (Binnemans et al., 2013; W. Zhang et al., 2015). The concentrations vary significantly from these resources from as low as 300 ppm to 30%. Research focused on the development of processes and/or circuitry needed to extract the REEs from secondary sources is very limited. (Peelman et al., 2014). Among the investigations conducted, apatite ore in the phosphoric acid industry and the bauxite residue (red mud) have been the most intensively studied. It is noted that the mineralogy composition of red mud has some similarity to coal refuse which is the resource being investigated in this study.

2.3.3.1. Apatite ore

Apatite ore $[Ca_5(PO_4)_3(OH,F,Cl)]$ contains low concentrations of REEs (0.1%~1%) due to the presence of phosphate (Habashi & Awadalla, 1986; Hogarth, 1988). Apatite ore is primarily the major source for phosphorous in the phosphoric acid producing industry (Peelman $et\ al$, 2016). The REEs present in apatite are an isomorphous ion substitution form for calcium within the crystal lattice (Habashi, Awadalla, & Zailaf, 1986; R. Kim, Cho, Han, Kim, & Mun, 2016). The main reaction that describes the phosphoric acid production from fluorapatite is (L. Wang et al., 2010):

$$Ca_5(PO_4)_3F + 5H_2SO_4 + xH_2O \rightarrow 3H_3PO_4 + 5CaSO_4 \cdot \frac{x}{5}H_2O(s) + HF(g) \qquad \text{(Eq. 9)}$$
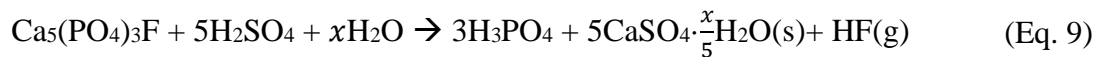
In this case, the fluorapatite is completely dissolved thereby releasing the associated REEs into solution. However, the process produces insoluble $CaSO_4$ (gypsum) that consumes nearly 80% REEs from solution as co-precipitation. The action taken to recover

the lost REEs was to re-leach the gypsum with 0.5–1M H_2SO_4 at room temperature (Habashi et al., 1986) which recovered 50% of the REE without destroying the gypsum crystal structure (Peelman *et al*, 2016). An alternative way of producing phosphoric acid and, at the same time, avoiding the loss of REE due to gypsum generation is to dissolve apatite using HNO_3 instead of H_2SO_4 (H. Li, Guo, Zhang, Li, & Wang, 2006). The aqueous stability of $Ca(NO_3)_2$ in product is easy to control thus can be precipitated after solvent extraction of REEs from the leachate solution. A benefit is that $Ca(NO_3)_2$ is marketable as fertilizer (Peelman et al., 2016). Leaching with HCl could also prevent the loss of REE caused by co-precipitation. However, the product $CaCl_2$ is very soluble in leachate that report together with REEs to solvent extraction process (Peelman et al., 2016).

Kim et al. (2016) investigated the REE leaching characteristics from a low-grade sheet-like magnetite apatite ore containing 95% REOs after physical processing. The concentrated ore was leached using sulfuric acid and hydrochloric acid in different concentrations. Sulfuric acid achieved REE recovery values no greater than 80% even with an excessive acid concentration of 13 mol/L, whereas using 2M of hydrochloric acid, nearly 100% of REEs were recovered in 10 minutes. Their conclusion on the differentiated leaching efficiency was that the high Ca content in the sample produced a large amount of $CaSO_4$ which covers the solids and causing the REEs to co-precipitate.

In apatite leaching, three major chemical reactions are taking place:

$$Ca_{10}(PO_4)_6X_2 + 20H^+ = 10Ca^{2+} + 6H_3PO_4 + 2HX \text{ (X= F,OH,Cl)} \qquad \text{(Eq. 10)}$$

$$Ca_3(PO_4)_2 + 6H^+ = 3Ca^{2+} + 2H_3PO_4 \qquad \text{(Eq. 11)}$$

$$REEPO_4 + 3H^+ = REE^{3+} + H_3PO_4 \qquad \text{(Eq. 12)}$$
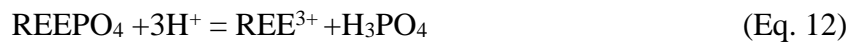
First, the reaction free energy change of Fluorapatite leaching at standard conditions is thermodynamically favorable as the calculated $\Delta G_r{}^0$ is less than 0. Subsequently, the leaching pH of the chemical reactions listed in (Eq. 10), (Eq. 11) and (Eq. 12) can be calculated assuming C(Apatite)= C(Ca$_3$(PO$_4$)$_2$) =1 mol/L, and C(REEPO$_4$) = 0.1 mol/L using thermodynamic data. In this condition, the pH values providing dissolution of Fluorapatite, Hydroxyapatite, and Chlorapatite are 1.0, 3.2, and 2.3, respectively, as shown in Table 2. These values agree with reported experimental data where apatite was dissolved with 1.0 M hydrochloric acid. However, the reported data do not address the reaction rate and the impacts from the presence of other species (ΔG_f^0 of H$^+$ = 0 kJ/mol; ΔG_f^0 of Ca^{2+} = -553.58 kJ/mol; ΔG_f^0 of H$_3$PO$_4$ = -1142.54 kJ/mol).

Table 2. Leaching pH of apatite and Ca$_3$(PO$_4$)$_2$ based on Gibbs free energy change data. Assuming c(Apatite)=c(Ca$_3$(PO$_4$)$_2$) =1 mol/L. Adapted from (R. Kim et al., 2016)

Apatite	$\Delta G^0{}_f (\frac{kJ}{mol})$			Leaching pH
	Apatite	HX*	$\Delta G^0{}_{rxn}$	
Ca$_{10}$(PO$_4$)$_6$F$_2$ Fluorapatite	-12885.9	-296.82	-98.76	1.00
Ca$_{10}$(PO$_4$)$_6$(OH)$_2$ Hydroxyapatite	-12503.5	-237.18	-361.93	3.24
Ca$_{10}$(PO$_4$)$_6$Cl$_2$ Chlorapatite	-12403.0	-131.23	-250.50	2.33
Ca$_3$(PO$_4$)$_2$	-3884.82	-	-61.00	1.84

*X= F, OH, Cl for fluor, hydroxy and chlorapatite, respectively.

2.3.3.2. Red mud

Red mud is the waste material produced in the Bayer process, i.e., the process of recovering Al from Bauxite (Binnemans *et al*, 2013). Bauxite ore is the primary mineral

resource required for the production of aluminum worldwide. The minerology of bauxites consists of various aluminum oxides [(γ- or α-AlO(OH)], hematite (Fe_2O_3), goethite [FeO(OH)], anatase (TiO_2), and clay minerals like kaolinite [$Al_2Si_2O_5(OH)_4$] (Mouchos, Wall, & Williamson, 2016).

Red mud is a byproduct of bauxite desilication produced by NaOH roasting of bauxite at 100-150 °C, which is the first step in Bayer process. The byproduct material contains a high concentration of other metals as well, especially iron with a content of up to 60%. As, such, many investigations have been carried out to recover the valuable metals with limited success (Peelman *et al*, 2016). The special interest on recovering REEs from red mud is because of its outstanding concentration of scandium (Sc), which is between 130 to 390 ppm on average (Binnemans et al., 2013). In recent decades, studies focused on the extraction of REEs used two major approaches: (1) physically upgrading REE concentration followed by leaching, and (2) direct leaching. Physical upgrading is mainly a pretreatment for leaching to reduce the volume and the amount of contamination that could cause acid consumption in the hydrometallurgical processes (Peelman et al., 2016).

Since scandium content is considerably high in red mud and has a higher economic value, many studies placed focus on the forms of Sc presence in red mud and recovery efficiency (Borra, Pontikes, Binnemans, & Van Gerven, 2015; Davris, Balomenos, Panias, & Paspaliaris, 2016; Petrakova, Panov, Gorbachev, & Milshin, 2015). Borra et al. conducted leaching experiments on a Greek bauxite residue using HCl solutions, achieved 80% REEs recovery and 60% Fe, 30-50% Al, Si, and Ti dissolution. Data implied a close association of Sc with the iron oxide phases (Borra et al., 2015). A similar conclusion was reported by Davis et al. who directly leached the red mud utilizing a diluted functionalized

26

ionic liquid betainium bis(trifluoromethylsulfonyl)imide (HbetTf2N) which achieved selective dissolution of RE oxides relative to Fe and Ti. By elevating temperature and retention time, 70-80% REEs was leached whereas Sc recovery was less than 45% while recovery lower than 3% of the Fe (Davris et al., 2016).

Petrakova et al. (2015) tested the approach to selectively recover Sc over the other REEs from red mud based on the ability of Sc to dissolve and form an anionic complex of $Sc(CO_3)_2$ in excessive carbonates and hydro-carbonate environment. By continuously gassing the system with carbon dioxide at a high pressure, the reactions were enhanced as shown in (Eq. 13) and (Eq. 14):

$$Sc(OH)_3 + NaHCO_3 \rightarrow Na[Sc(CO_3)_2] + NaOH + 2H_2O \qquad \text{(Eq. 13)}$$

$$NaOH + CO_2 \rightarrow NaHCO_3 \qquad \text{(Eq. 14)}$$
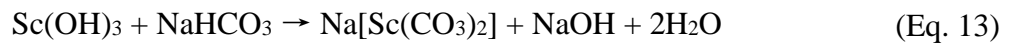
This approach achieved 26.5% Sc recovery (Petrakova *et al.*, 2015). However, with all the investigations and experimental efforts, H_2SO_4 is considered as the most economical and efficient way to recovery rare earths from bauxite residue (Binnemans *et al.*, 2015).

2.4. LEACHING RATE PROCESS

2.4.1. Thermodynamic viability

The leaching process of metal and minerals includes various types of reactions, such as hydrolysis, electrochemical, complexation, precipitation, conversion, solvation, ionic disassociation, and gas dissolution (Free, 2013). For a reaction,

$$aA + bB \rightarrow cC + dD$$ (Eq. 15)

the Gibbs free energy change of reaction (ΔG_r) can be calculated by

$$\Delta G_r = \Delta G_r{}^0 + RT \ln \frac{a_C{}^c a_D{}^d}{a_A{}^a a_B{}^b}$$ (Eq. 16)

where a, b, c, and d represent moles of substance A, B, C, and D, respectively; $a_A, a_B, a_C, and\ a_D$ represent the activity of substance A, B, C, and D, respectively.

The standard free energy change of a reaction ($\Delta G_r{}^0$) can be calculated from the sum of standard free energy of products minus the sum of standard free energy of reactants. The formation Gibbs free energy of individual species involved in a reaction can be obtained from various sources and literature (Pourbaix, 1966).

In leaching reactions, which are usually mineral or metal dissolution in the presence of H^+ ions, thermodynamic calculations can provide the information of whether the leaching reaction is likely to occur or favorable. Under a given condition, if $\Delta G < 0$, the reaction takes place spontaneously. Conversely, if $\Delta G > 0$, the reaction does not occur. It also provides the information of the maximum performance a reaction can achieve in terms of

the equilibrium constant K (Kenneth N. Han, 2002). At equilibrium, $\Delta G_r = 0$ and the reaction equilibrium constant K is quantified by:

$$K_a = \frac{a_C{}^c a_D{}^d}{a_A{}^a a_B{}^b}$$ (Eq. 17)

(Eq. 18)

$$\Delta G_r{}^0 = -RT \, lnK$$

where a is the activity described as a function of the activity coefficient (γ) and molar concentration (C) at equilibrium.

Since the activity of the hydrogen ion is expressed as pH = -log(a[H^+]), the required H^+ concentration for a certain reaction to occur can be calculated with a valid reaction equation and known concentration of reactants. Thus, the solution pH required for the leaching reaction to take place can be calculated.

2.4.2. Aqueous stability

The chemical potential of a species i (μ_i) is

$$\mu_i = \mu_i{}^0 + RT \, lna_i$$ (Eq. 19)

$$a_i = \gamma_i C_i$$ (Eq. 20)

The activity a_i is a measure of thermodynamic availability of a species i, which depends on the activity coefficient (γ) and molar concentration (C). When species i is found in the environment, activity decreases and $\gamma_i < 1$, whereas if the species i dislikes the environment, activity increases, $\gamma_i > 1$. In a diluted solution where $C_i < 10^{-3}$ M, the system

is considered as ideal and $\gamma_i=1$ (Habashi, 1999). The activity coefficient can be calculated in multiple ways, such as the Debye-Hukel method (Free, 2013), i.e.,

$$-\log\gamma_i = \frac{Az_i^2\sqrt{I}}{1 + d_iB\sqrt{I}}$$ (Eq. 21)

where the values of A and B are a function of temperature, d_i is the effective ionic diameter ($1\sim10\cdot10^{-8}$ cm), z_i is the valence number of the ion, and I, represents the ionic strength which can be quantified using the expression:

$$I = \frac{1}{2}\sum_i^n C_iz_i^2$$ (Eq. 22)

If the number of species increases in the system, the ionic strength I increases, whereas the activity coefficient for individual species γ_i decreases. This fact indicates that only a portion of the concentration of species i is activating in this reaction, thus effective activity decreases.

The oxidation-reduction potential and the hydrogen ion activity (pH) in solution environment are essential indications in the metal dissolution behavior. At certain conditions, the metal may exist in an inert oxide form or a dissolved metal ion form. The thermodynamically stable form under such condition depends on the solution oxidation potential and the pH (Kenneth N. Han, 2002). The Eh-pH diagram was introduced by Pourbaix in 1966 which included most of the metal stability diagrams (Pourbaix, 1966). Losing electrons indicates the metal oxidization (E_h increases), whereas gaining electrons represents the reduction of metal ions (E_h decreases).

The standard redox potential E^0 is associated with the standard Gibbs free energy change (ΔG^0) as described by the equation (Kenneth N. Han, 2002):

$$E^0 = -\frac{\Delta G^0}{nF} \qquad \text{(Eq. 23)}$$

where F is the Faraday constant quantified by:

$$F = eN_A = 1.602 \cdot 10^{-19} \frac{J}{V} * 6.02 \cdot 10^{23} \frac{1}{mol} = 96485 \text{ J/V} \cdot \text{mol} \qquad \text{(Eq. 24)}$$

n is the number of electrons involved in the reaction.

For a system with a known E^0 value, the potential can be obtained using the Nernst equation:

$$E = E^0 - \frac{RT}{nF} \ln \frac{a_{reduzate}}{a_{oxidant}} \qquad \text{(Eq. 25)}$$

Under standard conditions (T=298K, P=1 atm.), the standard hydrogen electrode (SHE) potential is always zero for reaction (Kenneth N. Han, 2002):

$$2H^+ + 2e \rightarrow H_2 \qquad \text{(Eq. 26)}$$

$$E = E^0 - \frac{2.303RT}{nF} \log \frac{a_{H_2}}{(a_{H^+})^2} \qquad \text{(Eq. 27)}$$

For other metals, their standard redox potential E^0 are measured by referencing to the SHE. As such, the potential (volt) can be calculated using the Nernst equation ((Eq. 25) for half-cell reactions, and using the free Gibbs energy equation (Eq. 28) for non-half-cell reactions, i.e., (Free 2013):

$$\Delta G^0 = -2.303RT \log \frac{\prod a_{product}}{\prod a_{reactant}} \qquad \text{(Eq. 28)}$$

The plots in Figure 4 demonstrates the potential-pH diagram for the Th– H_2O, Nd– H_2O, Ce-H_2O, and La–H_2O systems under standard conditions with concentration under the ideality condition (C<10^{-3} M) conducted by Kim et al. (E. Kim & Osseo-Asare, 2012). Other researchers carried out the calculation to generate a potential-pH diagram for REEs in a more complicated system. For example, Yamamura et al. generated a potential-pH

diagram for Ce-O-Cl system (*Yamamura et al*, 2004). Al-Nafai studied the cerium potential diagram in a bastnaesite-water system as shown in Figure 5 (a) and (b). Cerium exists as Ce-F and Ce-C compounds over a wide range of pH values when the concentration of F and C is dominating the system, whereas Ce exists in ionic form Ce^{3+} or Ce^{4+} at low pH values (< 1.3) when the ligand concentrations were comparative to Ce (Al-Nafai, 2015).

Speciation stability diagrams can help to identify the major species existing at a certain pH value and elemental concentrations and provide the ability to predict the change in composition when there is a change in condition. However, the diagram only indicates the stable composition at equilibrium based on reaction viability calculated from thermodynamic equations. It is very ideal and has limitations when the reaction kinetics is excessively slow to reach equilibrium (Free, 2013).
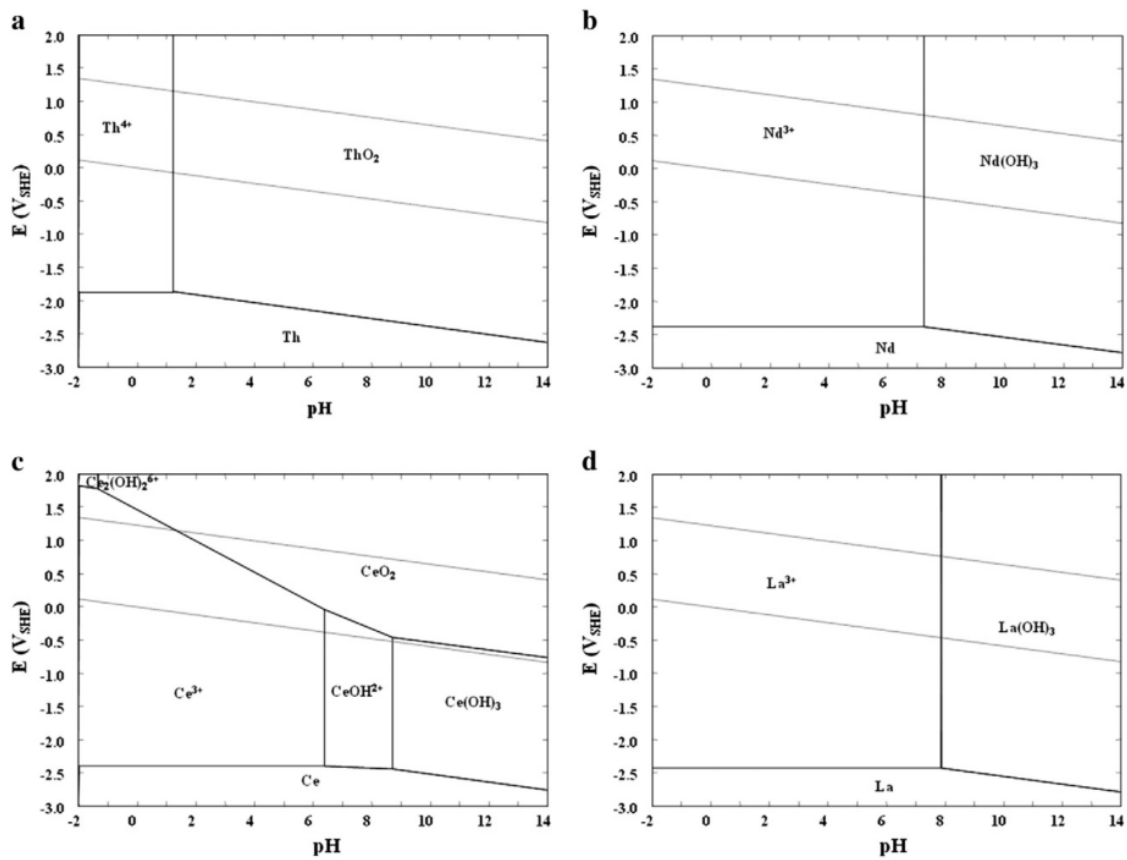
Figure 4. Potential-pH diagrams for the Th–,Nd–,Ce–, and La–H2O systems at 25 °C: (a)
{Th}=10^{-3} M, (b) {Nd}=10^{-3} M, (c) {Ce}=10^{-3} M, (d) {La}=10^{-3} M (E. Kim & Osseo-
Asare, 2012).
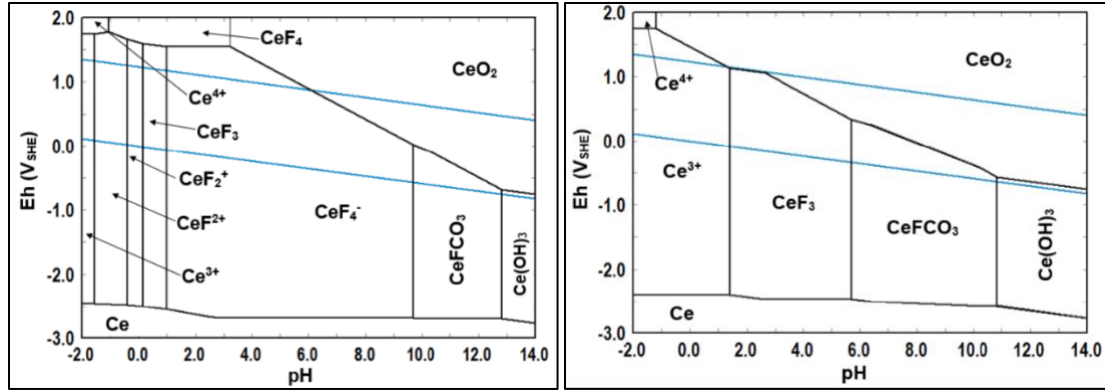
Figure 5. Ce-F-CO$_3$-H$_2$O system. (a){Ce}= 10^{-6} mol/kg, {F}={C}=1.0 mol/kg. (b) {Ce} = {F} = {C} = 10^{-3} mol/kg. (Al-Nafai, 2015)

2.4.3. Shrinking Core Model

The leaching process is classified as a fluid-particle heterogenous reaction in which a liquid reacts with a solid by contacting and transforms the solid into a product (Levenspiel, 1999). According to Levenspiel, the reaction can be represented by the following forms:

A (liquid) + B (solid) → C (liquid)   (Eq. 29)

A (liquid) + B (solid) → D (solid)   (Eq. 30)

A (liquid) + B (solid) → E (liquid) + F (solid)   (Eq. 31)

In the reaction described by Eq. 29, solid particles shrink in size during reaction and form a flaking ash material as it dissolves in liquid. When solid particles contain a large amount of unreacted impurities, the particle does not participate in a change in size during the reaction and thus remains as a non-flaking solid or forms a firm solid product per the reactions of Eq. 30 or Eq. 31. Two critical factors need to be considered in a heterogenous reaction other than a homogeneous reaction: 1) modified kinetic expression due to mass

transfer between phases and 2) the form of phases contacting and interacting (Levenspiel, 1999).

Mathematical models are usually developed to predict outcomes, which require the closest possible regressions of the reality with the minimum mathematical complexities. A schematic diagram of different reaction behavior of solid particles is as shown in Figure 6. To develop an acceptable model to describe the abovementioned types of reaction rate, two types of models are considered:

(1) The progressive-conversion model (PCM), which describes a reaction that the reactant enters the particle and reacts throughout continuously. The reaction rate varies at different position of the particle radial and the reaction takes place with time; and

(2) The shrinking core model (SCM), in which the reaction occurs from the outer layer of the particle to the inner layer. The effective reaction zone erodes into the solid and generates completely reacted material and un-reacted core. This core material presents and shrinks in size throughout the reaction time (Levenspiel, 1999).
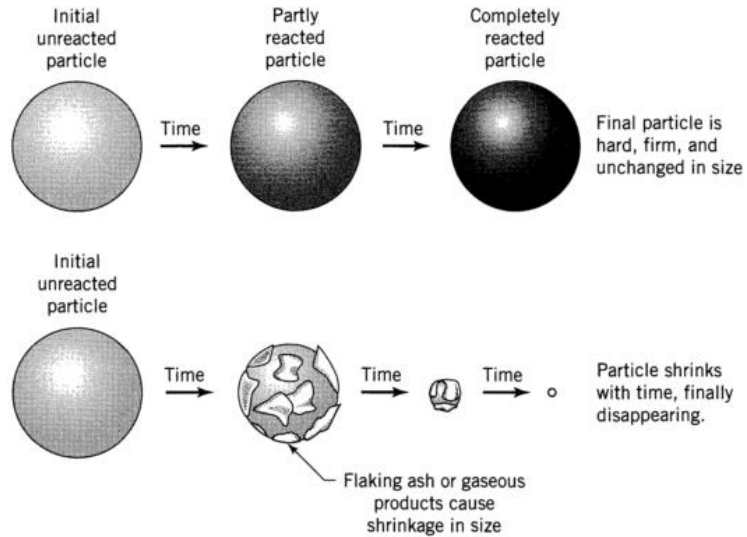
Figure 6. Different solid particle behaviors in leaching reaction (Levenspiel, 1999).

The shrinking core model describes the leaching reactions more accurately in most of the situations. It was first developed by Yagi and Kunii who divided the reaction process into five steps for spherical particles with unchanging size (Yagi & Kunii, 1955). Figure 7 demonstrates the five-step process: diffusion through the film layer, diffusion through the product layer, chemical reaction on surface, product diffusion through the product layer, product diffusion through the film layer to the solution (Xiao, Chen, et al., 2015). Without considering the "flaking ash" (sponge like solid product) formed by reaction, the kinetic rate for shrinking core model of spherical particles was simplified into three steps, that were contributing to the major resistance of rate-control, i.e.,

Step 1: Diffusion and penetration of reactant film from the bulk fluid to the solid surface;

Step 2: Chemical reaction between reactant and solid;

Step 3: Diffusion of the reaction product from the solid surface through the film of reactant to the bulk fluid.
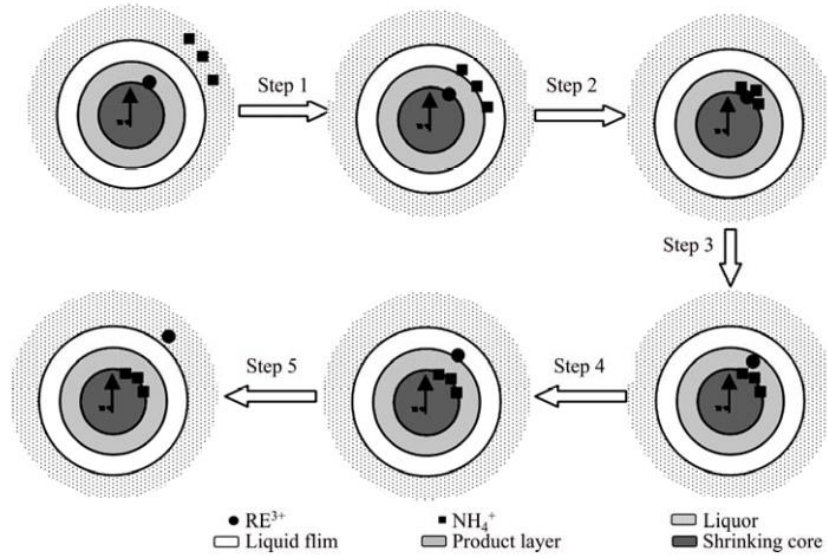
Figure 7. Shrinking core model of ore particles in 5 steps. (Xiao, Chen, et al, 2015)

The shrinking core model is controlled either by the diffusion process where the concentration of substance on solid surface plays an important role, or by the chemical reaction of the solid and liquid. The model equation to determine the rate constant of either process are as shown in (Eq. 32) for diffusion, and (Eq. 33) for chemical reactions (Gharabaghi, Noaparast, & Irannajad, 2009; Levenspiel, 1999):

$$\left[1 - \frac{2}{3}\alpha - (1-\alpha)^{\frac{2}{3}}\right] = \frac{2M_B D C_A}{\rho_B a r_0} t = k_d t \qquad \text{(Eq. 32)}$$

$$\left[1 - (1-\alpha)^{\frac{1}{3}}\right] = \frac{k M_B C_A}{\rho_B a r_0} t = k_r t \qquad \text{(Eq. 33)}$$

where α is the fraction that reacted; k the kinetic constant; M_B the solid molecular weight; C_A the acid concentration (% by weight); a the stoichiometric coefficient of the component in reaction; r_0 the initial radius of particle; t the reaction time; D the diffusion coefficient in porous product layer; and k_d, k_r the diffusion rate constant and chemical reaction rate constant, respectively.

2.4.4. Activation energy

Based on the Arrhenius Law's equation (1889) (Levenspiel, 1999),

$$k = Ae^{(\frac{-E_a}{RT})}$$

(Eq. 34)

where E_a is the activation energy of the reaction (J/mol) which the minimum required energy for the reaction to occur and A the frequency factor (considered as constant over small temperature ranges) (Habashi, 1999).

For a given reaction knowing the reaction rate k under various temperature, the ln(k) is correlated inversely with temperature. From a plot of ln(k) versus 1/T, the activation energy can be determined from the slope ($l = \frac{E_a}{R}$), and the plot intercept $= \ln(A)$. An example shown as in Figure 8.
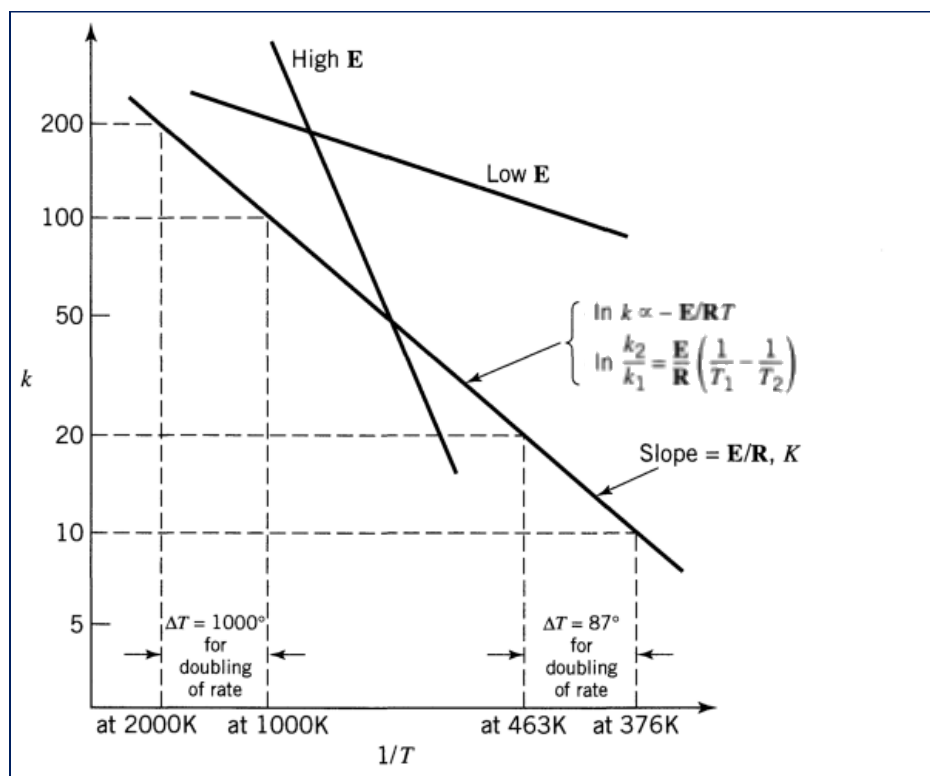
Figure 8. Temperature dependency of the reaction rate. (Levenspiel, 1999)

In other words, higher the activation energy, more sensitive the reaction rate is to the change of temperature. An elevation of 10°C in temperature to ambient only leads to 2.7% increase of reaction rate for a reaction that has an activation energy of 2000 J/mol. However, a 10°C increase in temperature for an activation energy of 20000 J/mol can provide about 30% increase in reaction rate (Free, 2013). Since the activation energy was less than 20 kJ·mol^{-1} which is the energy barrier for diffusion-controlled process (Sparks, 1986), the leaching process of rare earth from ion adsorbed clay mineral was concluded to be controlled by film diffusion process (Xia*o, Feng, et al*, 2015).

CHAPTER 3. MATERIAL AND METHODS

3.1. MATERIALS

3.1.1. sample Collection and characterization

Representative bulk samples of source B in Table 3 were collected from a coal processing plant located in Webster County, KY that processed the Western Kentucky No. 13 seam coal. The coal source was a high-volatile, bituminous coal source. The plant uses dense medium cyclones to clean the material finer than 75 mm and coarser than 1 mm, and spiral concentrators for the 1 x 0.15 mm fraction. The reject from these two circuits report to the coarse refuse stream. During the period of sample collection, the specific gravity in the dense medium cyclone circuit was approximately 1.35 which resulted in a plant weight recovery to the product stream of around 45%. Fine reject was produced from the treatment of material finer than 0.15 mm and accounted for nearly 5% of the preparation plant feed. A belt sweep sampler was used to collect a representative sample of the coarse refuse material. The processing plant treated the fine reject stream using a thickener to clarify the process water and to concentrate the waste solids material to the thickener underflow stream (TUF). A valve located in the pump discharge line of the TUF stream was opened periodically to collect a representative sample of the fine refuse. A bulk sample of each waste material was obtained by taking incremental samples every 20 minutes for a period of three hours and placing each increment into a common container. A middlings material was obtained from the coarse refuse material by subjecting a representative sample of the bulk to a float-sink analysis using a medium having a 1.8 specific gravity. The middlings material was the fraction that floated in a 1.8 specific gravity medium comprised of water and ultrafine magnetite.

Coal samples representing sources A and C in Table 3 were collected in barrels from sweep-belt samplers located on the feed streams of coal preparation plants treating the respective sources. Upon arrival at the university laboratory, the coal samples were processed following a characterization procedure depicted in Figure 9. The coal was initially screened at 9.5 mm and 1 mm. The plus 9.5 mm and 9.5 x 1 mm size fractions were subject to density fractionation using an ultrafine magnetite-based media adjusted to specific gravity (SG) values of 1.4, 1.8 and 2.2. Magnetite-based media was chosen instead of salt-based and organic chemical options to prevent pre-leach and contaminations on the solid particles from the chemical reagents. A heavy medium bath was developed using heavy duty plastic tank. The suspension was provided by air injected tubing laying on the bottom with needle poked holes. The material finer than 1 mm was wet screened at 100 mesh (150 microns) on a vibration screen. The 1 x 0.15 mm size material was subjected to density separation at a SG value of 2.2 using a heavy liquid comprised of lithium metatungstate (LMT). The material finer than 0.15 mm was decarbonized using a three-stage froth flotation (Rougher-Cleaner-Recleaner) process to obtain a low ash clean coal from the froth and a combined tailings material from all three stages for REE recovery tests.

Table 3. Coal source sample identification and sample locations.

Source	Coal Seam	Location	Operation
A	Fire Clay	Eastern Kentucky	Leatherwood (Blackhawk Mining)
B	Kentucky No. 13	Western Kentucky	Dotiki (Alliance Coal)
C	Illinois No. 6	Southern Illinois	Hamilton (Alliance Coal)
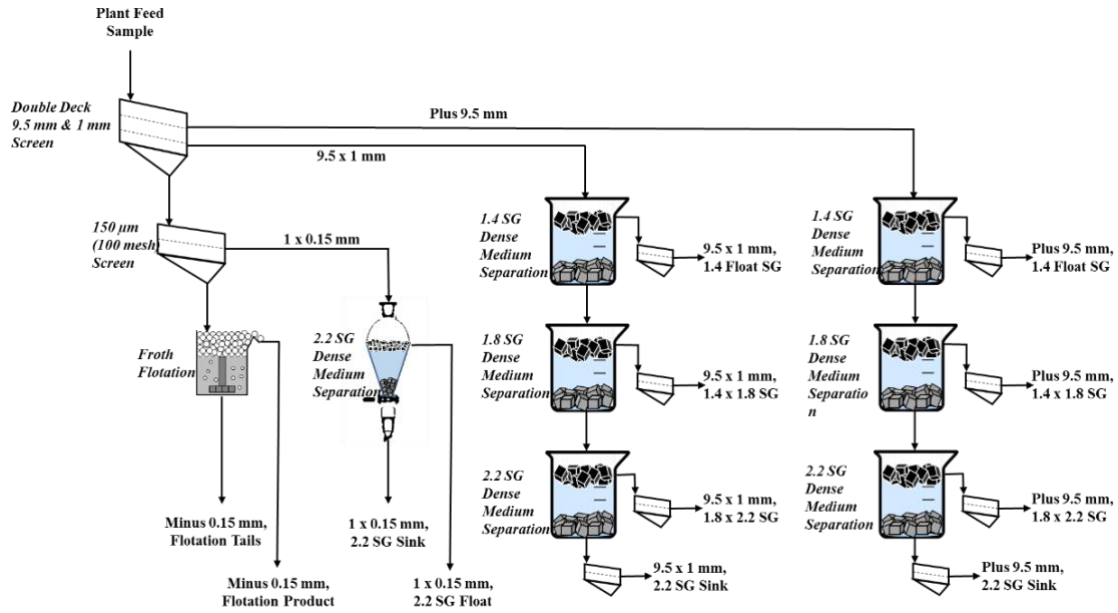
Figure 9. Flowsheet showing the sample preparation process conducted on the feed coal.

3.1.2. Geological core sample

To investigate the REE distribution and the leaching characteristics of various geological segments, a geological core sample of the West Kentucky No. 13 coal bed was obtained from operators of the mining and processing complex. A petrographic analysis was performed and each segment analyzed for REE content. As shown in Figure 10, a thin parting material measuring around 7-cm thick and located near the roof contained nearly 1000 ppm of total REEs. The next highest REE contents were found in a relatively thick parting and the direct floor material. Organic matter tends to dilute the REE content as shown by the low REE contents in the coal-rich segments.

To assess the REE recovery potential, a representative sample from each core segment was obtained and reduced to an 80% passing size of 15 microns using a shatter box. The

adjacent coal-rich segments along the length of the core were combined into four sets of coal samples. The coal-rich segments were decarbonized by a low-temperature oxygen plasma ashing unit to expose the finely dispersed mineral matter contained within the coal. Low temperature ashing (LTA) was used as method of sample preparation for analytically characterizing the mineralogy within the rich-coal segment of the channel sample (Bond & Giroux, 2013; Richaud, Herod, & Kandiyoti, 2004). The process involved placing the coal samples in a controlled oxygen plasma environment under vacuum at a temperature between 110-120°C.
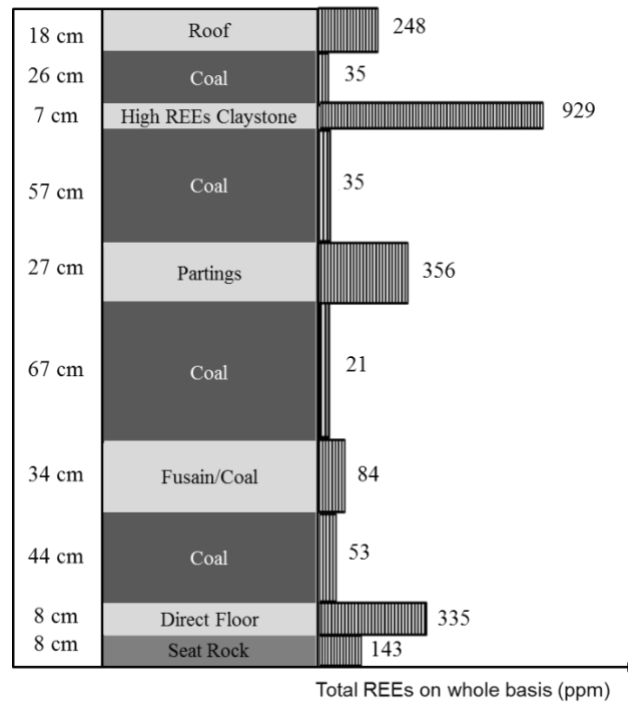
Figure 10. Total REE concentrations on a dry, whole sample basis for each core segment in a West Kentucky No. 13 seam core sample.

3.1.3. Leaching SAMPLE PREPARATION

The particle size of the middling and coarse refuse samples was reduced using a laboratory jaw crusher, hammer mill and a pulverizer in sequence to obtain a feed for the leaching tests. The material used in the leaching experiments was finer than -177 microns (80 mesh) as shown in Figure 11. To evaluate the potential benefits of improved mineral liberation, a few tests involved grinding representative samples of the pulverized material in an attrition mill for up to 60 minutes. As a secondary benefit to REE recovery, any coal liberated during crushing and pulverization as well as grinding was recovered from the material using flotation. Froth flotation involved the use of 0.5 kg/t of diesel fuel No. 2 as the collector and 4-methyl-2-pentanol (MIBC) as the frother at a concentration of 15 ppm. The first stage flotation process was carried out in four steps (rougher-cleaner-recleaner-recleaner) to ensure optimum separation efficiency and to minimize the recovery of ultrafine particles due to water entrainment which maximized REE recovery to the flotation tailings. The pH value of the slurry was adjusted and maintained at 7.0 during flotation.

Given that coal tailings material generally contains calcite, dolomite and other alkali earth minerals, which are acid consuming materials, the tailings material collected from the coal recovery process was further treated by a second flotation step using hydroxamic acid at a pH value of 9.5. The secondary flotation step also added the potential of recovering rare earth mineral grains to the froth concentrate as previously reported by Zhang et al. (2017) (W. Zhang, Honaker, & Groppo, 2017). The tailing of this flotation step was filtered and subsequently used as the feed material for the leaching tests.
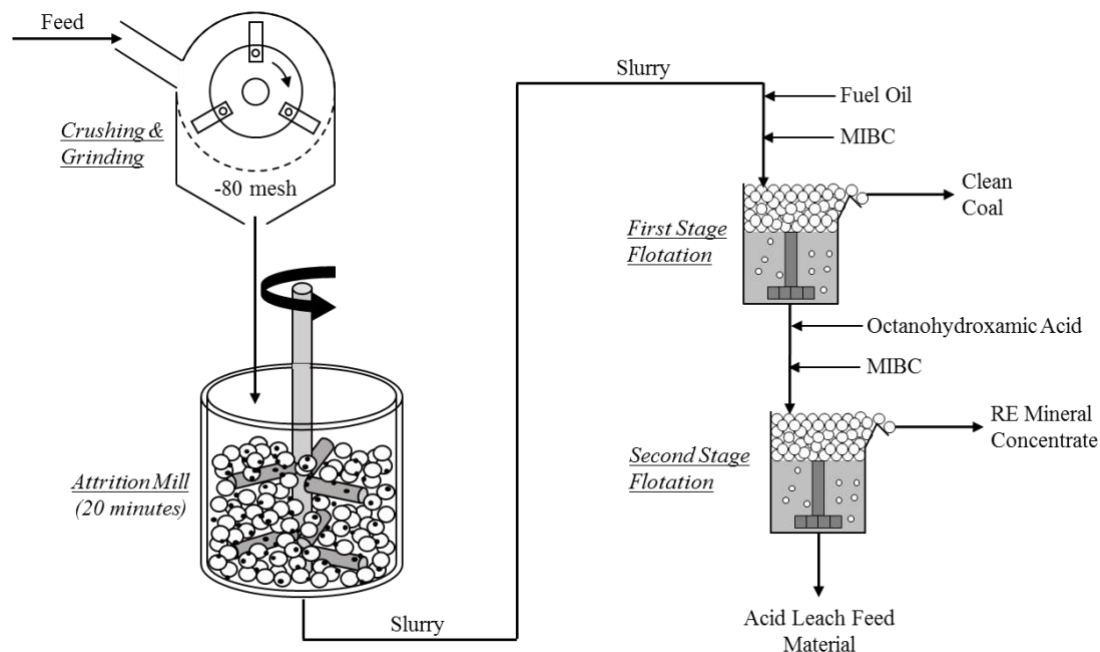
Figure 11. Grinding and flotation circuit for sample preparation on middling material.

3.2. METHODOLOGY AND APPARATUS

The leaching experimental apparatus consisted of a heating and stirring system, a reactor, and a reflux condensing system as shown in Figure 12. A magnetic stirrer hot plate was employed to provide heat to the water bath and a stream of recycling water was injected in the water bath to adjust and maintain the temperature at a predetermined level up to 80 °C. The mixing speed provided by the magnetic stirrer was of approximately 530 rpm. A round bottom triple neck flask was used as the main reactor with a total reflux condenser connected to the middle neck to eliminate any liquid loss during reaction. Cooling water was continuously flowing through the jacket of the condenser to maintain the environment pressure inside the reactor to reflux evaporated liquid. Side necks were closed using stoppers except when sampling and pH adjustment was needed. A pH meter used in this

45

project was the Orion™ Versa Star Pro™ pH meter from Thermo Scientific which operated in a range of pH -2.000 to 20.000 under operating temperatures between -0.5ºC to 105ºC.

Lixiviate agent solution was prepared with deionized water based on designated concentrations and mixed with a solid sample to obtain a total 1 L of slurry. At different time intervals during the test, 25 ml of slurry sample was collected into a 50-ml centrifuge tube using a volumetric pipette. The slurry sample was weighed and subjected to liquid-solid separation in a high-speed centrifuge for 10 minutes. At the end of the experiment, the slurry sample was filtered under vacuum using ultra fine analytical grade filter paper. The filtered solid residue was thoroughly washed using deionized water and the wash water collected for analysis. The solid residue sample was dried in an oven and weighed to obtain percentage solids loss. The specific gravity of separated leachate was measured to obtain the leachate volume.
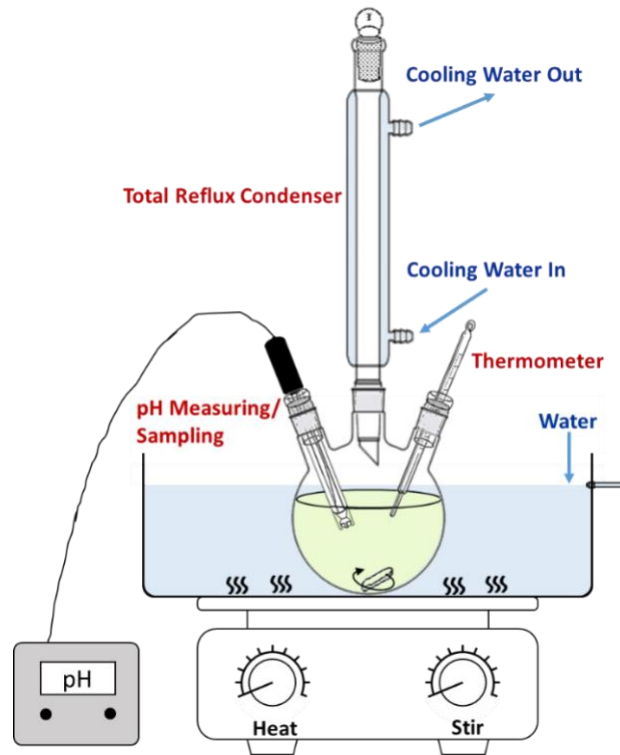
Figure 12. Experimental apparatus for ion exchange and/or acid leaching tests.

Both leachate and solid residue samples collected from the tests were subject to ICP analysis for individual REE concentrations and other major elements present in the sample. The standard solution used in the ICP analysis was the VHG-SM68 multi standard which contained 48 elements. The inductively coupled plasma optical emission spectrometry (ICP-OES) instrument was calibrated using a standard solution over a range of 0.2 to 10 ppm for each individual RE elements. To examine the lower limit of the calibration curve, low concentration standard solutions were generated of each individual RE element with concentrations as low as 0.01 ppm. The examination indicated that the lower limit for cerium was 0.02 ppm and for other REEs were 0.01 ppm in liquid form.

Leaching recovery represents the amount of material in the test feed source that was solubilized into solution during the leaching process. The value was determined using the following expression:

$$\text{Leaching recovery (\%)} = \frac{c_L * V_L}{c_L * V_L + c_{SR} * m_{SR}} * 100\%$$

where c_L is the elemental concentration in the leachate solution (μg/ml); V_L the volume of the analyzed leachate solution (ml); c_{SR} the elemental concentration in solid residue (μg/g); and m_{SR} the weight of solid residue (g).

3.3. CHARACTERIZATION AND ANALYTICAL METHOD

3.3.1. ICP analysis

All liquid and solid samples along with a representative feed solid sample were subject to REE analyses using an Inductively Coupled Plasma Optical Emission Spectrometry (ICP-OES) located at the Kentucky Geological Survey Analytical Laboratory as shown in Figure 13. The REE analyses included Sc, Y, La, Ce, Pr, Nd, Sm, Eu, Gd, Tb, Dy, Ho, Er, Tm, Yb, and Lu. The leachate liquid sample was directly subject to ICP analysis and the value of individual REE concentration was based on liquid volume in terms of ppm (μg/ml). Solid sample preparation for ICP analysis followed a slightly modified ASTM digestion procedure which included the addition of extra nitric acid to eliminate any undissolved solid particles. The solid digestion procedure involved: 1) Ashing: a representative sample of 1 gram was ashed at 500°C for 3 hours in a muffle furnace; 2) Acid digestion: 100 mg of the ash sample was mixed with 20 ml of Aqua Regia (HCl: HNO_3 = 3: 1 by volume) plus 20 ml of hydrofluoric acid followed by heating the mixture at 150 °C using a hot block to evaporate all liquid components; 3) Reflux: 10 ml of HNO_3 was added to the solid

residue with 30 ml of deionized water and heated to 120 °C to bring the total volume to 10 ml. After this process, the solid material was completely dissolved. The abovementioned acids were TraceMetal™ grade purchased from Fisher Scientific. Finally, the liquid volume was fixed at 20 ml to convert the REE concentration from liquid form (μg/ml) to the original solid (μg/g).

The ICP-OES unit was calibrated using four liquid standards having the following concentrations: 0 ppm, 0.2 ppm, 1.0 ppm and 10.0 ppm. The calibration was verified by two independently sourced check standards at the frequency of not less than every 20 samples. The recovery of the check standards was maintained within +/- 10% RSD. The standard deviation for the total REE content analyses of all samples was less than 5 ppm on a whole sample basis.
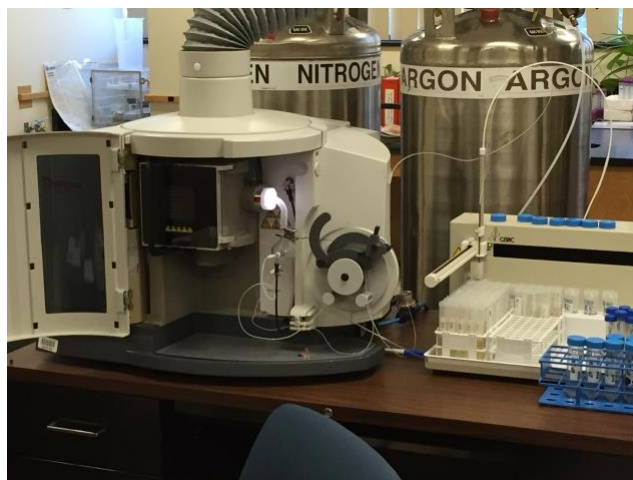
Figure 13. The Inductively Coupled Plasma Optical Emission Spectrometry (ICP-OES)

for REEs and other major elements analyses.

3.3.2. X-ray diffraction (XRD)

Samples were prepared for mineralogy analysis by X-ray Diffraction (XRD) shown in Figure 14. For the coal-rich segment, the carbon was removed using low temperature (110°C), oxygen-enriched plasma ashing which prevented a change in the mineral chemical structures while removing the carbon components [22]. X-ray diffraction (XRD) analyses were conducted on each sample using an Advance D8 instrument produced by the Bruker company. The scanning was performed from 10° to 70° with a stepwise increase of 0.02° and a scanning speed of 0.5°/min. The XRD spectra were analyzed to estimate concentrations of major mineral components using the EVA software developed by the Bruker company.

Figure 14. XRD instrument used for mineralogy analysis.

3.3.3. BET Surface analysis

The BET surface area and pore size distribution analyses were conducted at the Center for Applied Energy Research (CAER) lab which is affiliated with the University of Kentucky. The instrument used for surface analysis is shown in Figure 15. The test was initiated with measuring an accurate mass of solid sample after low temperature drying followed by immersion in nitrogen for adsorption of nitrogen onto the particle surfaces. Next, heat and vacuum were applied to desorb the nitrogen from the sample. The amount of nitrogen adsorbed and desorbed at the sample surface under different relative chamber

pressures was plotted as the isotherm sorption curve which was used to calculate the surface area and pore distribution of the solid sample using different models.

The isotherm sorption curve obtained for the solid sample follows multi-layer adsorption with capillary condensation. The isotherm curve was type IV with a type IV hysteresis. The surface area of each sample was calculated using the Brunauer–Emmett–Teller (BET) method where the single point total volume was equal to the volume of nitrogen that was dosed in the system at a specific P/Po. Since the sample did not appear to have cylindrical pore geometry, the average pore diameter was calculated using the Barrett-Joyner-Halenda (BHJ) method. The BHJ method assumes capillary condensation of the liquid nitrogen within the pores. The desorption branch was used to plot the pore size distribution since it considers the meniscus which was not formed during adsorption.

Figure 15. Instrumentation used for surface area and pore volume analyses.

3.3.4. XPS

The X-ray photoelectron spectroscopy (XPS) analysis was used to measure the elemental composition, chemical state, and electronic state of elements on a material surface by irradiating the surface with a beam of X-ray and collecting the emitted electron energy, intensity and direction. The XPS characterization was performed on a PHI Versa Probe III scanning XPS microscope using monochromatic Al K-alpha X-ray source (1486.6 eV) in the Surface Analysis Laboratory at Virginia Tech (Figure 16). Spectra were acquired with 100 µm/100 W/20 kV X-ray and dual-beam charge neutralization over a 1400 µm × 100 µm area. All binding energies were referenced to C-C at 284.8 eV. Peak

deconvolution and chemical state of elements were assigned based on the PHI and NIST

XPS.

Figure 16. PHI Versa probe II scanning XPS microscope at Virginia Tech.

CHAPTER 4. LEACHING CHARACTERIZATION OF REES IN COAL

4.1. LIBERATION OF REES IN COAL

The coarse and fine refuse materials produced during the coal cleaning process primarily represent material extracted from the floor, roof and parting segments which need to be removed to meet contract specifications. To track the REEs and understand their leaching characteristics in a plant product stream, a series of leach kinetic tests were conducted on three different plant samples collected from source B. The coarse samples were ground to a particle size finer than 177 µm and treated using froth flotation for carbon removal. The REE contents in the original plant samples and the flotation tailings are listed in Table 4. The REEs contents in the original coarse refuse, middling, and fine refuse samples were 320 ppm, 102 ppm, and 278 ppm on a dry mass basis, respectively, and modified to 289 ppm (σ = 5.51 ppm), 297 ppm (σ = 7.94 ppm), and 273 ppm (σ = 3.51 ppm) after coal and calcite removal. Some RE minerals were removed together with calcite in the flotation process. The ash contents of the flotation tailing materials from the three different streams were in a range of 84% to 86%. The REEs content of middlings after coal removal was significantly increased due to the reduced amount of organic matter.

To evaluate the effect of particle size and liberation on leaching performance, a representative sample of the pulverized middling material was ground in an attrition mill for 60 minutes to obtain a particle size less than 10 microns. Both the ground (-10 µm) and unground (-180 µm) material were treated in a primary flotation step to recover clean coal and a secondary flotation step to remove the alkali metal minerals. The tailings stream of the last flotation step was the feed source for the leaching tests.

Table 4. REE contents of representative plant samples before and after coal removal by froth flotation reported on a dry, whole mass basis.

Rare Earth Elements / Samples	Original Plant Samples			Flotation Tailings		
	Coarse refuse (CR)	Middling (Mids)	Fine refuse (TUF)	Coarse refuse (CR)	Middling (Mids)	Fine refuse (TUF)
Sc	19.1	7.6	14.6	16.5	14.4	18.7
Y	28.5	14.6	20.8	27.2	30.9	26.7
La	51.2	12.6	37.9	44.8	33.1	41.3
Ce	119.4	30.5	121.5	102.2	79.8	96.5
Pr	19.2	10.3	13.6	23.8	38.0	24.6
Nd	45.0	12.4	37.5	38.6	30.7	36.8
Sm	10.8	4.6	8.6	12.2	49.9	10.0
Eu	1.8	0.6	1.5	1.6	1.2	0.7
Gd	9.0	3.5	7.5	8.6	7.7	7.7
Tb	0.8	0.5	0.7	0.8	1.1	0.4
Dy	4.5	1.7	5.2	2.6	1.6	2.8
Ho	1.2	0.2	1.3	1.1	0.4	0.4
Er	4.7	1.2	3.8	4.0	1.0	3.2
Tm	1.0	0.2	0.9	0.9	0.2	0.1
Yb	3.4	1.8	2.8	3.7	4.5	2.9
Lu	0.0	0.1	0.0	0.5	2.0	0.0
Total	319.6	102.3	278.3	289.1	296.6	273.1
Ash Content (%)	85.0	22.9	68.8	84.7	84.9	86.0

(REEs Content on Whole Mass Basis (mg/kg))

REE content values for the leach feed material were significantly higher for the unground material (392.5 ppm) as compared to the ground material (296.5 ppm) as shown in Table 5. The grinding activity likely released RE minerals or REE-associated minerals from the organic matrix similar to previously reported findings (Wencai Zhang, Yang, & Honaker, 2018b). The difference between ground and unground material suggests a significantly higher loss of REEs to the concentrate in one or both stages of flotation because of the improved liberation realized from grinding to a particle size. Possible explanations include: 1) the liberation of the RE bearing mineral particles from the cracks

and micropore structures during grinding followed by recovery into the flotation concentrate prior to leaching the flotation tailings and 2) loss of the REEs associated with alkali metal minerals existing in an isomorphous ion substitution form due to liberation and recovery into the second stage flotation concentrate due to interactions with hydroxamic acid used as a collector. Both scenarios are possible and provide an explanation for the reduced REE contents in the -10 µm leach feed.

The dissolved solids values listed in Table 5 represents the solids loss during leaching as a result of mineral dissolution. Based on the dissolved solids values, the leaching reaction achieved on the unground material was more selective than that of the ground material. For the -180 µm material, the amount of feed material dissolved into solution was around 21.4% after 24 hours of leaching which resulted in a total REE recovery of 34.7%. The REE content in the dissolved solids was 791 ppm after 30 minutes of leaching experiment and slowly shifted downward to 635 ppm after 24 hours. The leaching of middlings finer than 10 µm resulted in the dissolution of 43.3% of the solids over the same time period and recovered 49.6 % of the total REEs. The incremental recovery gain from grinding may be attributed mostly to the solid loss thereby indicating a minimal amount of selective leaching. For the -10 µm material, the REE content in the dissolved solids approached the content in the leach feed material. A general finding was that ultrafine grinding of the middlings material in this study caused significant loss of REEs in the concentrate of the second flotation step and dissolution of the minerals associated with the REEs in the de-alkalined second stage flotation tailings material under the given leaching conditions.

An element-by-element assessment found that grinding had nearly no effect on the leaching recovery of heavy REEs as shown in Table 5. However, the leaching recovery of light REEs nearly doubled after grinding. As shown in Figure 17, an increase in scandium recovery by nearly eight absolute percentage points may provide significant economic reasons to support ultrafine grinding. Since yttrium content was the highest among all the other heavy REEs in the middlings material, its leaching recovery contributed the most and dominated the overall HREE leaching recovery. As shown in Figure 17, grinding and liberation did not impact yttrium recovery. On the other hand, the recovery of Pr and Sm increased dramatically after grinding which contributed to the recovery improvement of light REEs. The recovery values of La, Ce, and Nd, which are the most abundant light REEs, were not sensitive to grinding and liberation. This finding may indicate that the La, Ce, and Nd left in the solid residue are bound/associated with a mineral type insoluble under the given leaching conditions.

Table 5. Leaching kinetics on middling sample with and without ultrafine grinding using 1.2 mol/L sulfuric acid and a 10 g/L solids concentration.

Middlings	Retention Time	Dissolved Solids		REEs content on whole mass basis		REEs Recovery		
		Yield	REEs	Solid	Leachate	Total REEs	Light REEs	Heavy REEs
	(hours)	(%)	(mg/kg)	(mg/kg)	(mg/L)	(%)	(%)	(%)
-180 μm	Feed	-	-	392.5	-	-	-	-
	0.5	10.6	791.2	-	0.84	21.37	17.24	24.68
	1	11.7	781.5	-	0.91	23.30	18.95	30.98
	3	15.8	678.3	-	1.07	27.31	21.82	39.97
	5	16.8	685.3	-	1.15	29.33	23.32	47.33
	10	18.9	656.1	-	1.24	31.59	25.07	50.99
	24	21.4	635.4	-	1.36	34.65	27.37	59.72
	Solid Residue	-	-	279.1	-	-	-	-
-10 μm	Feed	-	-	296.5	-	-	-	-
	0.5	28.6	281.6	-	0.91	30.71	31.45	27.10
	1	30.8	293.3	-	1.02	34.44	34.75	32.93
	3	32.3	319.6	-	1.17	39.28	39.02	40.53
	5	31.7	338.1	-	1.21	40.87	40.57	42.30
	10	37.2	318.0	-	1.34	45.08	43.86	50.93
	24	43.3	301.1	-	1.47	49.64	48.29	56.16
	Solid Residue	-	-	224.8	-	-	-	-
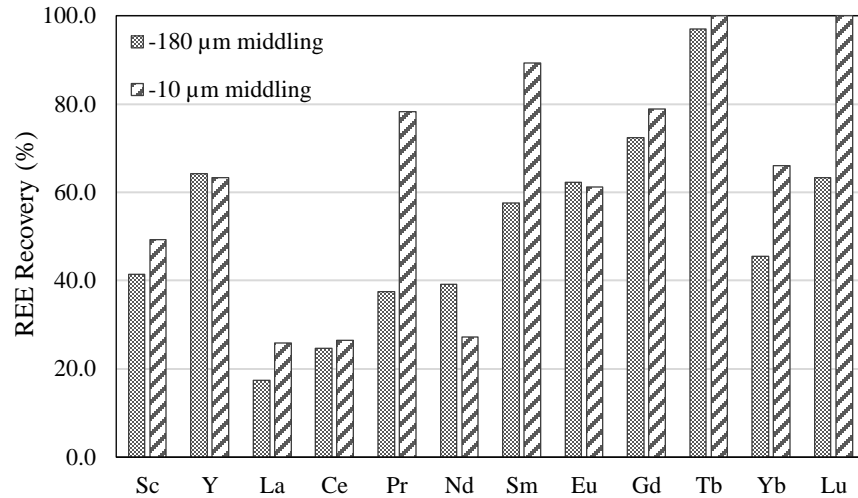
Figure 17. Individual REE recovery values achieved from leaching -180 µm and -10µm middlings material after 24 hours using 1.2 mol/L sulfuric acid.

4.2. LEACHING CHARACTERISTICS ASSESSMENT

4.2.1. Ion exchange

The REEs in coal sources may exist in different states including an aqueous soluble state (clay adsorbed), ion-exchangeable state, colloid sediment and mineral state. For the ion-exchangeable state, REEs can be exchanged using a salt cation solution (Xiao et al., 2016). To investigate the ion exchangeable REEs in the given coal source, tests were performed using 0.1 mol/L ammonium sulfate and an initial solution pH of 5 using HNO_3. Since the West Kentucky No. 13 coal samples contained a significant amount of acid generating material, the final pH dropped to around 4.0 after 24 hours leaching at 75 °C. At a solid concentration of 5% by weight, the stoichiometric amount of NH_4^+ favored the reaction towards the exchange of $REE^{3+/4+}$s.

The total REEs recovered from the coarse and fine refuse and the middling material was around 9~10% as shown in Figure 18. The overall heavy REEs (HREEs) recovery was nearly twice of the light REEs (LREE) recovery, which was similar to the preferential leaching realized from the treatment of the core segments. The elements Eu, Dy, Gd and Tb were the major elements that contributed to the HREE recovery. It is interesting to note that, although Ce and La account for 38% to 50% of the total REEs in the three coal sources, their recovery by ion exchange was the lowest which suggests differences in the mode of occurrence between the light and heavy REEs.

The approach of extracting REEs from the thickener underflow sample using salt ion exchange was further examined at different pH levels (1, 3, and 5). For pH 1 conditions, 12 ml of nitric acid (67% concentration) was added prior to the start of the test and an additional 2.5 ml was injected in increments during the test to maintain the desired pH value. The test involving a solution pH value of 3 required an initial 2.5 ml of nitric acid and the incremental addition of 0.55 ml to maintain the pH value. For the test at pH 5, 0.5 ml of nitric acid was added to achieve the initial pH of 5 and the pH naturally drifted to a value of 4 after 24 hours of leaching time.

Results in Figure 19 show significant improvement of REE recovery by reducing the pH value. Although all recovery values increased with a decrease in pH, the effect was most notable for Pr, Sm and Tb. The recovery values for La, Ce and Nd remained low under all conditions which may be indicating a common association in regard to the mode of occurrence that differs from the other REEs.

60
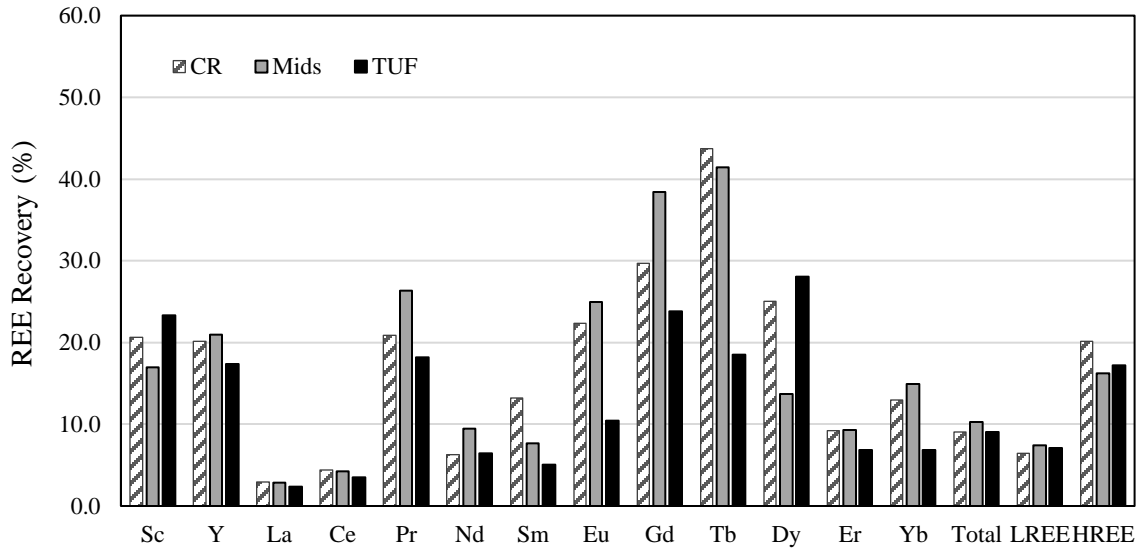
Figure 18. Ion exchangeable REEs in plant samples recovered using 0.1 mol/L
$(NH_4)_2SO_4$ at an initial pH of 5.
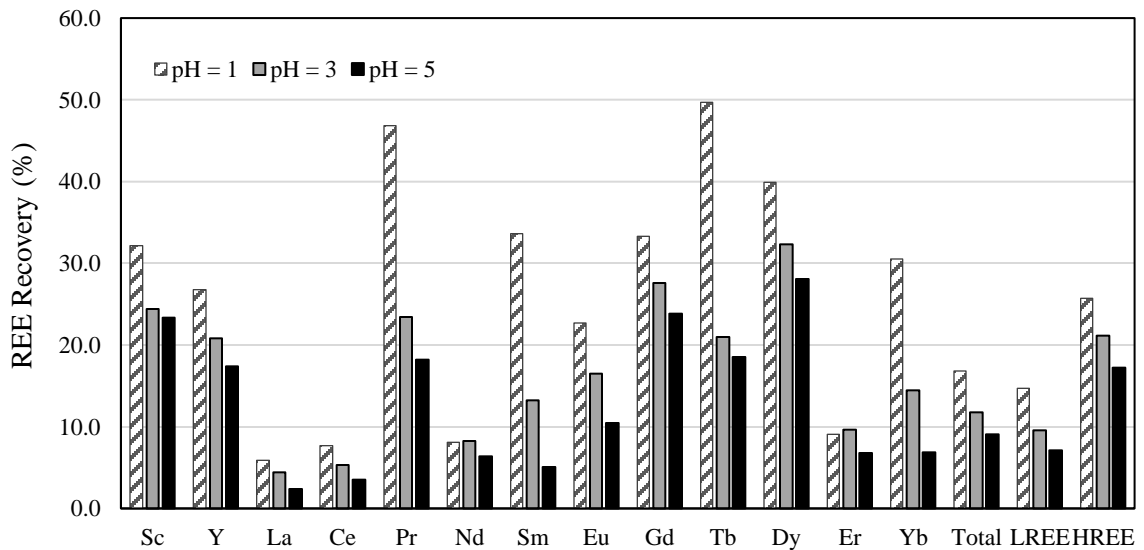
Figure 19. Effect of pH on REE recovery from thickener underflow fine refuse (TUF)
sample using 0.1 mol/L $(NH_4)_2SO_4$ and nitric acid for pH adjustment.

4.2.2. Acid leaching

Leaching kinetics data obtained from the treatment of the three plant samples using 1.2
mol/L sulfuric acid at 75°C are shown in Figure 20. The REE recovery rate from the

leaching of the middling material was found to be significantly higher than the fine and coarse refuse samples. The variable results were likely due to the origin of the components in each stream, i.e., dispersed mineral matter within the coal, partings within the seam, roof and floor materials. For all samples, REE recovery increased rapidly within the first 30 minutes of the experiments which suggested a portion of REEs were associated with soluble minerals and/or ion adsorbed clays. Most of the REEs that were leachable under the test conditions were recovered into solution within the first five hours of the test followed by small incremental recovery increases which indicates suppressed reaction rates for the remaining REEs.

REE recovery rate for the fine and coarse refuse were nearly identical to each other from element-to-element as shown in Figure 21. Recovery values for cerium, lanthanum and neodymium were the lowest among other elements in all three sample types. The finding indicated that the abovementioned three elements may be co-existing in a similar form throughout the coal seam. The recovery of Pr was notably high at around 73% for the fine and coarse refuse materials and 88% in the middlings material. The leachability of Sm from the middling material was also extraordinary high at around 95%. As shown in Table 2, the decarbonized middling material contained 38 ppm of Pr and 50 ppm of Sm, whereas the chondrite concentrations of Pr and Sm were only 9.1 ppm and 6.1 ppm, respectively, on average (Gromet, Dymek, Haskin, & Korotev, 1984). The concentration and leaching recovery data suggests that the coal source is a viable source for these two elements.

Scandium currently has significantly higher market value relative to any other REE. A recent study indicated that 36.8% of scandium in a coal reject was present in an aluminum substitution form in the Al-O octahedrons structure of kaolinite, 55.6% present in boehmite,

and a small portion of the scandium in the Si-O tetrahedrons structure (P. Zhang et al., 2017). As shown in Figure 21, the leaching recovery for scandium was around 40% for all three materials. The coarse refuse material is a more valuable source of Sc given that 1) there was significantly more mass in the coarse refuse relatively to the other materials, 2) the Sc concentration was higher in the coarse refuse according to Table 4 and 3) leaching data for Sc was nearly equal.
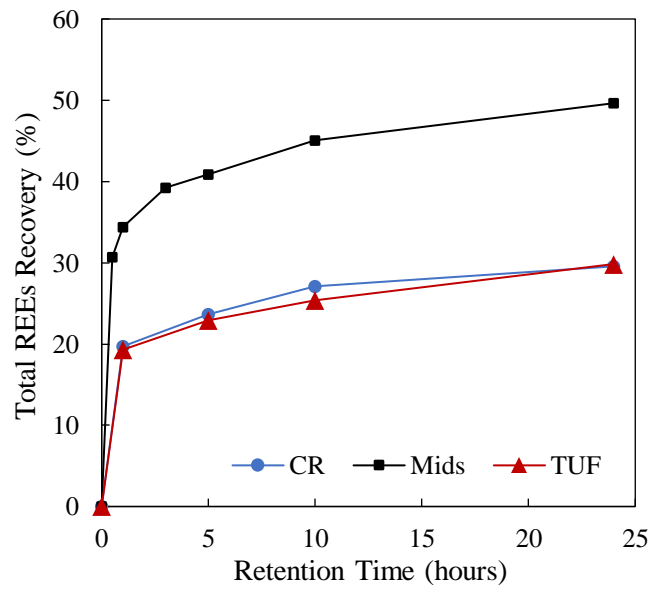
Figure 20. Acid leaching kinetics of REEs leaching recovery from plant samples using 1.2 mol/L sulfuric acid: CR- Coarse refuse, Mids- Middling, TUF- Thickener underflow.
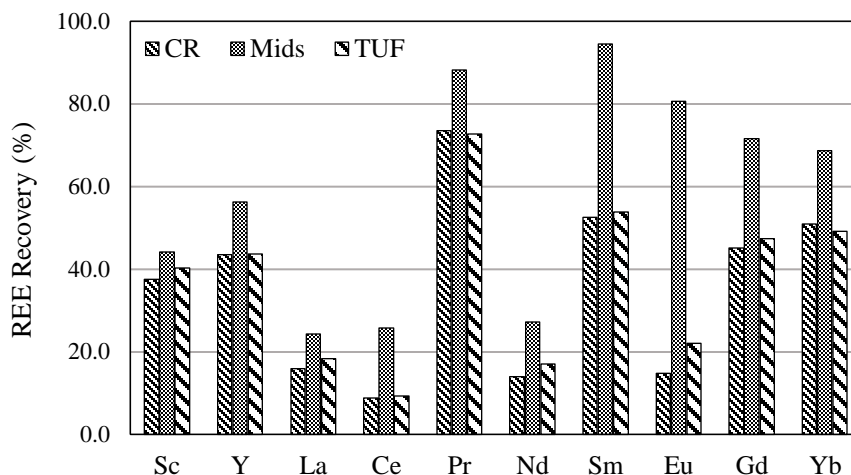
Figure 21. Selective RE element recovery from three different plant samples after 24 hours of leaching using 1.2 mol/L sulfuric acid.

4.2.3. Thermal and chemical activation

To further improve the leaching recovery of REEs from coal refuse materials, pretreatment methods were evaluated with a focus on 1) creating more exposed surface area to allow greater access to the ion exchangeable rare earth and the rare earth oxides/hydroxides; and 2) oxidizing the RE minerals and REE-enriched minerals that are relatively difficult to leach due to their existence within the crystal structures. Effective leaching usually requires pretreatment to transform the RE phosphate or silicate crystal minerals to a more leachable form such as RE oxide or chloride, followed by treatment in a leaching process (Jha et al., 2016; Kumari et al., 2015; Merritt, 1990; Sadri, Nazari, & Ghahreman, 2017). The pretreatment methods include several different roasting techniques, i.e., concentrated sulfuric acid roasting, ammonium chloride roasting, salt roasting and alkaline roasting (W. Zhang et al., 2015).

The middling fraction finer than 180 µm sample was treated by blank roasting (no chemical additives) at 750°C for 2 hours to oxidize the REEs followed by leaching using 1.2 mol/L sulfuric acid at 75°C. The leaching results obtained for both the non-treated and thermally-activated middling samples are compared element-by-element in Figure 22. The thermal activation treatment significantly improved the total REEs recovery from 31% to 74%. In particular, the effect was the greatest for all the LREEs. The recovery of neodymium, which is the most important and valuable element among the LREEs, increased by over 45 absolute percentage points. The improvement in scandium recovery was greater than 15 absolute percentage points which was significant given its market value.

The chemical transformation of RE minerals when treated with sodium hydroxide results in RE hydroxide and oxidization during blank roasting as described by (W. Zhang et al., 2015):

$$REPO_4 + 3NaOH \rightarrow 3RE(OH)_3 + Na_3PO_4.$$

$$RE_2(CO)_3 \rightarrow RE_2O_3 + 3CO_2(g)$$

$$REFCO_3 \rightarrow REOF + CO_2(g)$$
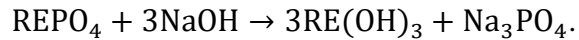
A representative sample of the fine refuse material obtained from a thickener underflow (TUF) stream was pre-leached using 8 mol/L of NaOH solution at a solid/liquid ratio of 1/10 (w/v) for 2 hours at 75°C. The solid residue was then filtered in a vacuum flask and washed thoroughly using deionized water. The dried solid residue and a non-treated TUF sample were leached using the same standard leaching conditions with 1.2 mol/L sulfuric acid. As shown in Figure 23, the total REE recovery increased from around 22% to 75% which was a slightly better improvement than the thermal activation treatment of the

middlings material. Similar to the thermal treatment, the effect was selective with the highest recovery improvement realized for the LREEs. Recovery gains of around five absolute percentage points were realized for most of the HREEs and scandium. The preferential improvements in the leach recovery values of Ce, La and Nd using both pretreatment methods may be an indicator of RE phosphate minerals.
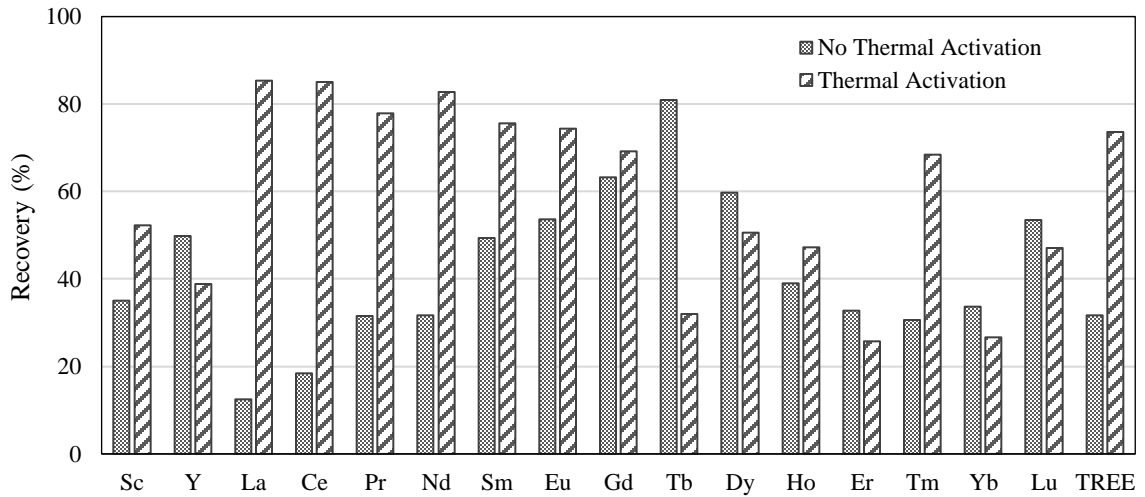
Figure 22. Improvement in REE leaching recovery after thermal activation pretreatment of the de-carbonized -180 µm middlings material and five hours of leaching using 1.2 mol/L sulfuric acid solution at 75℃.
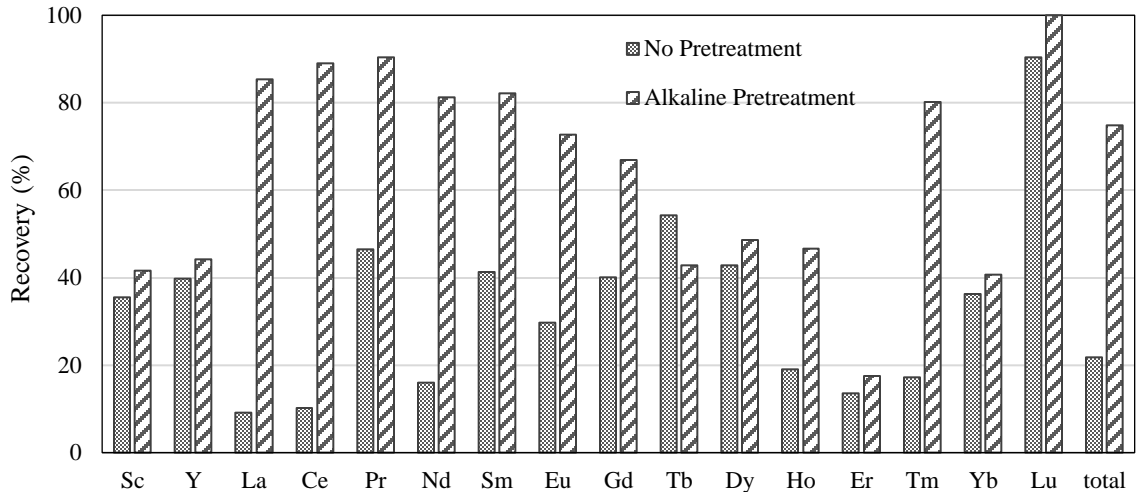
Figure 23. Improvement in REE leaching recovery after pretreatment of the de-carbonized fine refuse (thickener underflow) material in a NaOH solution followed by five hours of leaching in a 1.2 mol/L sulfuric acid solution.

4.2.4. Low temperature plasma treatment

The low-temperature plasma ashing technique has been widely used as an analytical procedure to determine mineral matter content and mineralogy structure in coal and coal byproducts (Adolphi & Stör, 1985; Kuhn, Fiene, & Harvey, 1978). Some studies compared the inorganic constituents of samples using various ashing methods and concluded that the low temperature ashing (LTA) procedure provided accurate analyses on elements with high volatility, such as mercury, zinc, lead, arsenic, and manganese (Richaud et al., 2004).

Carling et. al. (1986) investigated the microstructure change of coal in LTP using a LTA-504 unit obtained from LFE Corporation (Carling, Allen, and VanderSande, 1986). The high-vol-C bituminous coal sample showed a radical structure changes observed by a Scanning Transmission Electron Microscope (STEM). A "gauze" appearance of individual

ash particles was observed which was likely to be a three-dimensional network where denser particles were suspended in the ash matrix. These denser particles were the same types of mineral inclusions as those in the raw coal. A high-vol-B bituminous coal sample reacted slightly differently after LTA. The gauzy-type structure was still observed but to a smaller degree. The ash particles were more agglomerates of quartz, clay and pyrite. Bassanite ($CaSO_4 \cdot 2H_2O$) was detected as one of the three major mineral components in the ash matrices after LTA treatment together with quartz and kaolinite. The formation of bassanite likely took place under three mechanisms: 1) dehydration of gypsum; 2) reaction of organic sulfur and calcite; 3) reaction of organic Ca and S. Pyrite was remained in the ashing process based on XRD analysis however, the Fe: S ratio of ash sample was higher than the ratio of the original pyrite composition (Carling et al., 1986). The oxidation of pyrite can positively contribute to the REE leaching process due to its acid generation property.

The LTA process on organic surfaces can be described as shown in Figure 24. As the mixture of ionized oxygen gas reaches the surface of particles, the singlet oxygen particles tend to chemically react with the radical hydrogen of the alkyl group. The reaction can occur at low temperature and produce hydroxyl and carboxyl ions which further react with singlet oxygen to produce oxidative carbonylation. The reaction is merely happening at the interface between solid and gaseous phases, therefore the heat generated during the oxidation reaction is released in the forms of CO_2 and H_2O vapor. The organic material at the surface is gradually peeled away and the process continued into the deeper layers of the solid surfaces. The kinetic rate of this process is controlled mainly by the concentration of oxygen.

Since coal particles have micro pores and small microcracks due to the size reduction processes, surface treatment provides more exposure of surfaces and micro dispersed minerals that may contain loosely bound REEs or RE bearing minerals. By implementing the plasma treatment, the surface property and pore structure of a coal particle can be altered in the severe oxidizing environment. The open surface area is provides enhanced REE liberation from the coal organic matrix and an improved diffusion rate of lixiviate to the particle core when expose to subsequence leaching treatment. For leaching purpose, it is not necessary to completely ash the material to provide an advanced REE extraction rate in leaching process. The optimal degree of oxidation of the sample needs to be evaluated and determined by the leaching process performance with respect to the REEs recovery.
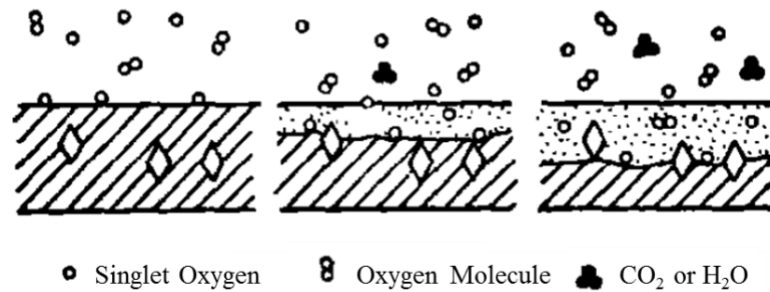
Figure 24. Oxygen plasma treatment on organic surface. Adapted from (Hozumi, 1971, 1976, 1977)

Leaching recovery of REEs from the plasma-treated LTA coal 1 segment with sulfuric acid solution at pH of 0, ammonium sulfate salt solution at pH of 3, and deionized water at pH of 3 were compared in Figure 25. Since pyrite was proved to be one of the major components present in the LTA coal, the material was naturally an acid producer. The final pH of the leaching environment dropped to 3 after 5 hours of leaching under 75 °C with no acid added. For most of the REEs, the magnitude of recovery followed the order of acid

leach> salt leach> water leach. However, scandium recovery values achieved under all three leaching conditions were above 80%.

Scandium (Sc) recovery values are plotted in Figure 26 as a function of solids loss, which represents the %weight of the feed material that dissolve during leaching. Any data points on or below the dotted lines given in these plots indicate non-selectivity in the chemical leaching process (i.e. digestion). Thus, the further a point is away from the line, the higher the selectivity. Alkaline assisted roasting is a sample pre-treatment process that oxidizes the targeted minerals at a rigorous condition (temperature at 750ºC). The process is commonly used to decompose the mineral crystal structure so that the REEs are easier to dissolve in solution. The roasted sample yielded over 70% Sc recovery in one of the tests, however, with almost 70% solid loss. The optimal recovery value obtained on the untreated sample was around 40% leaching under a condition of pH 0 and 75 ºC. However, as shown in Figure 26, scandium recovery from the plasma treated sample was greater than 80% while solids loss was around 40% which reflects a higher degree of selectivity. High selectivity mean less contamination in the leachate and, thus, a less complex, lower cost solvent extraction circuit.
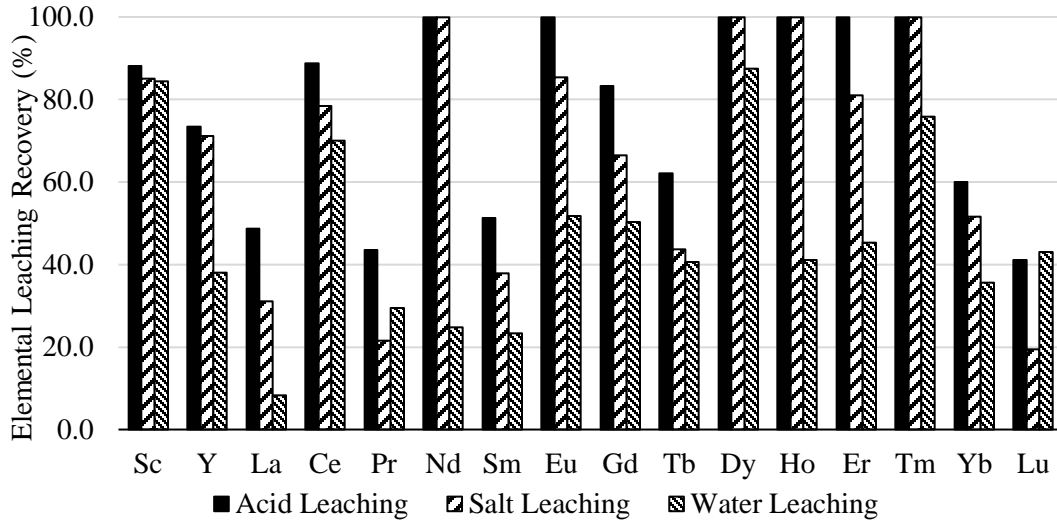
Figure 25. Recovery of REEs from low-temperature plasma treated coal under various leaching conditions for 5 hours. (Acid Leaching with sulfuric acid at final pH of 0; Salt Leaching with ammonium sulfate at final pH of 3; Water Leaching with deionized water at final pH of 3.)
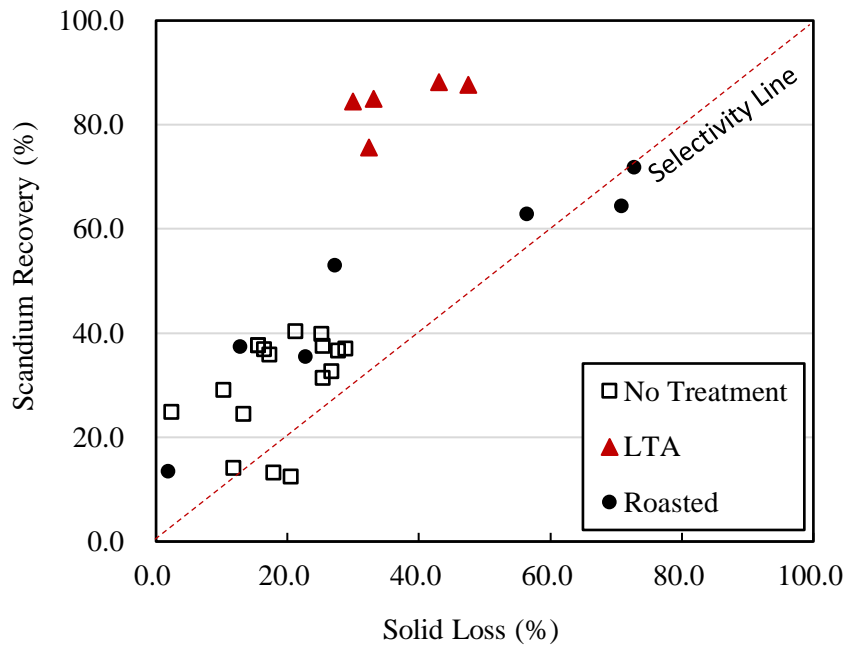
Figure 26. Enhanced Scandium recovery and leaching selectivity of WKY13 coal after low-temperature plasma treatment compare to that of decarbonized WKY13 coal and coal byproducts under various leaching conditions. (pH value of 0-3, solid concentration of 10 g/L, temperature of 75°C).

4.3. Geological Core Leaching

To identify the mineral sources of the REEs and identify the minerals dissolved under the standard leach conditions, XRD analyses were conducted on selected samples before and after the leaching test. As shown in Table 6, quartz, kaolinite and illite were the three major minerals comprising the mineral matter within the coal seam including the roof and floor material. Pyrite content is known to be high in Illinois basin coal with values in the range of 0.5% to ~18.5% by weight of the total mineral matter (Korose & Elrick, 2010). The coal segments and the fusain layer within the West Kentucky No. 13 seam contained significantly greater amounts of pyrite by weight ranging from 20% to ~53%. An issue pertaining to acid leaching in the presence of pyrite was the relatively large amount of iron in the leachate solution which was a major contaminant in the final leachate. The high iron and low REE contents in the leachate presented challenges for the downstream REE refining processes. However, pyrite oxidation occurring in the natural environment produces sulfuric acid which helps reduce the cost of the leaching process. As such, the high pyrite content in the West Kentucky No. 13 coal refuse material has the potential to provide effective self- leach action subject to a proper temperature and oxidation environment.

Fluorapatite ($Ca_5(PO_4)_3F$) was detected in a core segment identified as "high REEs claystone" which represented 5.5% by weight of the total segment. The fluorapatite mineral is a major source of phosphoric acid production and considered as a secondary source of REE production (Gupta & Krishnamurthy, 2015; Jha et al., 2016).

Table 6. XRD analysis on major segments of the core sample.

Minerals / Core Segments	Quartz %	Kaolinite %	Pyrite %	Illite %	Muscovite %	Fluorapatite %
Roof Rock	60.5	16.7	1.3	8.3	13.3	0
LTA Coal 1	22.6	21.8	53.3	0.6	1.8	0
High REE Claystone	31.4	48.8	1.3	6.3	6.7	5.5
LTA Coal 2	20.1	42.9	30.8	0.7	6.3	0
Claystone Partings	32.9	55.0	1.0	4.6	6.5	0
LTA Coal 3	30.8	15.8	47.9	1.4	4.1	0
Fusain Layer	22.9	31.3	38.4	3.4	4.0	0
LTA Coal 4	40.8	20.6	31.2	1.7	5.7	0
Direct floor	48.7	14.9	9.3	10.7	16.4	0
Seat Rock	52.1	27.5	8.5	3.4	8.5	0

The results indicated that the light REEs are more likely existing as finely dispersed minerals in coal, whereas the heavy REEs are more likely existing as ionic form entrapped in the carbon matrix and/or adsorbed onto clay surfaces. The low-temperature ashed coal segments consisted of quartz, kaolinite, illite, pyrite, and calcite as the major mineral components of the ash-forming material analyzed by XRD as shown in Figure 27. The composition of LTA coal was identical to the typical composition of the roof and floor materials. However, under the same leaching condition, the REE recovery values obtained from the LTA coal samples were much higher than those obtained from the treatment of the roof, floor, or inner parting materials. Therefore, two possibilities exist to explain this observation: 1) The REEs that are ionically associated with the clay material and other inorganic minerals are oxidized creating rare earth oxides that are soluble under mild pH

conditions and 2) the REEs minerals in coal are exposed and oxidized under the oxygen plasma environment and also become more easily dissolved in water.

The REE leachability from the mineral matter that was micro-dispersed within the coal rich segments was evaluated by first subjecting the material in each coal segment to low-temperature ashing and performing the leach test on the remaining material. It was noted by the ash contents in Table 7 that the total removal of the carbon material from the samples subjected to leaching tests was not totally complete. As summarized in Table 7, the recovery of the total REEs from the coal-rich segments was greater than 65%. The results showed that the recovery of HREEs in three of the four coal-rich segments was significantly higher with values around 80%. Explanations for the preferential leaching behavior could be reflective of the differences in the modes of occurrence. If the presence of the REEs was originally due to the chelating properties of specific components of the organic matter, the chelating efficiency favors the higher ionic charge of the heavy REEs while the preferential leaching of heavy REEs is suspected to be due to adsorption onto the micro-dispersed clay particles due to their higher charge density. A greater recovery differential between the heavy and light REEs was obtained from the direct floor material and the claystone parting located near the roof. The roof rock, a middle claystone parting, and the seat rock material were relatively difficult to leach as indicated by recovery values of 27%, 7%, and 23%, respectively. Given that these segments likely account for most of the coarse and fine refuse due to their cumulative thickness, their poor leaching characteristics help to explain the relatively low recovery values obtained from the refuse samples. On the other hand, the good leachability characteristics of the middling material, which is comprised of both coal and rock, may be reflective of the leaching performances

obtained from the coal-rich segment, direct floor and thin claystone parting.

The coal splits and claystone parting in the upper coal bench are also the best source of REEs due to the high recovery values for critical REEs and scandium. Scandium recovery is particularly high (i.e., 70% to 80% range) in the upper bench and the coal-rich fragments in the lower bench. The direct floor material appears to be an excellent source of the critical elements based on REE concentration and high recovery values.

The REEs present in fluorapatite as an isomorphous ion substitution form for calcium within the crystal lattice (Habashi et al., 1986; R. Kim et al., 2016). The main reaction that describes the phosphoric acid production from fluorapatite is (Bandara & Senanayake, 2015a):

$$Ca_5(PO_4)_3F + 5H_2SO_4 + 5x\ H_2O = 5CaSO_4 \cdot x\ H_2O + 3H_3PO_4 + HF\ (x=2\ or\ 0.5).$$

The process produces insoluble $CaSO_4$ (gypsum) which consumes nearly 80% REEs from solution by co-precipitation. In a study reported by Kim et. al. (2016), around 40% of the Ca, Ce, La, Nd, and Pr were recovered from apatite ore using 1.0 mol/L of sulfuric acid (R. Kim et al., 2016). However, nearly 50% of the leached REEs were precipitated with $CaSO_4$ due to Ca ion substitution. The leaching process also produces H_3PO_4 and HF which can interfere with leaching efficiency since the REEs as well as other non-REE metal ions can complex with PO_4^{3-} and F^- thereby forming precipitates as phosphate or other salts (Bandara & Senanayake, 2015a). Fluorapatite is readily soluble under the general leaching conditions used in the study as indicated by the XRD results presented in Figure 27.

Table 7. Acid leaching of REEs from core segments after five hours of treatment.

WKY#13 Core	Ash Content	Core Segment TREEs		Solids Loss	REE Leaching Recovery		
		Dry Ash Basis	Whole Mass Basis		Total REEs	LREEs + Sc	HREEs + Y
	(%)	(ppm)	(ppm)	(%)	(%)	(%)	(%)
Roof Rock	92.2	268	248	23.7	26.8	21.7	48.0
LTA Coal 1	59.0	294	174	43.0	72.5	73.9	66.8
High REE Claystone	81.2	1144	929	22.8	56.2	49.4	89.7
LTA Coal 2	67.9	318	216	33.8	66.2	63.0	78.8
Claystone Partings	88.2	404	356	17.9	6.8	2.8	26.0
LTA Coal 3	72.7	331	241	32.4	66.4	61.4	78.4
Fusain Layer	44.1	190	84	31.6	46.3	45.8	51.3
LTA Coal 4	67.8	252	171	47.5	74.5	66.1	82.0
Direct Floor	85.9	390	335	30.8	62.9	47.8	93.6
Seat Rock	88.9	161	143	10.3	22.9	22.8	23.4
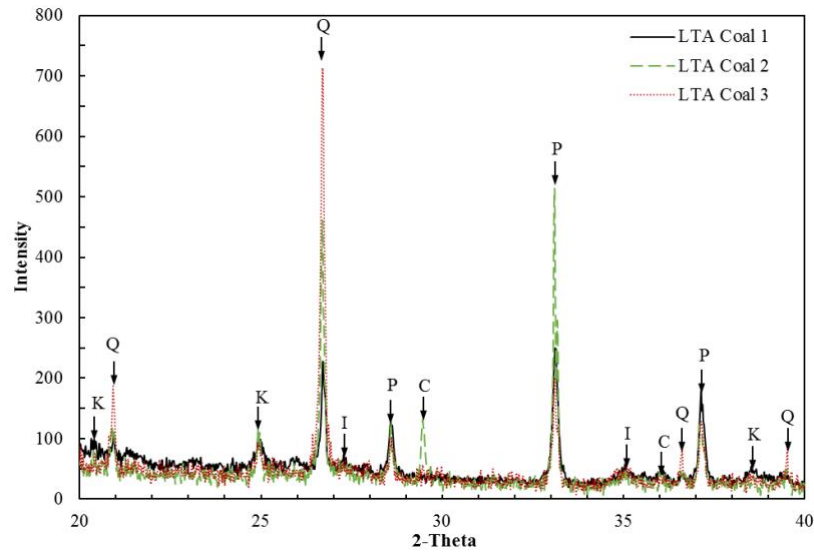
Figure 27. X-Ray Diffraction patterns of several combined coal segments in WKY #13 geological core sample after low-temperature plasma treatment. (Major minerals include K: Kaolinite; Q: Quartz; I: Illite; P: Pyrite; C: Calcite.)

4.4. CONCLUSIONS

In this chapter, the leaching characteristics of the REEs distributed in different particle size and density fractions of two coal sources were studied. The results indicated that the REEs associated with different compositions in heterogenous coal material shared had different leaching characteristic which proved that the mode of occurrence of REEs differs between in coal sources was not in the same manner and thus requires different intensity levels of leaching strategies to achieve economical extraction to recover. The specific findings include:

(1) Most of the REEs are concentrated in the inorganic fractions in of bituminous coal. The total REE concentration on an ash basis of the low ash fractions was significantly higher compared to high ash fractions due to the dilution effect of the carbon content organic matter. With physical liberations of carbon content and inorganic material, the REEs are concentration in the inorganic minerals.

(2) The smaller size of particles liberated from coal material contains higher concentration of REEs, which indicated that the REEs are finely disseminated in coal structure.

(3) Ion-adsorbed REEs onto clay particles surfaces is one of the modes of occurrence associated with coal sources. The recovery values obtained for of a number of heavy REEs including Gd , Tb, Dy, Y as well as Sc than that of the light REEs, such as Ce, La and Nd, which indicated the potential of utilizing ion exchange for selective extraction.

(4) For the coal-rich segments in the vertical profile of a coal seam, the micro-dispersed mineral matter was liberated using a low-temperature plasma furnace prior to the

leaching tests. Overall REE recovery values of around 60% and higher were obtained for the direct floor, claystone parting material and the micro-dispersed mineral matter while significantly lower recovery values were realized for the roof, other parting segments and the seat rock.

(5) Thermal activation by roasting or chemical activation pretreatment provided a significant increase in overall REE recovery. The recovery of the light REEs was affected the most as indicated by an increase in La and Ce recovery which indicated the conversion of the RE minerals to a soluble rare earth metal hydroxide form.

(6) Light REEs are more likely existing as finely dispersed minerals in coal, whereas the heavy REEs are more likely existing as ionic form adsorbed onto clay surfaces or entrapped within the organic matrix...

CHAPTER 5. LEACHING KINETICS

5.1. INTRODUCTION

The leaching kinetic rate is affected by a series of major variables including the type of lixiviant, the lixiviant concentration, solid-to liquid-ratio, particle size, mixing conditions, temperature and reaction time. The type of lixiviant affects the REE leaching characteristics by changing the solution speciation stabilities due to the existence of various anions in varying concentrations. Sulfate ions have a higher coordination ability with rare earths than chloride ions even in high monovalent concentration solutions (Xiao et al., 2016). Solid-to-liquid ratio corresponds to the stochiometric ratio of reactants which directly affects the reaction equilibration. Leaching process that is mainly controlled by a diffusion process is more dependent on mixing conditions whereas temperature has a more significant effect on chemical reaction controlled processes (Levenspiel, 1999).

The leaching process is classified as fluid-particle heterogenous reaction in which a liquid reacts with a solid by contacting and transforms the solid into a product (Levenspiel, 1999). A solid particle that reacts with a liquid and shrinks in size during the reaction can be described by a shrinking core model. The reaction is a five-step process, i.e., 1) diffusion through the film layer, 2) diffusion through the product layer, 3) chemical reaction on the surface, 4) product diffusion through the product layer and 5) product diffusion through the film layer to the solution (Xiao et al., 2015). The slowest step is known as the rate determining process. By selecting a correct rate equation, the activation energy of certain leaching step can be calculated. In this chapter, the major variables of leaching process are evaluated and the activation energy of the REE leaching is determined.

5.2. PARTICLE SIZE EFFECT

A reduction in the particle size may provide two significant benefits, i.e.: 1) liberation of the clay particles which exposes more surface area and exchangeable REEs for lixiviants to interact and extract the RE ions and/or 2) liberate nano-sized RE minerals and RE oxides that can be dissolved in acid. On the negative side, by reducing the particle size to micron level, the newly released surface area is increasing exponentially which escalates the consumption of hydrogen ions by dissolving more contaminate metal ions. Acid leaching on finer size material can provide faster kinetic rates and higher efficiency on REE extraction. The ultrafine material could reduce selectivity and increase the cost of leach and the downstream concentration processes, significantly increase the cost of energy to achieve the required grinding and cause difficulties in thickening and dewatering.

In the previous chapter, particle size showed a significant effect on leaching kinetic rate, where the leaching rate is faster with smaller particle size, but the contamination level is higher in leachate solution due to the higher solid loss. To assess the effect of particle size on leaching performance, a samples of the Fire Clay middlings material were ground for different lengths of time before the de-carbonization step to generate samples having a range of 80% passing sizes (P80). The Fire Clay middling material was obtained from the material coarser than 9.5 mm and with a specific gravity between 1.4 and 1.8. The sample was crushed and ground to finer than 212 microns (-80 mesh) and then dispersed in a slurry and ground in an attrition mill under different conditions (grinding time and RPM). The attrition mill product was then de-carbonized in a flotation cell followed by secondary flotation to remove calcite and other acid consuming minerals. The tailings material of the second flotation step was filtered and dried in preparation for the leaching tests. Kinetic

leaching tests were conducted using 1.2 mol/L of sulfuric acid with a solid concentration of 1% by weight at 75 °C. The REE recovery was measured after leaching for five hours.

To establish a baseline, the contents of the de-carbonized Fire Clay middling material after dry grinding to a top size of 212 microns (80 mesh) was analyzed. The material was analyzed for REE content by ICP-OES and mineralogy using XRD. The decarbonized Fire Clay middling material contained 607 ±18 ppm of total REEs of which Ce content accounted for 42% of the total REEs as shown in Figure 28(a). The Fire Clay material was rich in light REEs as indicated by a content of 534 ppm or 88.0% of the total. Yttrium was the most abundant heavy REE with a concentration of 47 ppm. The major minerals present in the sample are quartz, kaolinite, illite, and muscovite as shown in the XRD plot in Figure 28 (b). A previous study found that REEs in the Fire Clay coal were strongly associated with micro-dispersed kaolinite which may be liberated and released through size reduction (Wencai Zhang et al., 2018b).

The results shown in Table 8 indicated that reducing the particle size liberated mineral matter containing higher concentrations of REE. For example, the least amount of grinding produced a P80 size of 32 microns and flotation tailings material or leach feed containing 444 ppm of total REEs. The REE concentration of 444 ppm reflects the content of the coarser mineral matter dispersed in the middling particles. By grinding for greater lengths of time and applying more energy, the P80 size was reduced to five microns and the two stages of flotation produced a leach feed material containing 751 ppm of total REEs. This finding indicates that the finest mineral matter dispersed within the Fire Clay coal has the highest concentration of REEs.

Reducing particle size also resulted in a significant increase in leach recovery from 71.2% to 83.6% over the range of P80 sizes. As such, the size reduction increased the amount of REEs reporting in the leach feed and increased the percentage of the REEs being recovered through leaching. These two positive outcomes suggest that the REEs associated with micro-dispersed mineral matter in the Fire Clay middlings are more concentrated and more easily extractable by leaching. In addition, the finer mineral matter is more soluble as indicated by the increase in the amount of solid loss shown in Table 8. As much as 20% of the solids in the finest sample tested was dissolved under the standard leaching conditions which may reflect both the mineral matter type and surface area exposure.
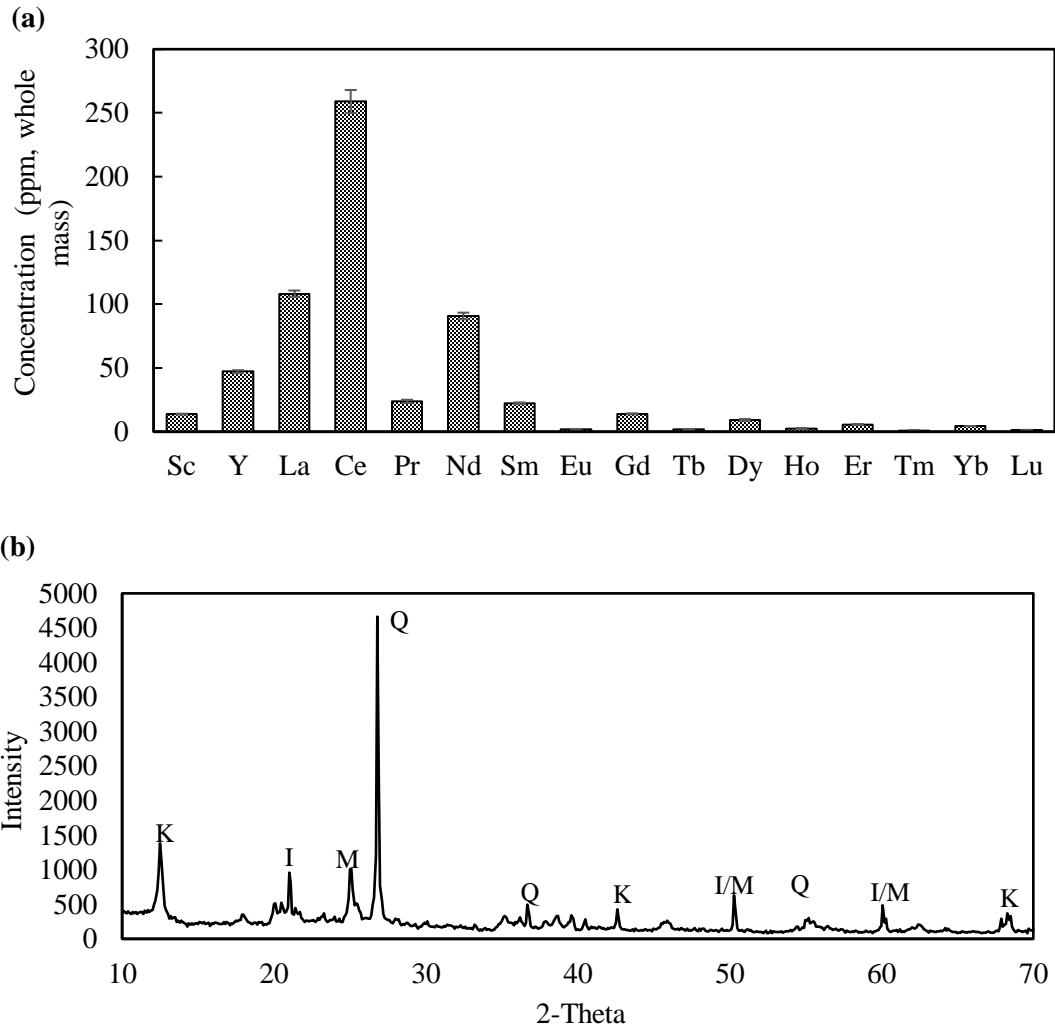
Figure 28. The contents of the decarbonized Fire Clay middlings material ground to a top size of 212 microns (80 mesh) on the basis of (a) rare earth content and (b) mineralogy as determined by X-ray Diffraction analysis (Q-quartz, K-kaolinite, I-illite, M-muscovite).

Table 8. Particle size reduction effect on acid leaching of the de-carbonized Fire Clay middlings material (1.2 M/L H_2SO_4, solid concentration = 1%, temp = 75 ºC).

P80	Leach Feed TREE	Solid Loss	TREE Recovery
(micron)	(ppm)	(%)	(%)
32	444	11.85	71.22
14.5	499	9.92	74.78
10.2	531	9.2	79.00
8.7	622	16.18	82.88
7.33	705	16.18	83.72
6.5	737	17.2	84.34
5	751	20.36	83.62

5.3. EFFECT OF MAJOR VARIABLES ON REE LEACHING

5.3.1. Effect of acid type

Leaching experiments were conducted using different inorganic acids using an acid concentration of 1M, solid/liquid ratio of 10 g/L and a temperature of 75℃. Sulfuric acid (H_2SO_4), hydrochloric acid (HCl), and nitric acid (HNO_3) were used to study the leaching process. Figure 29 compares the REE leaching recovery and reaction rate between the different lixiviants. The total REE (TREEs) recovery values of 80%, 76%, and 74% were achieved after 3 hours of leaching using HCl, HNO_3, and H_2SO_4 solution, respectively. The pH of the leachate solutions at the end of the tests were 0.105, 0.113, and 0.112, respectively.

Hydrochloric acid provided the fastest leaching rate which achieved 73% recovery after the first 5 minutes of leaching, and slowly reached equilibrium after 3 hours. Nitric

acid also provided fast leaching rate at the first 30 minutes. Sulfuric acid was the least effective under the leaching conditions and provided the slowest leaching rate. This finding is likely due to the fact that sulfate ions have a higher coordination ability with rare earths than chloride ions even in high monovalent concentration solutions (Xiao et al., 2016).

The coal-based leachate contained high concentrations of trivalent ions that may coordinate with sulfate ions resulting in depression of the rare earth-sulfate coordination. In addition, sulfuric acid requires two steps of dissociation reaction to release H^+ into solution whereas hydrochloric acid and nitric acid dissociates more rapidly into solution. Viscosity of the sulfuric acid solution is another factor that could have resulted in the slower reaction rate as the wetting rate of the solid particle surfaces is reduced when the solution viscosity is high. Despite the negative aspects of sulfuric acid, the lixiviant is still considered a viable lixiviate due to its relatively low cost and the negative aspects of the other lixiviants including the volatility of hydrochloric acid and the decomposability of nitric acid under 75 ℃ (Yu, Guo, & Tang, 2013).

Figure 29. Effect of acid type on the leaching recovery of total rare earth elements contained in the Fire Clay coal middlings (75℃, 530 rpm, S/L=10g/L, d_{80}=8.7 micron).

5.3.2. Effect of stirring speed

The stirring speed affects the film thickness around the film layer of a solid particle suspended in the lixiviate solution. A high stirring speed creates an enhanced shear rate in solution which reduces the film layer thickness thereby increasing the mass transfer rate through the film diffusion layer (Makanyire, Jha, & Sutcliffe, 2016). The effect of stirring speed was evaluated at 300 rpm, 530 rpm, 760 rpm, and 900 rpm as shown in Figure 30. The leaching condition included a 1M sulfuric acid solution and a solid/liquid ratio of 10 g/L at 75 °C. The test results indicate a stirring speed of 300 rpm had a negative effect on leaching kinetics while stirring speeds of 530 rpm to 900 rpm provided nearly equal kinetics. The recovery at a 900-rpm stirring speed was slightly lower than that obtained at

760 rpm. A stirring speed of 530 rpm was established as an adequate value for the standard test conditions.

Figure 30. Effect of stirring speed on the leaching recovery of total rare earth elements contained in the Fire Clay coal middlings (75℃, 1 M H_2SO_4, S/L=10g/L, d_{80}=8.7 microns).

5.3.3. Effect of solid-to-liquid ratio

The effect of solids-to-liquid ratio on rare earth leaching recovery was investigated in the range of 10g/1L to 200g/1L while maintaining the other parameters constant at 75 ℃, 1 M H_2SO_4 and 530 rpm. The association between reactants decreased with an increase in the solid/liquid ratio which resulted in a decrease in the extraction rate as shown in Figure 31. Leach recovery was reduced from 74% to 40% after increasing the solid-to-liquid ratio from 10g/L to 200 g/L. The magnitude of the recovery reduction is not commonly observed in other metal leaching operations. In the metallic copper leaching process, the leaching

reaction was more effective when the Cu^{2+} concentration in solution was higher because the Cu^{2+} reacted with metallic Cu to Cu^+ (Z. Wang, Guo, & Ye, 2016). This type of reaction mechanism does not occur in a REE solution since the REEs exist mostly as a compound. Niobium leaching from titanium oxide residues did not show any effect of solid-to-liquid ratio on leaching recovery (Makanyire et al., 2016). However, Li et. al. (2013) reported on a study on rare earth concentrate leaching that found the solid/liquid ratio to have a negative effect when the ratio was higher than 100 g/L. (Mei Li et al., 2013) Therefore, the solid/liquid ratio effect varies from source to source in different leaching environments.
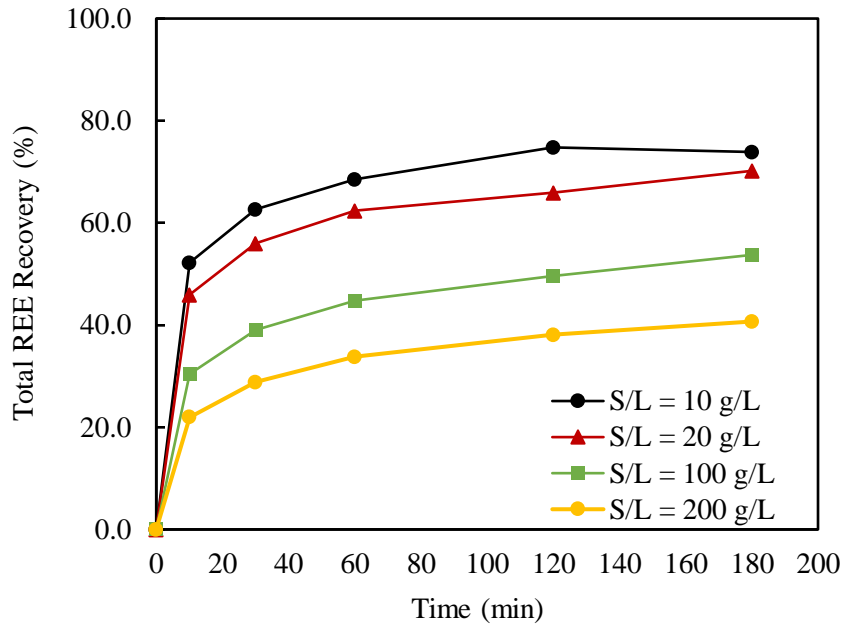
Figure 31. Effect of solid to liquid ratio on the leaching recovery of total rare earth elements contained in the Fire Clay coal middlings (75℃, 1 M H_2SO_4, 530 rpm, D_{80}=8.7 micron)

5.3.4. Effect of acid concentration

The effect of sulfuric acid concentration on leaching recovery was studied using 0.1 M, 0.5 M, 1 M, and 2 M acid concentrations and the standard conditions for temperature, stirring speed, and solid- to-liquid ratio. The initial acid concentration of 0.1 M, 0.5 M, 1 M, and 2 M resulted in ending pH values of 1.04, 0.38, 0.11, and -0.25, respectively, after 3 hours of leaching. As shown in Figure 32, the total REE recovery increased substantially from 40% to 74% by increasing acid concentration from 0.1 to 1 M. However, from 1 M to 2 M, recovery only increased by 2.5%. The optimal acid concentration was selected to be 1 M since higher concentrations of acid did not provide a significant increase in recovery of REEs and adds significantly to the contaminant concentration.
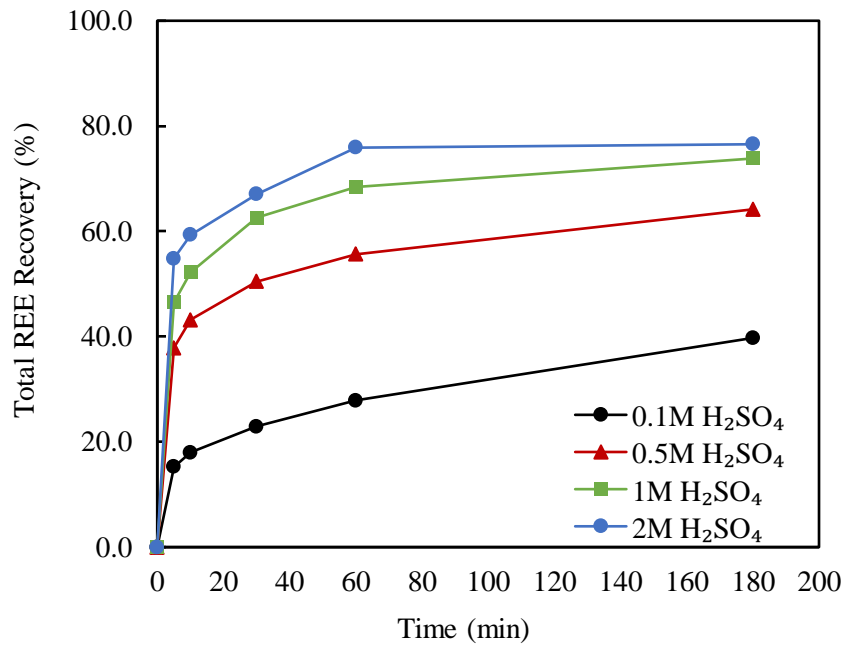
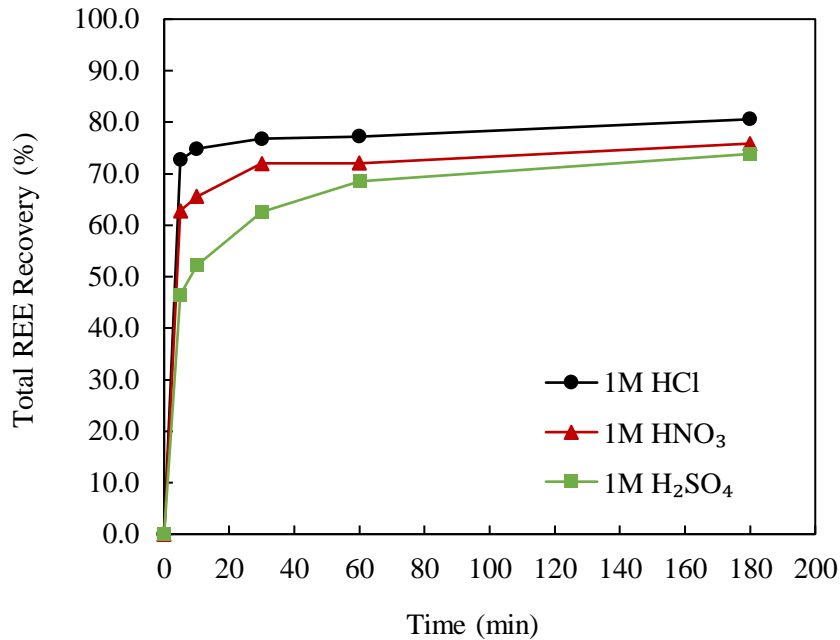Figure 32. Effect of sulfuric acid solution concentration on the leaching recovery of total rare earth elements contained in the Fire Clay coal middlings (75℃, 530 rpm, S/L=10g/L, D_{80}=8.7 micron).

5.3.5. Effect of temperature

The effect of temperature on REE leaching using 1 M H_2SO_4 was investigated with stirring speed of 530 rpm and the S/L of 10 g/L for 2 hours. Samples were taken over shorter time increments due to the relatively fast kinetics over the first 20-30 minutes. Figure 33 demonstrates that the REE leaching recovery increased with an elevation in leaching temperature. When the temperature was increased from 298 K (25℃) to 348 K (75℃), leaching recovery increased from 35% to 75% after 2 hours of leaching. The data suggests the existence of a relatively fast leaching process during the first 20 minutes followed by a slow process. As such, two or more reaction mechanisms may be occurring when leaching the coal source.

The effect of temperature on individual REEs is shown in Figure 34. Most of the light REEs (i.e. La, Ce, Pr, Nd, Sm) appeared to be very sensitive to temperature which indicated that the leaching mechanism of light REEs was mostly chemical reaction controlled. The recovery of Ce, Pr, and Nd increased from 36%, 39%, and 36% to 79%, 84%, and 80%, respectively, by increasing the temperature from 25 ℃ to 75 ℃. The heavy REEs and scandium recovery improved with higher temperature, but the increase was not as significant. Scandium recovery rose from 29% to 36%. For the recovery of elements that were relatively insensitive to temperature, the activation energy is generally low and more likely to be a result of a diffusion controlled process (Free, 2013).
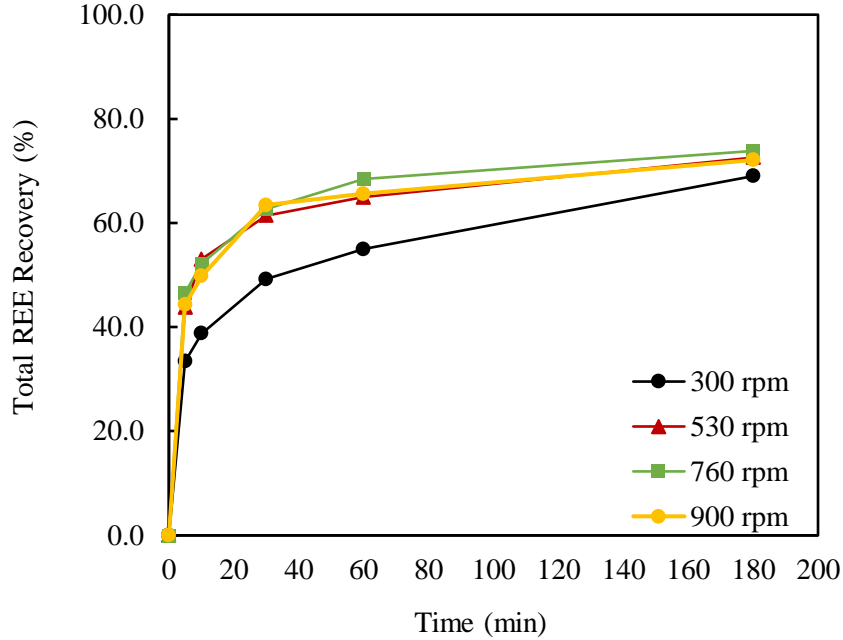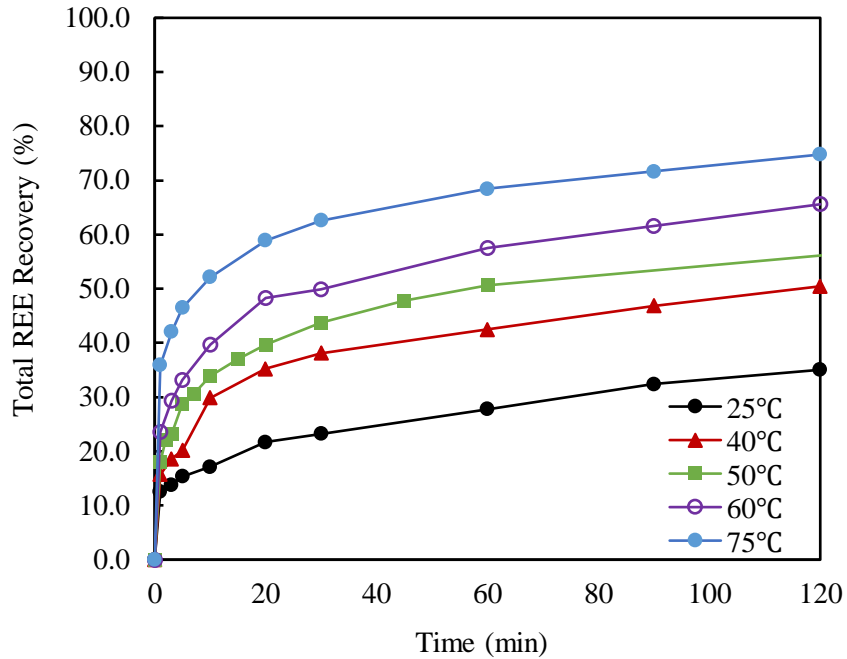
Figure 33. Effect of leaching reaction temperature on the leaching recovery of total rare earth elements contained in the Fire Clay coal middling (1 M H_2SO_4, 530 rpm, S/L=10g/L, D_{80}=8.7 micron)
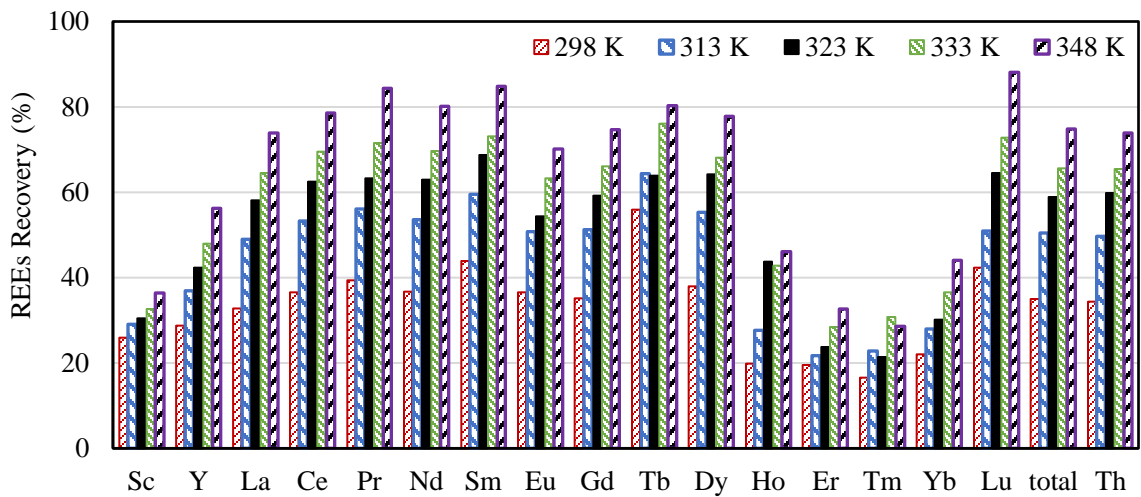
Figure 34. Effect of leaching reaction temperature on the leaching recovery of individual rare earth element. (1 M H_2SO_4, 530 rpm, S/L=10g/L, D_{80}=8.7-micron, retention time of 120 minutes)

5.4. MORPHOLOGY

The morphology of the Fire Clay coal middling particles before and after sulfuric acid leaching was studied using SEM. As shown in Figure 35 (a), the feed material consisted of heterogeneous particles comprised of mostly quartz and clay agrees well with the XRD analysis shown in Figure 28(b).

After 2 hours of leaching at 50 ºC, the particles were found to have a porous structure on the surface with a micro pore structure as shown in Figure 35 (b). After 2 hours of leaching at 75 ºC, the porous structure on some of the particle surfaces appeared larger size as shown in Figure 35 (c). The images showed no reaction product layer or any coating product on the surface. Therefore, the diffusion process in this reaction may be contributed by the interfacial transfer of the products and the reagent diffusion through the porous structure of solid particles.

The leaching process involved several simultaneous reactions due to the mineral composition and the variety of REEs associations. The REEs were found to exist in crystalized structures (mostly silicates and phosphate compounds) which usually require decomposition to be extracted under the current leaching condition. The REEs are mostly present as RE ion substitution in clays and as soluble RE containing minerals. Based on the experimental data, light REEs in this coal source were mostly mineral associated, whereas the heavy REEs were soluble metal oxides and ion-adsorbed onto clay minerals.
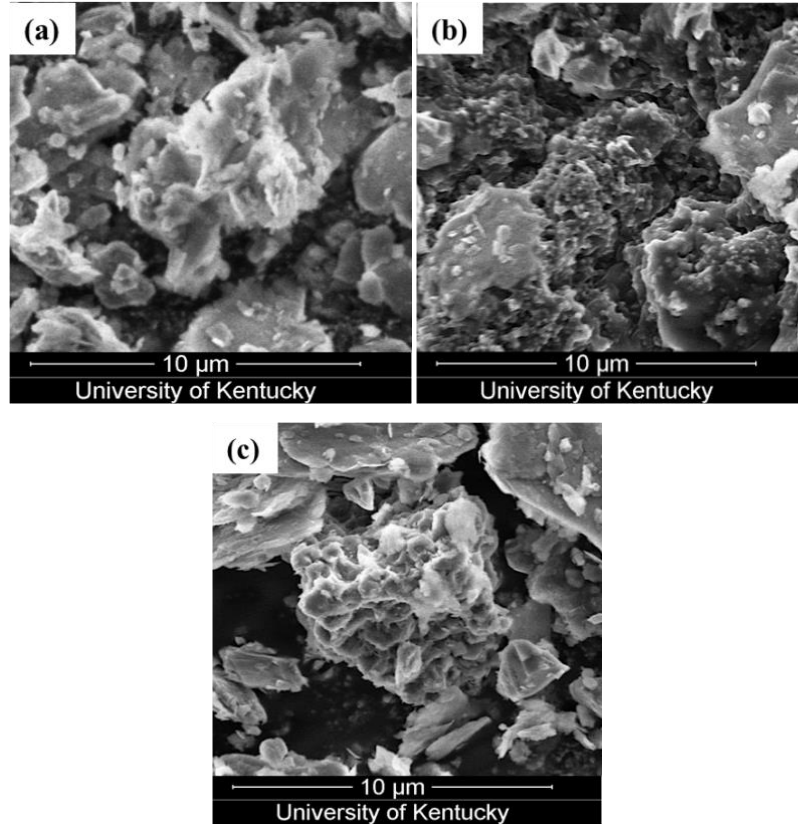
Figure 35. SEM images of particles found in (a) leaching feed material; (b) solid residue after 2 hours leaching at 50 ℃; (c) solid residue after 2 hours leaching at 75 ℃. (1 M H_2SO_4, 530 rpm, S/L=10g/L, D_{80}=8.7-micron)

5.5. KINETIC ANALYSIS

A variety of rate equations have been developed and reported in literature that describe the leaching rate process (Dickinson & Heal, 1999; Levenspiel, 1999; Salmi, Grenman, Warna, & Murzin, 2013). Among the equations, the rate equation (Eq. 35) developed by Crank–Ginstling–Brounshtein which describes the mass transfer across product layer fits the experimental data well, i.e.:

$$k_d t = \left[1 - \frac{2}{3}\alpha - (1-\alpha)^{\frac{2}{3}}\right]$$

Eq. 35

where α is the fraction that reacted; k the kinetic constant.

The Crank–Ginstling–Brounshtein equation was used to linearize the extraction fraction (α) among all the temperatures using the experimental data for the first 20 minutes of leaching and 20-120 minutes reaction as shown in Figure 36. The correlation coefficient values (R^2) and the corresponding slopes (k) of the plots are listed in Table 9. Rate constants were calculated and the Arrhenius plots of ln(k) versus 1/K are as shown in Figure 37 for the two leaching stages. The activation energy determined for the first 20 minutes was 36 kJ/mol and 27 kJ/mol for the following 20-120 minutes of leaching. The activation energy values for both leaching periods were close to the energy barrier that is typically used to identify a diffusion controlled or chemical reaction controlled process which is around 20 kJ/mol (Free, 2013).

Since the coal tailing material is a heterogenous material that contains a number of potential modes of occurrence of REEs, the leaching process is not a single reaction. The resulting requirement for activation energy is a combination of the various forms of REEs. In addition, the material contains both calcite and pyrite among other soluble minerals which create a complex solution environment where the localized pH elevation on the solid particle surface could cause a product layer to be formed. The interfacial transfer of product through the porous structure of the solid particles requires high activation energies as reported by Li et.al. (2010 and 2013) which can be as high as 40 kJ/mol (Mei Li et al., 2013; Minting Li et al., 2010).

To support of the hypothesis, the activation energies for light and heavy REE groups were calculated using the data provided in Table 10 and Table 11, respectively. The activation energy values for leaching the light REEs leaching over the first 20 minutes and

the period between 20 and 120 minutes are 41.8 kJ/mol and 28.1 kJ/mol, respectively. Whereas, the activation energy for heavy REEs leaching for the first 20 minutes and the 20-120 minutes of reaction is 24.2 kJ/mol and 26.1 kJ/mol, respectively. These values indicate that the leaching of the light REEs during the initial stage is more of a chemical reaction followed by the formation of a product layer and a reduced activation energy. The activation energy required for leaching the heavy REEs during the initial stage was significantly lower than that of the later stage. This finding implies that the major mechanism for heavy REEs leaching is desorption, and the product layer forming does not significantly affect the leaching of the heavy REEs.
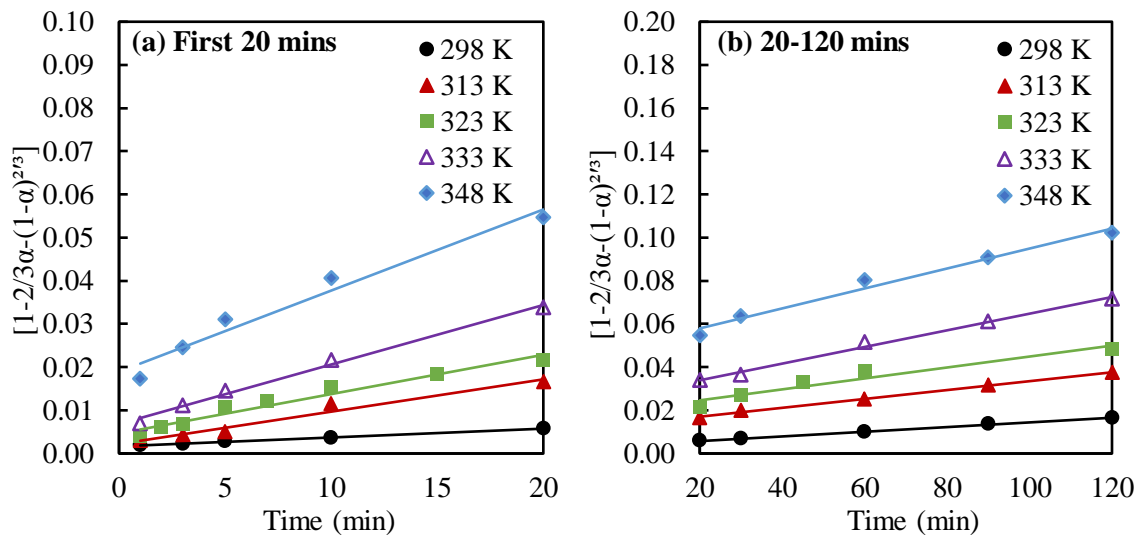
Figure 36. Kinetic modelling of total REEs recovery during the (a) first 20 minutes, and (b) 20-120 minutes of leaching at various temperatures for the Fire Clay middlings (1 M H_2SO_4, 530 rpm, S/L=10g/L, D_{80}=8.7-micron, retention time of 120 minutes).

Table 9. Correlation coefficients of diffusion-controlled kinetics models at different temperatures for total REEs.

T, K	Diffusion 1-20 mins			Diffusion 20-120 mins		
	k	a	R^2	k	a	R^2
298	0.0002	0.0017	0.9949	0.0001	0.0036	0.996
313	0.0007	0.0022	0.9648	0.0002	0.0129	0.9977
323	0.0009	0.0046	0.9616	0.0003	0.0196	0.9402
333	0.0014	0.0068	0.9919	0.0004	0.0262	0.9934
348	0.0019	0.0189	0.9627	0.0005	0.0487	0.9796
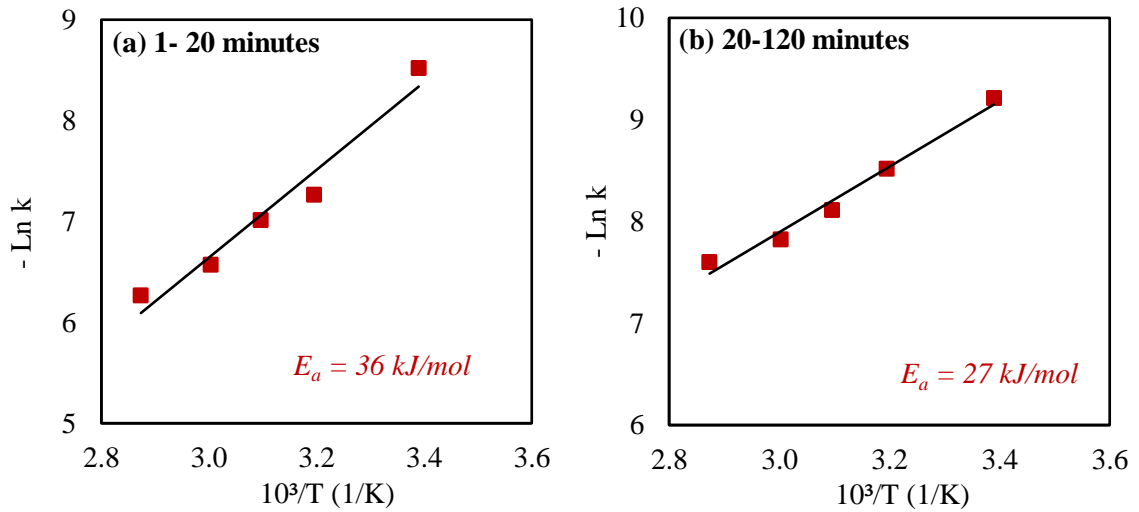
Figure 37. Arrhenius plot for the total REEs leached from the Fire Clay coal middlings during the (a) first 20 minutes, and (b) 20-120 minutes of leaching (1 M H_2SO_4, 530 rpm, S/L=10g/L, d_{80}=8.7-micron).

Table 10. Correlation coefficients of diffusion-controlled kinetics models at different temperatures for light REEs.

T, K	Diffusion 1-20 mins			Diffusion 20-120 mins		
	k	a	R^2	k	a	R^2
298	0.0002	0.0016	0.9975	0.0001	0.0034	0.9971
313	0.0005	0.0017	0.9963	0.0002	0.0115	0.9931
323	0.001	0.0042	0.9712	0.0003	0.0214	0.9542
333	0.0015	0.0068	0.9929	0.0004	0.0278	0.9928
348	0.0021	0.0198	0.9648	0.0005	0.0571	0.9888

Table 11. Correlation coefficients of diffusion-controlled kinetics models at different temperatures for heavy REEs.

T, K	Diffusion 1-20 mins			Diffusion 20-120 mins		
	k	a	R^2	k	a	R^2
298	0.0002	0.0028	0.9593	0.00005	0.0049	0.9634
313	0.0004	0.0032	0.9943	0.00008	0.104	0.98
323	0.0005	0.0051	0.939	0.00009	0.0127	0.9704
333	0.0007	0.0068	0.9803	0.0002	0.016	0.9972
348	0.0008	0.013	0.941	0.0002	0.0251	0.9857

5.6. CONCLUSIONS

The Fire Clay coal is an excellent source for REE extraction due to its relatively elevated REE contents and high leaching recovery values. Leaching at a temperature of 75ºC using 1.2 M sulfuric acid resulted in over 75% of the total REEs in the coal being recovered within 2 hours and over 85% after 24 hours. The kinetic data obtained from leaching over a range of temperatures suggested that the leaching process follows the shrinking core model with a mixed control mechanism that may be a result of several

heterogenous materials leaching simultaneously. The activation energy determined from test data obtained over a range of temperatures using 1 M sulfuric acid was 36 kJ/mol for the first 20 minutes of reaction time and 27 kJ/mol for the leaching period between 20 and 120 minutes. Additional conclusions derived from the finding presented in this chapter include:

(1) Reducing the particle size of the middings material prior to de-carbonization results in the liberation of associated mineral matter that has significantly higher concentrations of REE. Decreasing the P80 particle size from 38 microns to 5 microns nearly doubled the concentration of REEs in the flotation tailings which was the material used for the leaching tests. The major minerals present in the sample were quartz, kaolinite, illite, and muscovite;

(2) Exponentially increasing the particle surface area through grinding elevated the consumption of hydrogen ions due to greater dissolution of contaminate metal ions;

(3) The type of inorganic acid does not affect leaching recovery significantly but has an impact on the initial leaching rate. The mixing condition is sufficient at above 500 rpm. The solid concentration and acid concentration have a significant effect on leaching recovery of REEs;

(4) Scanning Electron Microscope (SEM) images showed no visible product layer or any coating product on the particle surfaces. Therefore, the diffusion process in this reaction may be contributed by the interfacial transfer of the products and the reagent diffusion through the porous structure of solid particles;

(5) The leaching of light REEs during the initial stage is more of a chemical reaction, followed by a formation of a product layer. The energy required for later stage of

leaching reduced significantly. However, the major mechanism for leaching of heavy REEs is desorption and the product layer forming does not affect the heavy REEs significantly.

CHAPTER 6.SURFACE CHARACTERISTIC CHANGES DURING LEACHING

6.1. INTRODUCTION

A shrinking core model describes the leaching process where the initial solid particle shrinks in size and forms flaking ash layer and/or gaseous products with leaching time. The reaction occurs on the particle surface where the reactants and products transport between the solid particle surface and the bulk solution. The rate of the leaching process is relevant to either the reaction rate on the solid surface or the rate of transport (diffusion) whichever is the slowest. The diffusion rate depends on different mass transfer mechanisms in a solid-liquid reaction, such as film diffusion, pore diffusion, and product layer diffusion. Film diffusion usually occurs on a nonporous particle where surface reaction is fast. Pore diffusion is reaction controlling when the particle is porous and usually limits the reaction rate internally. Product layer diffusion occurs when there are flaking ash (precipitates) or metal oxides/hydroxides formation on the surface of the particles that limits the reaction.

In the coal tailing material, clays and quartz are the major minerals with minor minerals such as calcite, pyrite, and a minimal amount of micron-size RE minerals (phosphates). An analysis presented in Chapter 5 showed that the leaching process was mostly diffusion controlled which required approximately 20-40 kJ/mol of activation energy. In the current leaching system, the reacted particles are mostly porous, and the concentrations of Fe and Ca are generally dominating in the leachate solution. Thus, the pore diffusion and product layer diffusion mechanisms are taking place and controlling the leach rate. A series of surface characterization analyses were performed to investigate the phenomenon.

6.2. LEACHING BEHAVIOR OF MAJOR CONTAMINANTS

6.2.1. Effect of acid type

The leaching recovery and reaction rate of TREEs, Al, Fe, and Ca using different acid solutions are shown in Figure 38. The total REEs (TREEs) recovery of 75%, 73%, and 71% were achieved after 2 hours leaching using 1M of HCl, HNO$_3$, and H$_2$SO$_4$ solution, respectively. Hydrochloric acid solution provided the highest leaching recovery; however, nitric acid achieved the fastest leaching rate which resulted in 60% leaching recovery in one minute. The ending pH of the leachate solutions were 0.14, 0.21, and 0.13, respectively, using 1M of HCl, HNO$_3$, and H$_2$SO$_4$ solution after 2 hours. The major increase of pH while leaching using HNO$_3$ was due to the high dissolution rate of pyrite in HNO$_3$. The Fe recovery was 95% leaching in 1M HNO$_3$, whereas only about 25% Fe were recovered using 1M H$_2$SO$_4$ or 1M HCl under the same leaching conditions. Among all three types of inorganic acids, nitric acid has a strong oxidation feature due to its +5-valence state of N and its completely disassociated in water. The pyrite reaction with nitric acid can be very complicated and sensitive to temperature and concentrations. In a 70℃ temperature leaching system, the dominate reaction between pyrite and nitric acid is as follows: (Kadoğlu, Karaca, & Bayrakçeken, 1995)

$$6FeS_2 + 30HNO_3 \rightarrow 3Fe_2(SO_4)_3 + 3H_2SO_4 + 30NO + 12H_2O$$
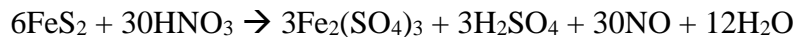
The XRD analyses on the samples before and after leaching using different acid types are shown in Figure 39. The pyrite peak completely disappeared after nitric acid leaching. The estimated mineral composition showed that the pyrite content was zero after nitric acid leaching, whereas the remaining pyrite content was 43% and 47% after leaching using sulfuric acid and hydrochloric acid, respectively. The leaching behavior of pyrite in this

material indicated that very limited REEs are associated with pyrite minerals in coal. Calcium recovery increased rapidly at the very beginning of the tests which agreed with the XRD results that calcite is the major source for Ca in this material.

The Al recovery was not very high in any of the three acids system which indicated that the dissolution of clays was not a major contribution to the REE recovery. The 1M HCl and H_2SO_4 systems both achieved about 7.4% Al recovery after 2 hours of leaching whereas Al recovery with 1M HNO_3 was 5.8%. This deduction was mostly due to the slightly higher ending pH of the nitric acid system which was 0.21. This finding indicated that Al recovery was very sensitive to the pH value.
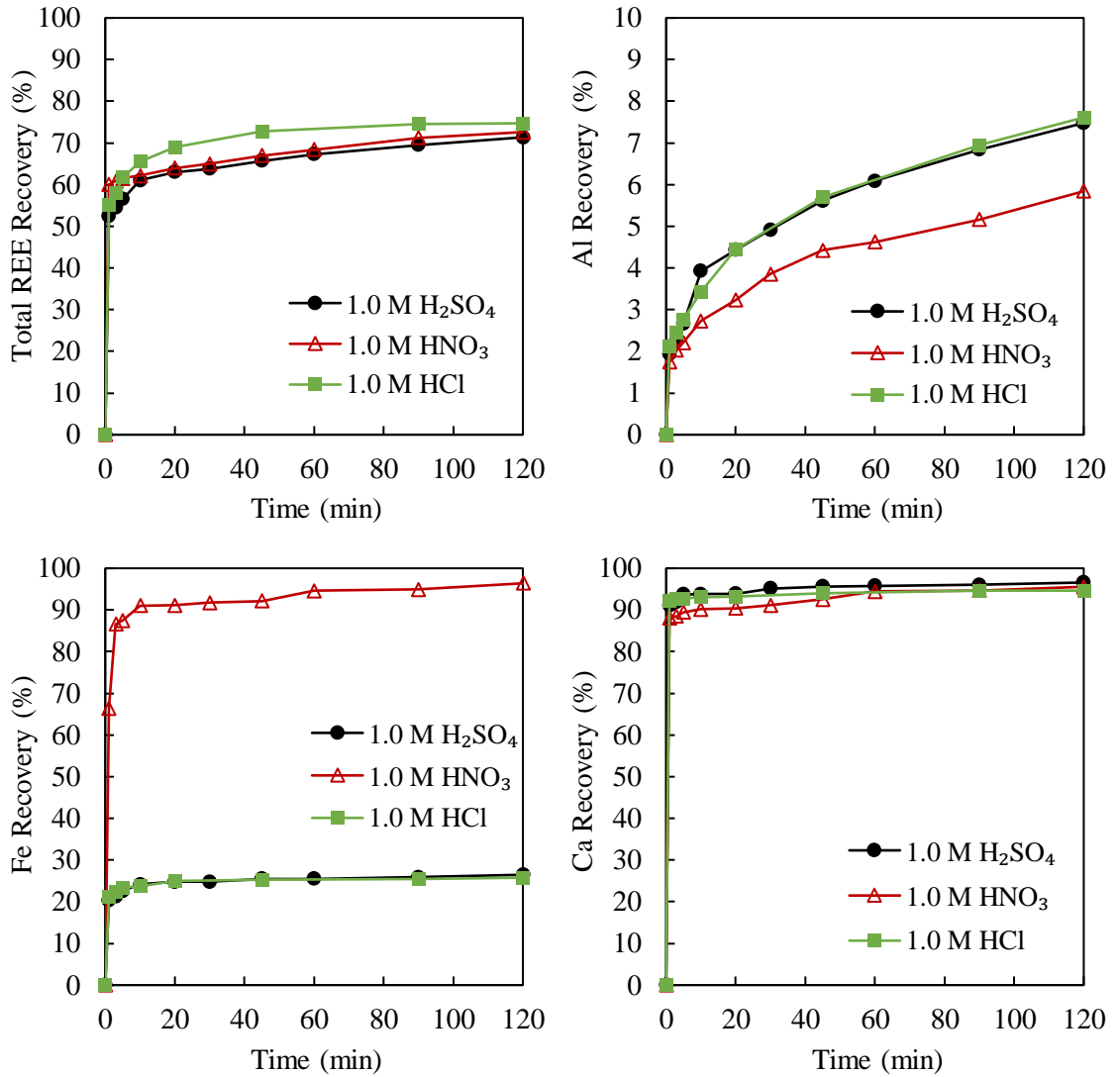
Figure 38. Effect of acid type on the leaching recovery of total rare earths from IL No. 6 coal material (75 ºC, 530 rpm, S/L=10g/L)
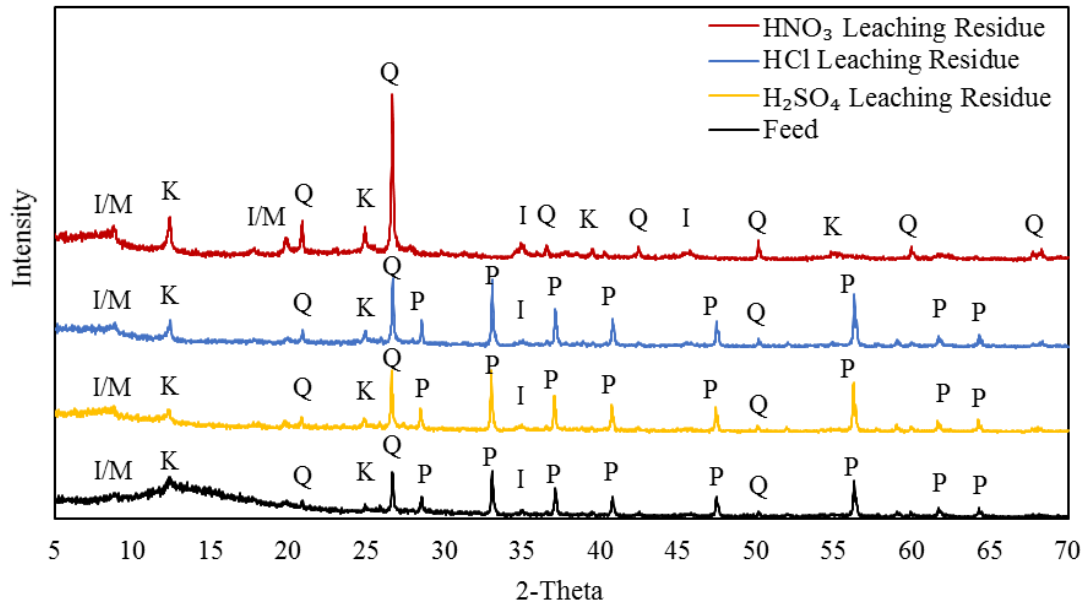
Figure 39. X-ray Diffraction analysis of the feed and solid residues after leaching using three different types of acids.

6.2.2. Effect of solid-to-liquid ratio

An increase in solid concentration was found to be having a significant negative effect on rare earth leaching recovery based on results presented in Chapter 5. The same trend was observed on this material while leaching with 1 M H_2SO_4 at temperature of 75℃ with 10 g/L, 100 g/L, and 200 g/L of solid-to-liquid ratios. The effect of solid-to-liquid ratio on REE and other elemental leaching recovery is shown in Figure 40. The association between reactants decreased with increasing the solid/liquid ratio which reduced the reaction rate. The REEs leaching recovery in 10 g/L, 100 g/L, and 200 g/L system were 71%, 59%, and 48%, respectively, after 2 hours of leaching. However, the reduction on leaching recovery due to the increased S/L ratio was not observed on Al and Fe leaching. The Al and Fe recovery of 7.4% and 25% were achieved regardless of the solid/liquid ratio in the system. Calcium recovery in 10 g/l and 100 g/L system was above 90%, however, in the high solid

concentration system, the Ca recovery only reached 80% recovery and slightly declined along the test. It was likely due to the high concentration of Ca and other anions in the leachate solution. The precipitation of Ca in acid leaching system was commonly seen in leaching processes (Bandara & Senanayake, 2015a; Seferinoglu et al., 2003; L. Wang et al., 2010).

Figure 40. Effect of solid to liquid ratio on the leaching recovery of (a) Total rare earths, (b) Aluminum, (c) Iron, and (d) Calcium. (75 ℃, 1 M H_2SO_4, 530 rpm)

6.2.3. Effect of acid concentration

The effect of sulfuric acid concentration on the leaching recovery of rare earths was studied using 0.1 M, 0.5 M, 1 M, and 2 M of initial acid concentration with keeping temperature, stirring speed, and solid to liquid ratio constant at 75°C, 530 rpm, and 10 g/L, respectively. The initial acid concentration of 0.1 M, 0.5 M, 1 M, and 2 M resulted in ending pH value of 1.13, 0.45, 0.14, and -0.23, respectively, after 2 hours of leaching. As shown in Figure 41, REEs recovery of 56%, 69%, 71%, and 74% were achieved after 2 hours leaching using 0.1 M, 0.5 M, 1 M, and 2 M of sulfuric acid, respectively. The concentration of acid did not play an important role on REEs leaching recovery when the pH was below 0.5. The Fe and Ca recovery showed very limited sensitivity on acid concentration since calcite dissolution can be completed at pH 4-5 and pyrite reaction with acid occurs at pH around 2 (Tessier et al., 1979). The acid concentration had a significant effect on Al recovery in the current leaching system. The Al recovery increased from 4.5%, 6.6%, 7.5%, to 8.7% while leaching using 0.1 M, 0.5 M, 1 M, and 2 M sulfuric acid. It indicated that a small portion of leachable REEs were associated with Al most likely in clay minerals as ion-substitution form, which would be extracted when the mineral dissolves.

106
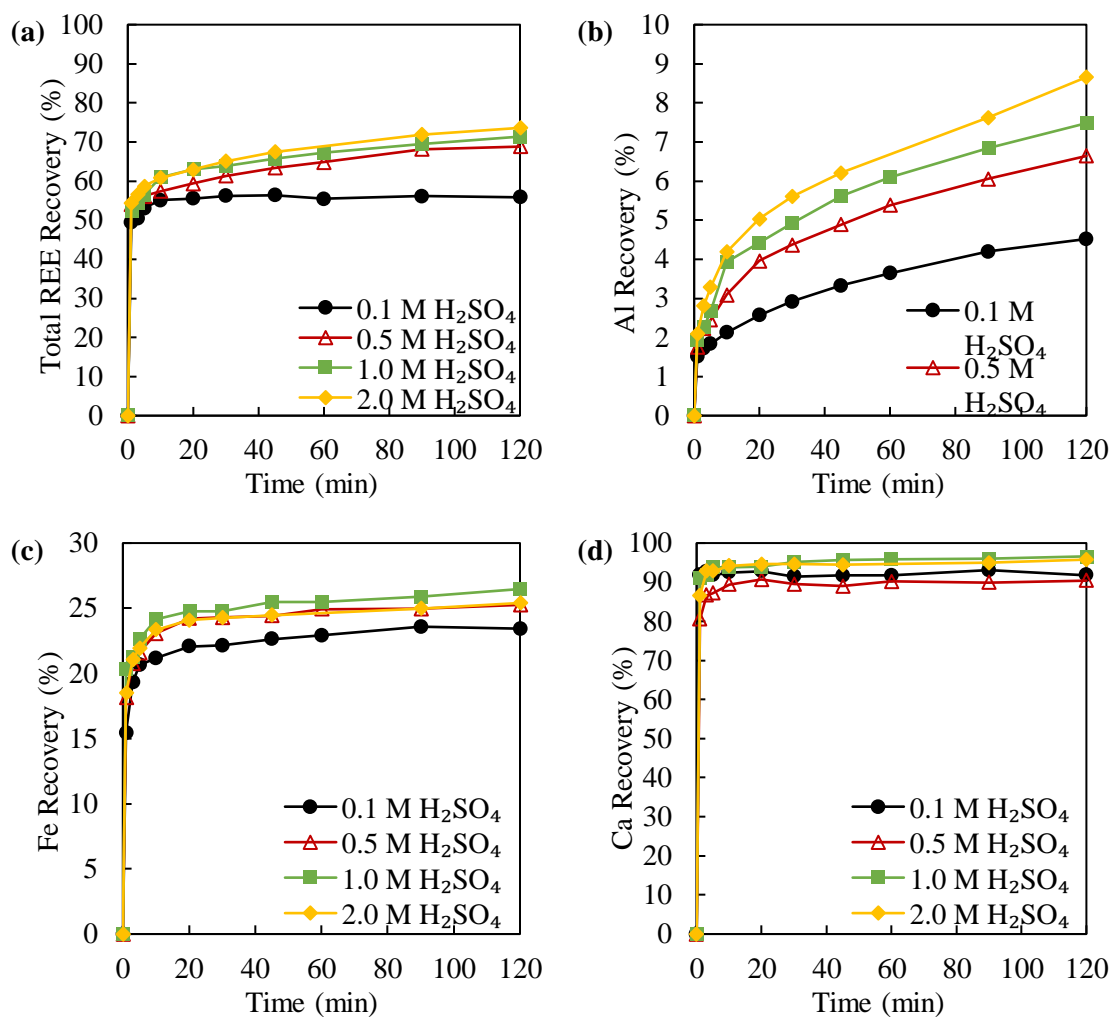
Figure 41. Effect of sulfuric acid solution concentration on the leaching recovery of (a) Total rare earths, (b) Aluminum, (c) Iron, and (d) Calcium. (75℃, 530 rpm, S/L=10g/L)

6.2.4. Effect of temperature

The effect of temperature on REEs leaching using 1 M H_2SO_4 was investigated with stirring speed of 530 rpm and the S/L of 10 g/L for 2 hours. The leaching recovery of REEs, Al, Fe, and Ca were displayed in Figure 42. The leaching recovery of REEs increased dramatically at the beginning of the reaction within one minute. At the first 10 minutes, the

temperature had almost no effect on the recovery of total REEs, which were 53%, 54%, 54%, 55%, and 58% leaching at temperature of 25°C, 40°C, 50°C, 60°C, and 75°C, respectively. From 10 minutes to 120 minutes of leaching, the recovery of REEs increased to be 56%, 59%, 62%, 65%, and 71% at temperature of 25°C, 40°C, 50°C, 60°C, and 75°C, respectively. For the elements recovery that were not very dependable on temperature, the activation energy is generally low and more likely to be diffusion controlled process (Free, 2013). The Al leaching recovery appeared to be sensitive to temperature all along the leaching process. The iron leaching recovery was slowly reaching the equilibrium after 30 minutes of leaching. At higher temperature, the equilibrium state was achieved faster than the lower temperature leaching. Calcium recovery was reaching 100% regardless of the temperature.

Using the method described in Section 5.5 in the previous chapter, the activation energy determined for the first 10 minutes leaching was 14.6 kJ/mol and 31.6 kJ/mol for the 10-120 minutes leaching, using diffusion model. It provides a direct evidence of different REE mode of occurrence present in different sources. The Illinois No.6 coal tailing contains more ion-adsorbed REEs than that of the Fire Clay coal source. It also shows an elevated energy requirement for the later stage of reaction which correlates well with the fact that the Illinois basin coal contains higher level of contaminations.
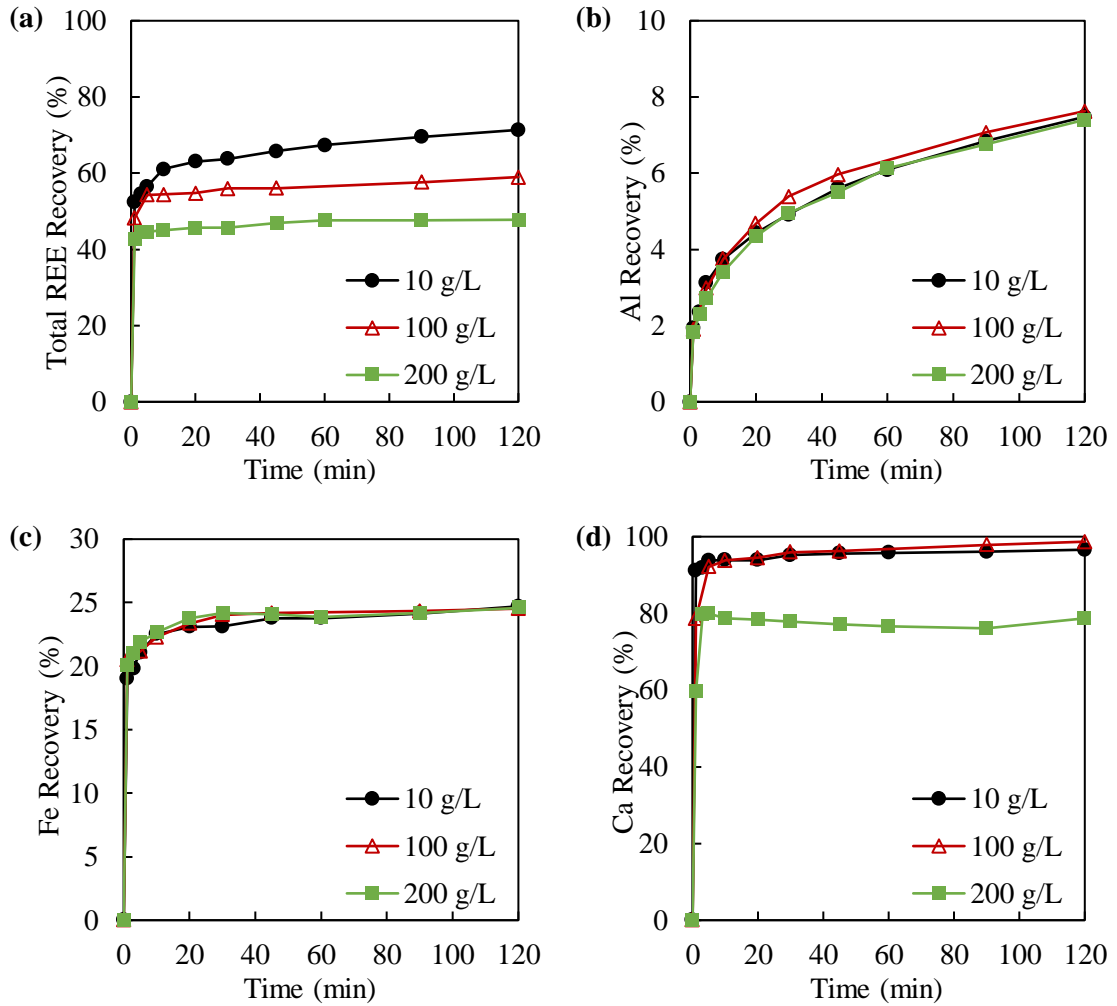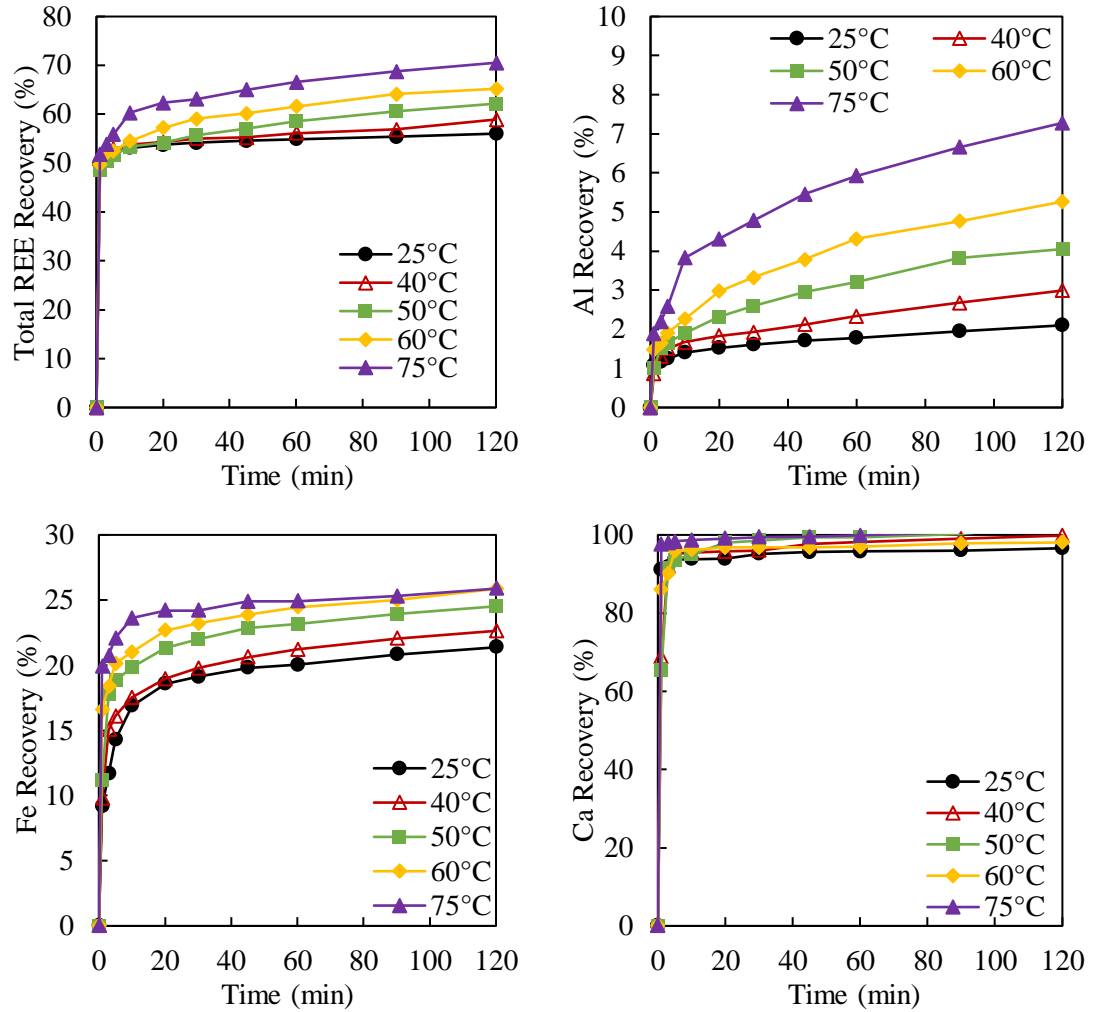
Figure 42. Effect of leaching reaction temperature on the leaching recovery of (a) Total rare earths, (b) Aluminum, (c) Iron, and (d) Calcium. (1 M H_2SO_4, 530 rpm, S/L=10g/L)

6.3. SURFACE AREA AND PORE DISTRIBUTION ANALYSIS

Leaching results showed that, with higher solid concentrations, leaching efficiency reduces even with an excessive amount of lixiviant as shown in Table 10. At a low solid concentration of 20 g/L, leaching recovery reached 16.3% after 5 hours. However, with 200 g/L solid concentration, the leaching recovery was 11.5% after 5 hours leaching. The BET analyses were performed to confirm the pore access change during leaching.

The results from surface area and pore distribution analyses on the leached samples under varying conditions are plotted in Figure 43 and summarized in Figure 44. The pore size of minerals are usually classified into three categories: micropores (< 2 nm), mesopores (2nm~50 nm), and macropores (>50 nm) (Zdravkov, Čermák, Šefara, & Janků, 2007). Figure 43 (a) shows that the pore size of the feed material was mainly 50 nm (500 Å) and above; thus, the pores can be classified as mostly mesopores and macropores. The surface area of the particles increased from about 21 m²/g to an average of about 32 m²/g after 5 hours of leaching at a solids concentration of 10 g/L. The surface area increased rapidly at the beginning then stabilized throughout the test which indicated that the reaction was rapid at the beginning and gradually slowed thereafter which was similar to the leaching kinetics. The leaching efficiency results in Table 12 indicate 11% of the TREEs were leached during the first 30 minutes then slowly increased to 16% after 5 hours. These findings implied that the accessible surface area played an important role in the initial stage. However, at the end of the test, the surface area did not vary significantly among tests with different solid concentrations.

The increased surface area also created more adsorption capabilities that should have positively impacted the leaching process and potentially allow selective adsorption of anions from the bulk solution onto the particle surface. In many applications, acid-activated clays were generally used as a bleach (adsorbent) to decolorize waste water in dying process (Komadel & Madejová, 2013; San Cristóbal, Castelló, Martín Luengo, & Vizcayno, 2009). The swelling type of clay has more potential of being activated such as smectite and bentonite, whereas kaolinite can only be slightly activated by acid treatment. The acid-

activated sample has higher capacity for cation exchange on the clay surface due to the change in Al coordination (San Cristóbal et al., 2009).

Table 12. Leaching efficiency of total REEs with different solid concentrations.

Test #	Time (min)	Solid Concentration	Lixiviate	Ending pH	TREEs Recovery (%)
1	30	200 g/L	1.6M H_2SO_4	0.03	7.71
	180				10.28
	300				11.50
2	30	100 g/L	1.4M H_2SO_4	0.04	8.32
	180				11.17
	300				13.21
3	30	50 g/L	1.3M H_2SO_4	0.02	9.70
	180				13.09
	300				14.45
4	30	20 g/L	1.2M H_2SO_4	0.08	10.84
	180				15.13
	300				16.33

The cumulative pore volume increased with retention time which indicated that the material porosity increased as shown in Figure 43 (d). Leaching with low solid concentration resulted in higher porosity compared to the that of the high solid concentration leaching on a per sample mass basis. While leaching with 20g/L of solids, the pore volume increased from about 0.04 cm³/g to about 0.065 cm³/g after 5 hours, which was more than a 50% increase. However, while leaching with 200 g/L solids, the pore volume only increased to 0.05 cm³/g. When leaching with 200 g/L of solid, there were 1400 ppm of Fe, 700 ppm of Ca, and 1000 ppm of Al in the leachate solution at the end of 5 hours leaching. A possible explanation is that, at the particle surface and in the inner pores, localized areas of high pH values can occur due to the dissolution of micro dispersed minerals such as calcite which consumes hydrogen ions. The dissolved Fe and Ca ions

form precipitates which block the pore access and creat a boundary to prevent further reactions with the lixiviants. This hypothesis may explain why the average pore size changed differently with leaching time for the solid concentrations evaluated. At low solid concentrations, the pore size increased with leaching time as shown in Figure 43 (c) due to the lower bulk concentrations of the metal ions and the pH shift to higher values was minimal. When treating high solid concentration solutions, the average pore size decreased with leaching time and the solution pH increase with time was significant. At a solid concentration of 200 g/L, pore size decreased slightly from 98 Å (9.8 nm) to about 83 Å (8.3 nm). Figure 45 shows the pore distribution shifts after leaching at varies solid concentrations which indicated that more macropores were generated during leaching, but the effect of pore blockage became more severe with an increase in solid concentration.
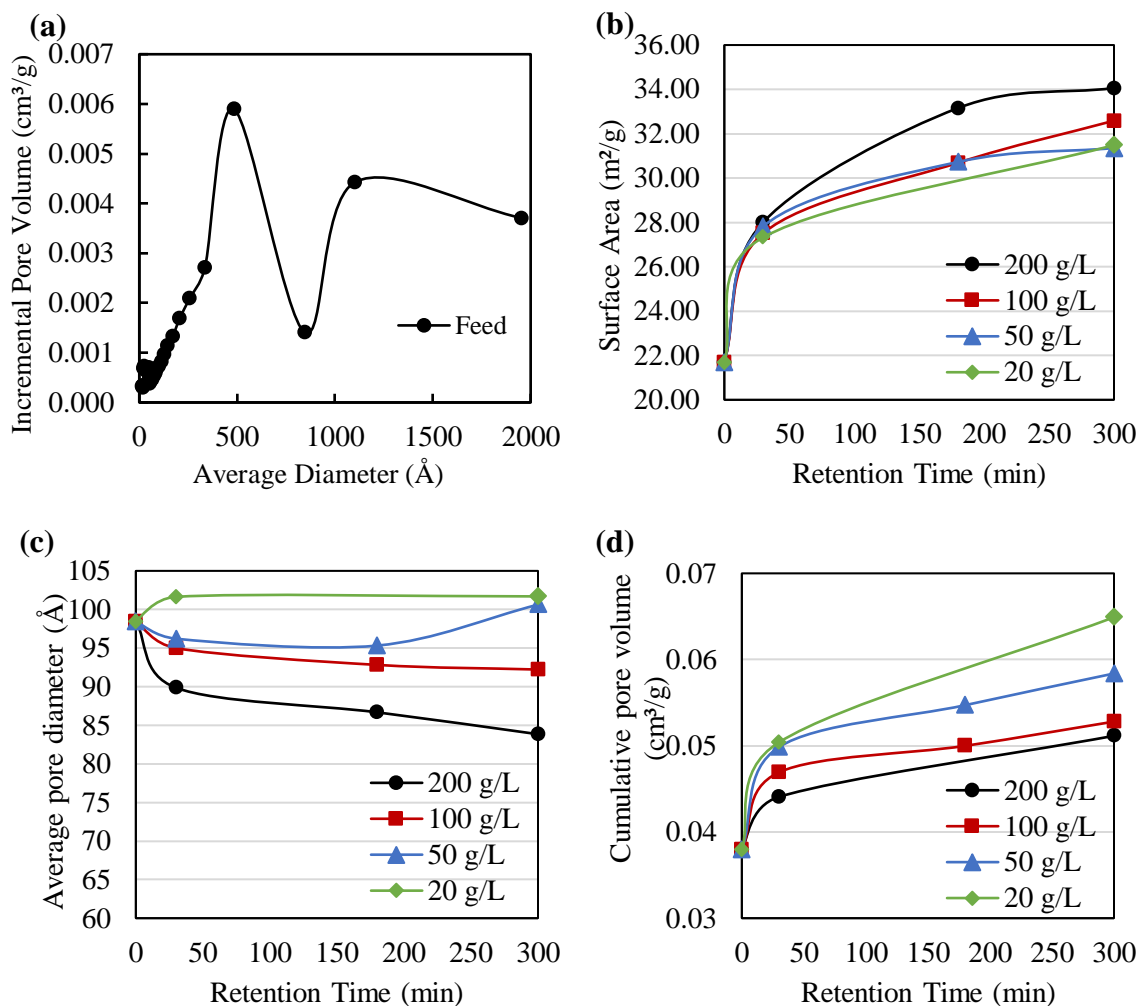
Figure 43. (a) Pore types in feed. (b) Surface area change during leaching; (c) Pore size change during leaching; (d) Pore volume change during leaching.
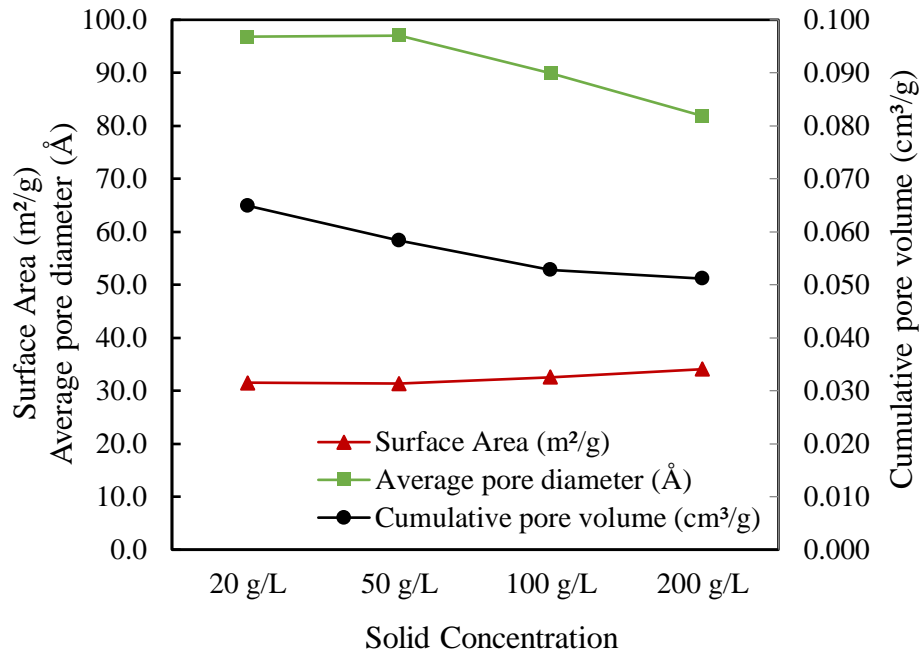
Figure 44. The effect of solid concentration on particle surface area, average pore size, and cumulative pore volume after 5 hours of leaching.
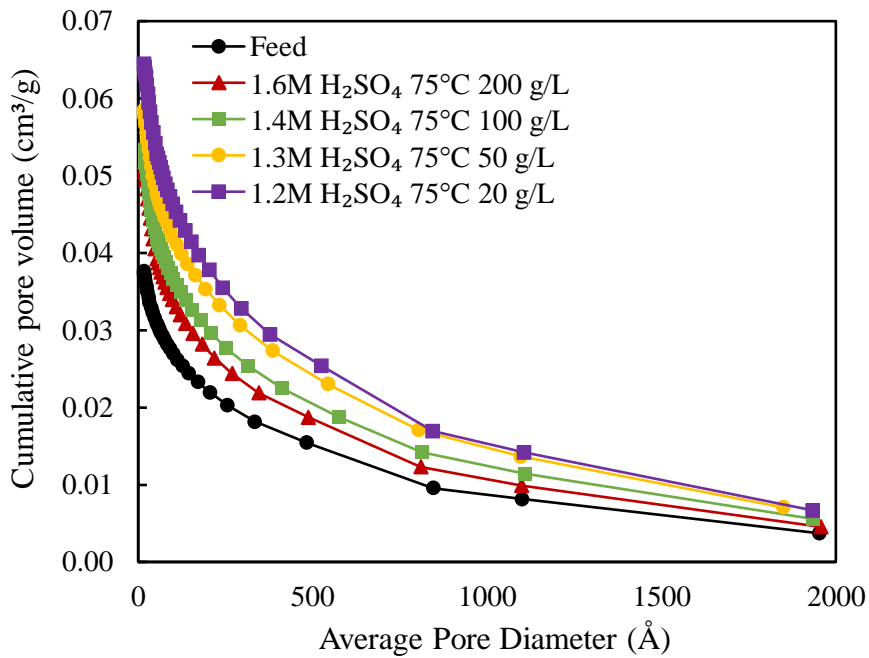
Figure 45. Pore size distribution before and after five hours leaching over a range of solid concentrations.

6.4. INVESTIGATION ON PRODUCT LAYER FORMATION

To investigate the product layer diffusion in the leaching process, a set of tests were performed on the prepared material and analyzed for surface characteristic changes before and after leaching. Leaching tests were conducted in a heated water bath that was maintaining a 75 °C temperature. The test lasted for five hours and the final solid sample was filtered on a vacuum filter and washed thoroughly with deionized water. The solid residue sample was dried at a low temperature in an oven. The solid and leachate sample was subjected to elemental analysis using ICP-OES by the Kentucky Geological Survey located at the University of Kentucky. As shown in Table 13, leaching conditions were varied to examine the effect of solid concentration and inorganic acid types. The feed sample and the solid residue samples were submitted for XPS analysis to obtain the knowledge of the state change in the elements at the solid surface.

Table 13. Leaching conditions and corresponding leaching recoveries of REEs and major metal elements.

Test #	Acid Type	Acid Concentration	Solid Concentration	Solid Loss (%)	Ending pH	Leaching Recovery At 5 hours (%)			
						TREE	Al	Ca	Fe
1	H_2SO_4	1 M	10 g/L	20.8	0.15	71.4	7.5	96.6	24.7
2	H_2SO_4	1 M	100 g/L	20.0	0.26	59.0	7.2	98.6	24.5
3	H_2SO_4	1 M	200 g/L	18.1	0.28	47.8	7.4	78.7	24.6
4	HCl	1 M	10 g/L	21.9	0.18	74.7	7.6	94.9	25.8
5	HNO_3	1 M	10 g/L	43.1	0.21	72.6	5.8	95.6	96.4

The XPS full spectra detected the presence of the following elements as shown in Figure 46: Mg, C, O, Fe, F, Ca, N, K, S, and Al. The O1s was overwhelmed by lattice oxygen in the clay, so oxygen in possible metal hydroxides or oxides could not be observed.

There was a noticeable chemical state change of iron as shown in Figure 47, where Fe2p3/2 peak at 707eV binding energy is Fe metal and the peak at 712eV could be multiple compounds such as FeOOH, FeSO$_4$, and Fe$_2$O$_3$. To provide further distinction, solution chemistry analyses were performed. Calcium (Ca) was mostly absent in the solid residue after leaching with the exception of the residues from the high solid concentration (200 g/L) test as shown in Figure 48. This finding indicated that calcium precipitates may be forming during the leaching process when treating elevated solid concentrations (e.g., gypsum). It should be noted that gypsum is relatively insoluble in a sulfuric acid solution.
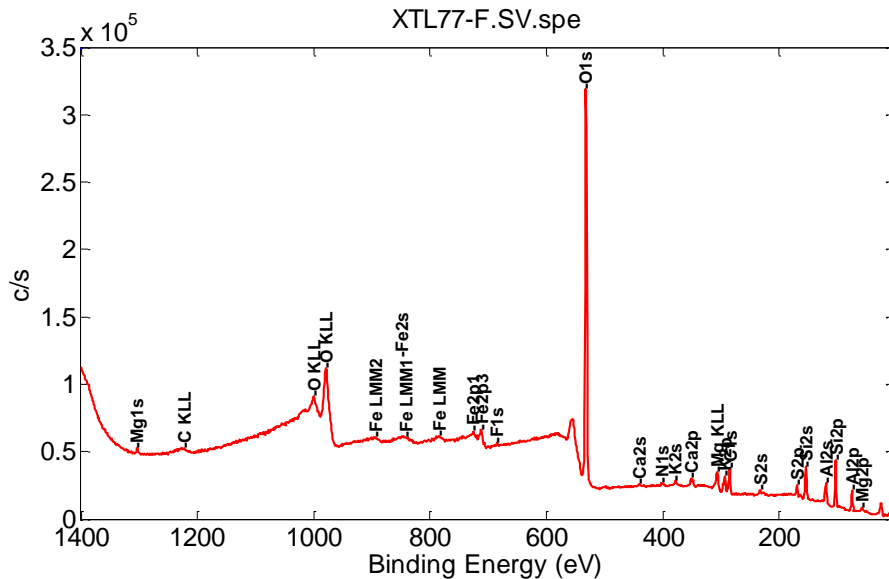
Figure 46. Full XPS spectra of the feed sample indicating major elements on the solid surface.

The reason for the difference in the Fe state in the sulfuric and nitric acid systems may be the varying levels of pyrite oxidation. The leaching reaction of pyrite with nitric acid in an aqueous environment can be described as:

$$FeS_2 + 5HNO_3 + 4H^+ = Fe^{3+} + 2SO_4^{2-} + 5NO(g) + 2H_2O.$$
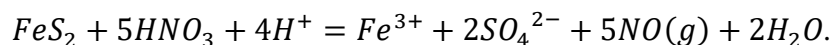
This reaction shows a natural production of the ferric (Fe^{3+}) ions in solution when using nitric acid. However, the reaction associated with pyrite in a sulfuric acid solution favors the generation of ferrous (Fe^{2+}) ions in solution. It should be noted that solutions that are aerated by mixing or other means will result in an oxidizing environment where Fe^{2+} is converted to Fe^{3+}.

In the nitric acid system, while increasing the solution pH, ferric ion hydrolysis will occur to form iron oxyhydroxide coatings on the particle surfaces. The coating acts as a product ash layer that reduces the exposure of the particle surface to the bulk solution. According to Huminicki and Rimstidt (2009), the formation of this product layer occurs in two stages: 1) The hydrolysis of Fe^{3+} forms iron hydroxide colloidal particles in the leachate solution which initiates the formation of a thin, porous layer (ash layer) on the solid surfaces; and 2) With the colloidal particle built up on the particle surfaces, the layer becomes thicker and less porous. A more structurally stable form of iron hydroxide such goethite (FeOOH) forms due to the presence of Fe^{3+} in solution. (Huminicki & Rimstidt, 2009)

However, pyrite reaction with sulfuric acid is less effective than that of nitric acid due to the generation of SO_4^{2-} in the solution. Considering that the redox potential change involved in ferric and ferrous systems, the Eh-pH diagram was generated for both nitric acid and sulfuric acid leaching systems with the actual concentrations of major elements in the coal-derived leachate solutions using a commercial software known as HSC Chemistry developed by Outotec. The input parameters and information are listed in Table 14. As shown in Figure 49 and Figure 50, the form of iron products in the sulfuric leaching system

is more complicated than that of the nitric acid leaching system. At a pH value of 0.15 and redox potential of 300~600 mV, the Eh-pH diagram when using a H_2SO_4 solution indicates the existence of $(H_3O)Fe(SO_4)_2(H_2O)_3$, which is a solid phase material that forms around the pyrite particles. This finding may explain why the Fe recovery was only about 25% in the sulfuric leaching system.
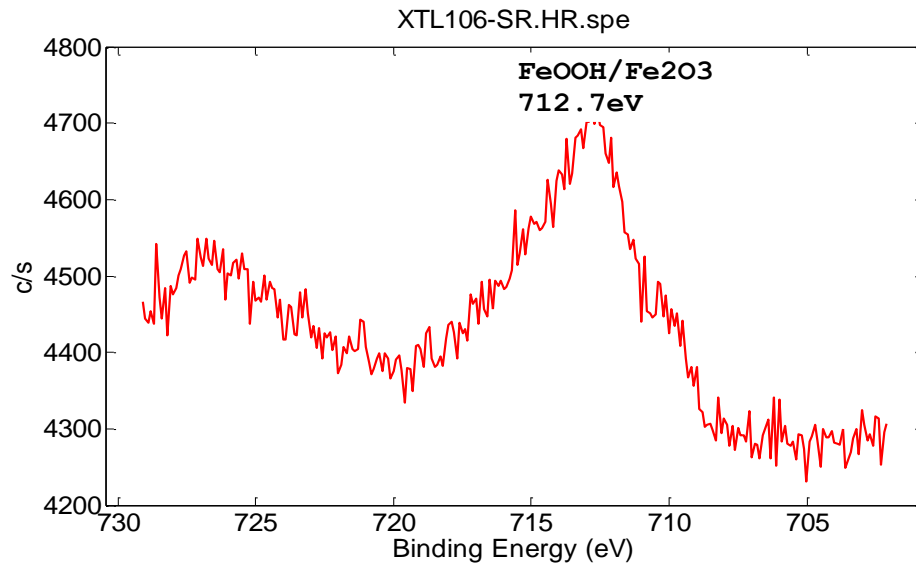
Figure 47. Fe state change on the particle surface after 5 hours leaching (1M HNO_3, 10 g/L solids, 75℃).
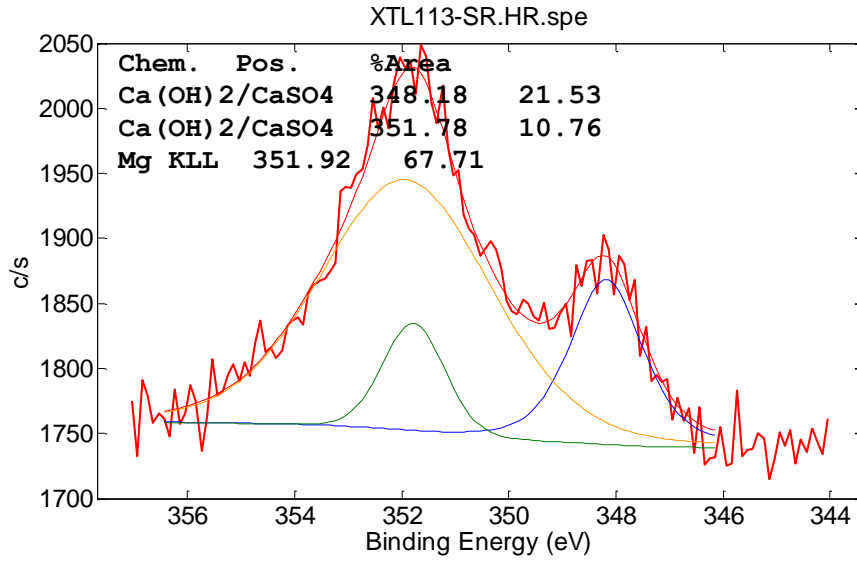
Figure 48. Ca state change on the particle surface after 5 hours leaching (1M H_2SO_4, 200 g/L solids, 75℃).

Table 14. The input elemental concentration in HSC Chemistry software (Temperature of 75℃).

Test #	Acid Type	Acid Concentration	Solid Concentration	Ending pH	Concentration (M)		
					Fe	Al	Ca
1	H_2SO_4	1 M	10 g/L	0.15	7.14E-06	1.73E-06	4.10E-06
5	HNO_3	1 M	10 g/L	0.21	2.50E-05	1.36E-06	4.03E-06
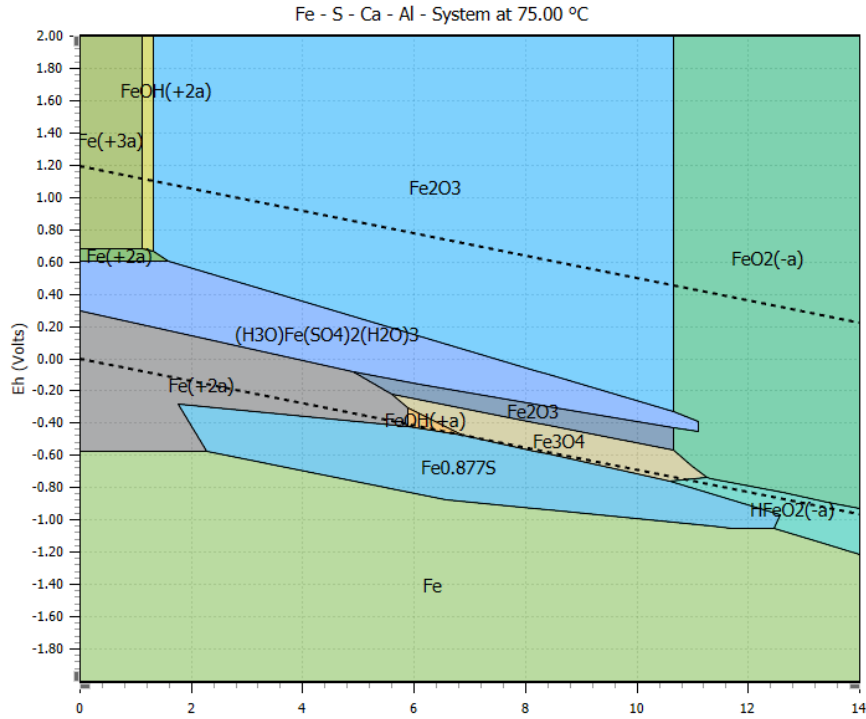
Figure 49. Eh-pH diagram of Fe in the system leaching with 1M H_2SO_4 and 10 g/L solid concentration at 75 ℃.
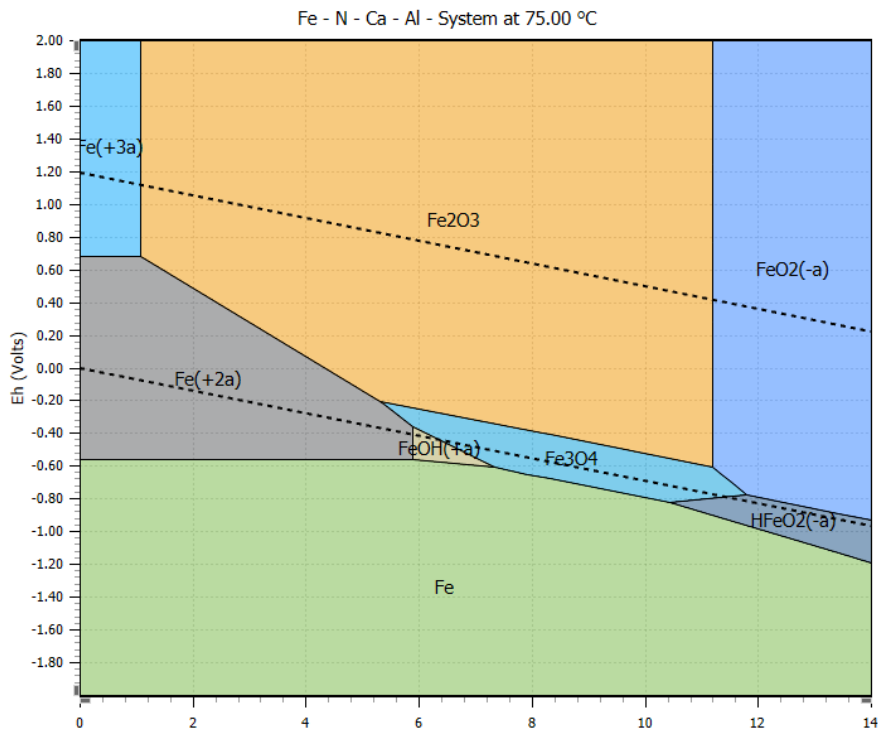
Figure 50. Eh-pH diagram of Fe in the system leaching with 1M HNO_3 and 10 g/L solid concentration at 75 ℃.

120

REEs are known to co-precipitate with the gypsum formation during the leaching process due to their similarity to the Ca ionic radii (Bandara & Senanayake, 2015b; Brahim et al., 2008; Dutrizac, 2017; L. Wang et al., 2010). In the current leaching system, the major Ca source was from calcite minerals that easily dissolve during leaching with 1M sulfuric acid. When leaching using a lower solid concentration, Ca recovery was close to 100% which indicated that no Ca was remaining in the solid. However, when the solid concentration increased to 200 g/L, the Ca recovery reached 99% at the beginning and then dropped to about 78%. The hypothesis is that the localized pH increases occurred at the particle surface and the inner pores during the leaching process which resulted in gypsum formation.

The rare earth ions are structurally incorporated in gypsum by replacing three Ca^{2+} ions with two trivalent rare earth ions and leaving a Ca^{2+} lattice. The findings of a study reported by Dutrizac (2017) indicate that the light REEs were more likely to co-precipitate with $CaSO_4$ compared to heavy REEs which was also observed in the current leaching system. From our experiments, the heavy REE recovery values at solid concentrations of 10 g/L, 100 g/L, and 200 g/L were 79%, 79%, and 76%, respectively, whereas the light REE recovery for 10 g/L, 100 g/L, and 200 g/L solid concentration were 68%, 53%, and 39%, respectively.

The XPS results showed a formation of either $Ca(OH)_2$ or $CaSO_4$, or a combination of both. The solution chemistry was further studied to identify the precipitation species using the software MINTEQ. The input information and parameters are listed in Table 15, where the major elements in solution were calculated based on the real leachate solution analysis. Figure 49 shows that the iron in the sulfuric leaching environment mainly exists as Fe^{2+}.

121

The concentration of SO_4^{2-} was assumed to be 1M since it was the initial concentration of acid and the molarity is much higher compare to other species.

The major species of the real leachate system and their corresponding concentrations and/or activities are listed in Table 16. The ionic strength calculated for this system is 0.82 M which is acceptable to validate the calculations. The major form of existence of Al, Ca, and Fe in the leachate solution was $Al(SO_4)_2^-$, Ca^{2+}, and Fe^{2+}, respectively. The formation of insoluble $Ca(OH)_2$ or $CaSO_4$ precipitation can be described as: (R. Kim et al., 2016)

$$Ca^{2+} + 2OH^- = Ca(OH)_2 , K_{s1} \tag{2}$$

$$Ca^{2+} + SO_4^{2-} = CaSO_{4(s)} , K_{s2} \tag{3}$$
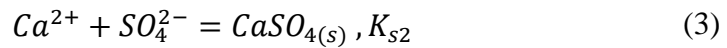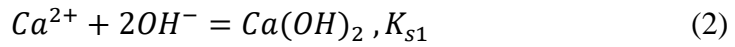
Using the calculated activities listed in Table 14, the solubility coefficients can be calculated for $Ca(OH)_2$ or $CaSO_4$ as shown below:

$$K_{s1} = [Ca^{2+}][OH^-]^2 = 3.8 \times 10^{-30} \tag{4}$$

$$K_{s2} = [Ca^{2+}][SO_4^{2-}] = 5.6 \times 10^{-8} \tag{5}$$

These solubility coefficient values indicate that $CaSO_4$ is the major calcium precipitate when using a sulfuric acid solution as the lixiviate.

Table 15. Input values and parameters in MINTEQ to estimate species and corresponding activities in the real leachate solution.

Input information	Value
pH	0.28
Temperature	75 °C
Ca^{2+}	7.00E-05 M
Fe^{2+}	0.0001 M
Al^{3+}	3.60E-05 M
SO_4^{2-}	1 M

Table 16. Estimation of species in leachate solution leaching with 1M sulfuric acid at 200 g/L, 75℃. (Calculated by MINTEQ). Ionic strength = 0.82.

Species	Concentration (M)	Activity (M)	Log activity
$Al(OH)_2^+$	8.3E-14	6.2E-14	-1.3E+01
$Al(OH)_{3\ (aq)}$	8.5E-19	1.0E-18	-1.8E+01
$Al(OH)_4^-$	1.9E-24	1.4E-24	-2.4E+01
$Al(SO_4)_2^-$	1.8E-05	1.4E-05	-4.9E+00
Al^{3+}	3.9E-06	2.9E-07	-6.5E+00
$Al_2(OH)_2^{4+}$	4.6E-17	4.5E-19	-1.8E+01
$Al_3(OH)_4^{5+}$	1.8E-26	1.3E-29	-2.9E+01
$AlOH^{2+}$	2.8E-10	8.8E-11	-1.0E+01
$AlSO^{4+}$	1.4E-05	1.0E-05	-5.0E+00
Ca^{2+}	5.4E-05	1.7E-05	-4.8E+00
$CaOH^+$	3.5E-16	2.6E-16	-1.6E+01
$CaSO_{4\ (aq)}$	1.6E-05	1.9E-05	-4.7E+00
$Fe(OH)_{2\ (aq)}$	2.2E-22	2.7E-22	-2.2E+01
$Fe(OH)_3^-$	3.1E-32	2.4E-32	-3.2E+01
Fe^{2+}	7.5E-05	2.4E-05	-4.6E+00
$FeOH^+$	6.0E-13	4.5E-13	-1.2E+01
$FeSO_{4\ (aq)}$	2.5E-05	3.0E-05	-4.5E+00
H^+	7.0E-01	5.2E-01	-2.8E-01
HSO_4^-	9.9E-01	7.4E-01	-1.3E-01
OH^-	6.3E-13	4.7E-13	-1.2E+01
SO_4^{2-}	1.0E-02	3.2E-03	-2.5E+00

6.5. CONCLUSIONS

The previous chapter presented evidence that the leaching of REEs from coal sources was mostly controlled by product layer diffusion. In this chapter, the elemental analyses showed that Fe and Ca were major contaminations in the leachate solution which potentially form precipitates due to localized pH and Eh variations on or near the particle surfaces during leaching reaction. Evidence suggests that the reaction products formed on the solid-liquid interface caused pore blockage as well as a barrier between the reactants and bulk solution. Additional conclusions include:

(1) The particle surface area increased rapidly at the beginning of the leaching process and then stabilized throughout the test which was a reflection of the rapid leaching reaction within the first several minutes which ultimately slowed after a given reaction time.

(2) The increased surface area created more adsorption capabilities that positively impacted the leaching process and potentially allowed selective adsorption of anions from the bulk solution onto the particle surface.

(3) Additional macropores were generated during leaching, but the effect of pore blockage became more severe with an increase in solid concentration. At low solid concentrations, the pore size increased with leaching time due to the lower bulk concentrations of the metal ions and the reduced pH shift to higher values. When treating high solid concentration solutions, the average pore size decreased with leaching time which corresponded to a larger upward shift in pH values.

(4) The hydrolysis of Fe^{3+} forms iron hydroxide colloidal particles in the leachate solution, near the particle surfaces and within the pores which initiates the formation of a thin, porous layer on the solid surfaces. The colloidal particle build up on the particle surfaces creates a thicker solid that is less porous.

(5) Localized pH increases caused by the dissolution of calcite, for example, may have occurred at the particle surfaces and the inner pores during the leaching process which may have caused gypsum formation. The light REEs appear to be more likely to co-precipitate with $CaSO_4$ compared to heavy REEs as observed in the current leaching system.

(6) XPS results supported the hypothesis of the formation of either $Ca(OH)_2$ or $CaSO_4$, or a combination of both on the solid surfaces. Solution chemistry was further studied to

124

identify the precipitation species using a software package commercially known as MINTEQ. The solubility coefficient values indicated that $CaSO_4$ was likely the major calcium precipitate when using a sulfuric acid solution as the lixiviate.

CHAPTER 7. SUMMARY AND CONCLUSIONS

REEs associated with different compositions in heterogeneous coal material shared different leaching characteristic which proved that there are different REEs mode of occurrence. The kinetic data obtained from leaching over a range of temperatures suggested that the leaching process follows the shrinking core model with a mixed control mechanism that may be a result of several heterogenous materials leaching simultaneously. The activation energy determined from experimental data suggested that leaching of REEs from coal sources were mostly controlled by product layer diffusion. The elemental analyses showed that Fe and Ca are major contaminations in the leachate solution which have potential to form precipitates due to the local pH and Eh variations on the particle surface during leaching reaction. The reaction products formed on the solid-liquid interface caused blockage of pores as well as a barrier between the reactants and bulk solution. The detailed findings of the present research dissertation were listed as follows:

(1) Most of the REEs are concentrated in the inorganic fractions in bituminous coal. The total REE concentration on an ash basis of low ash fractions was significant higher compare to high ash fractions due to the dilution effect of carbon content. With physical liberations of carbon content and inorganic material, the REEs are concentration in the inorganic minerals. The smaller size of particles liberated from coal material contains higher concentration of REEs, which indicated that a portion of the REEs are finely disseminated in coal structure.

(2) Thermal activation by roasting or chemical activation pretreatment provided a significant increase on the light REEs recovery which indicated the conversion of

the RE minerals to a soluble rare earth metal hydroxide form, whereas the heavy REEs are more likely existing as ionic form adsorbed onto clay surfaces.

(3) The particle size of coal before decarbonization affects the liberation of carbon and other inorganic material. The major minerals present in the sample were quartz, kaolinite, illite, and muscovite. Size reduction escalates the consumption of hydrogen ions by dissolving more contaminate metal ions.

(4) The type of inorganic acid does not affect the leaching recovery significantly but has an impact on the initial leaching rate. The mixing condition is sufficient at above 500 rpm. The solid concentration and acid concentration have a significant effect on leaching recovery of REEs.

(5) The SEM images showed no visible product layer or any coating product on particle surface. Therefore, the diffusion process in this reaction may be contributed by the interfacial transfer of the products and the reagent diffusion through the porous structure of solid particles.

(6) The light REEs leaching at the initial stage is more of a chemical reaction, and then, with the product layer formation, the energy required for later stage of leaching reduced significantly. However, the major mechanism for heavy REEs leaching is desorption, and the product layer forming does not affect the heavy REEs significantly.

(7) The surface area increased rapidly at the beginning then stabilized throughout the test which indicated that the leaching reaction was rapid at the beginning and gradually slowed thereafter.

(8) The increased surface area created more adsorption capabilities that positively impacted the leaching process and potentially allow selective adsorption of anions from the bulk solution onto the particle surface. At low solid concentrations, the pore size increased with leaching time due to the lower bulk concentrations of the metal ions and the pH shift to higher values was minimal. When treating high solid concentration solutions, the average pore size decreased with leaching time which indicates the pore blockage at high solid concentration.

(9) The hydrolysis of Fe^{3+} forms iron hydroxide colloidal particles in the leachate solution which initiates the formation of a thin, porous layer (ash layer) on the solid surfaces. With the colloidal particle built up on the particle surfaces, the layer becomes thicker and less porous.

(10) The localized pH increases occurred at the particle surface and the inner pores during the leaching process which resulted in gypsum formation. the light REEs were more likely to co-precipitate with $CaSO_4$ compared to heavy REEs which was also observed in the current leaching system.

(11) The XPS results showed a formation of either $Ca(OH)_2$ or $CaSO_4$, or a combination of both. The solution chemistry was further studied to identify the precipitation species using the software MINTEQ. The solubility coefficient values indicate that $CaSO_4$ is the major calcium precipitate when using a sulfuric acid solution as the lixiviate.

CHAPTER 8. RECOMMENDATIONS FOR FUTURE STUDY

The current study investigated the leaching process of REEs from pre-combustion bituminous coal sources. However, coal tailings are a heterogenous material that contains various modes of occurrence of the REEs. Additional efforts should be devoted to identify the mineral associations of REEs in coal, quantitative analysis of the REE mode of occurrence, and the associated leaching characteristics of different modes. Suggestions for future studies are provided as follows:

(1) The mineral associations of REEs were studied by extracting REEs using different types of lixiviants under various pH conditions. However, a quantitative procedure should be developed to sequentially extract REEs associated with each type of mineral present in coal refuse systems to fully understand the element by element association of REE.

(2) By identifying the mineral association of REE in coal refuse system, studies ought to be addressed on the leaching performance of individual type of association and identify the energy required to recover the REEs associated in various minerals. Surface characterization analysis ought to be performed on the individual minerals to understand the change of properties and the corresponding effect on leaching process.

(3) Considering the high concentration of pyrite existing in some of the coal sources, the potential of natural acid generation through pyrite oxidation should be further studied. The concept leads to a heap leach process of the coarse refuse stream that could be self-sufficient and maximize the REE recovery without additional acid consumption.

(4) For the purpose of designing a flowsheet, the economic value of individual REE need to be considered and systematically evaluated. The heavy REEs contain higher market values and can be extracted at milder conditions. A selective leaching process is more promising with extracting the heavy REEs priory to the light REEs. An economic feasibility analysis ought to be carried out with considering the chemical expenses on extracting different levels of REEs concentrations.

(5) Investigation on system scale up is needed for designing and operational purpose, especially on the mixing condition energy anticipation. Lab scale test showed that 500 rpm is required to eliminate the mixing condition effect, however, the corresponding shear rate needs to be determined.

(6) The REEs in coal sources is low in concentration, however, potential exists for significantly upgrading the content through particle size reduction and liberation followed by a physical concentration step. However, excessive size reduction creates difficulties on physical separation of REEs and carbon content. Efforts should be devoted to a feasible separation process for REE pre-concentration.

REFERENCES

Adolphi, P., & Stör, M. (1985). Glow discharge excited low temperature ashing. A new technique for separating mineral matter of coals. *Fuel*, *64*(2), 151–155.

Al-Nafai, I. S. (2015). Application of Pourbaix Diagrams in the Hydrometallurgical Processing of Bastnasite, (May). Retrieved from

Arbuzov, S. I., Maslov, S. G., Finkelman, R. B., Mezhibor, A. M., Ilenok, S. S., Blokhin, M. G., & Peregudina, E. V. (2018). Modes of occurrence of rare earth elements in peat from Western Siberia. *Journal of Geochemical Exploration*, *184*(February 2017), 40–48.

Bandara, A. M. T. S., & Senanayake, G. (2015a). Leachability of rare-earth, calcium and minor metal ions from natural Fluorapatite in perchloric, hydrochloric, nitric and phosphoric acid solutions: Effect of proton activity and anion participation. *Hydrometallurgy*, *153*, 179–189.

Bandara, A. M. T. S., & Senanayake, G. (2015b). Leachability of rare-earth, calcium and minor metal ions from natural Fluorapatite in perchloric, hydrochloric, nitric and phosphoric acid solutions: Effect of proton activity and anion participation. *Hydrometallurgy*, *153*(2015), 179–189.

Bao, Z., & Zhao, Z. (2008). Geochemistry of mineralization with exchangeable REY in the weathering crusts of granitic rocks in South China. *Ore Geology Reviews*, *33*(3–4), 519–535.

Binnemans, K., Jones, P. T., Blanpain, B., Van Gerven, T., & Pontikes, Y. (2015). Towards zero-waste valorisation of rare-earth-containing industrial process residues: A critical review. *Journal of Cleaner Production*, *99*(January 2016), 17–38.

Binnemans, K., Jones, P. T., Blanpain, B., Van Gerven, T., Yang, Y., Walton, A., & Buchert, M. (2013). Recycling of rare earths: A critical review. *Journal of Cleaner Production*, *51*(July), 1–22.

Blissett, R. S., Smalley, N., & Rowson, N. A. (2014). An investigation into six coal fly ashes from the United Kingdom and Poland to evaluate rare earth element content. *Fuel*, *119*, 236–239.

Bond, J., & Giroux, L. (2013). Low temperature plasma ashing of coal for quantitative mineral analysis.

Borra, C. R., Pontikes, Y., Binnemans, K., & Van Gerven, T. (2015). Leaching of rare earths from bauxite residue (red mud). *Minerals Engineering*, *76*, 20–27.

Brahim, K., Antar, K., Khattech, I., & Jemal, M. (2008). Effect of temperature on the attack of fluorapatite by a phosphoric acid solution. *Scientific Research and Essay*, *3*(January), 35–39.

Carling, R. W., Allen, R. M., & VanderSande, J. B. (1986). Microstructural changes in coal during low-temperature ashing. *Fuel*, *65*(3), 321–326.

Chi, R., Zhang, X., Zhu, G., Zhou, Z. A., Wu, Y., Wang, C., & Yu, F. (2004). Recovery of rare earth from bastnasite by ammonium chloride roasting with fluorine deactivation. *Minerals Engineering*, *17*(9–10), 1037–1043.

Chu, S., E. A. (2011). Critical Materials Strategy. *Energy*, 191.

Cotton, S. (2006). *Lanthanide and Actinide Chemistry - Cotton - Wiley Online Library*.

Dai, S., Graham, I. T., & Ward, C. R. (2016). A review of anomalous rare earth elements and yttrium in coal. *International Journal of Coal Geology*, *159*, 82–95.

Dai, S., Jiang, Y., Ward, C. R., Gu, L., Seredin, V. V., Liu, H., … Ren, D. (2012). Mineralogical and geochemical compositions of the coal in the Guanbanwusu Mine, Inner Mongolia, China: Further evidence for the existence of an Al (Ga and REE) ore deposit in the Jungar Coalfield. *International Journal of Coal Geology*, *98*, 10–40.

Davris, P., Balomenos, E., Panias, D., & Paspaliaris, I. (2016). Selective leaching of rare earth elements from bauxite residue (red mud), using a functionalized hydrophobic ionic liquid. *Hydrometallurgy*, *164*, 125–135.

Dickinson, C. F., & Heal, G. R. (1999). Solid–liquid diffusion controlled rate equations. *Thermochimica Acta*, *340–341*, 89–103.

Dutrizac, J. E. (2017). The behaviour of the rare earth elements during gypsum (CaSO4·2H2O) precipitation. *Hydrometallurgy*, *174*, 38–46.

Finkelman, R. B., Palmer, C. A., & Wang, P. (2018). Quantification of the modes of occurrence of 42 elements in coal. *International Journal of Coal Geology*, *185*, 138–160.

Free, M. L. (2013). *Hydrometallurgy: Fundamentals and Applications*. John Wiley & Sons, Inc.

Gharabaghi, M., Noaparast, M., & Irannajad, M. (2009). Selective leaching kinetics of low-grade calcareous phosphate ore in acetic acid. *Hydrometallurgy*, *95*(3–4), 341–345.

Gromet, L. P., Dymek, R. F., Haskin, L. A., & Korotev, R. L. (1984). The North American Shale Composite : Ist compilations, major and trace element characteristics.-. *Geochim. Cosmochim. Acta*, *48*, 2469–2482.

Gupta, C. K., & Krishnamurthy, N. (2015). *Extractive Metallurgy of Rare Earths*. *International Materials Reviews*.

Habashi, F. (1999). *Textbook of Hydrometallurgy* (Second). Quebec, Canada.

Habashi, F., & Awadalla, F. T. (1986). The recovery of uranium and the lanthanides from phosphate rock. *Journal of Chemical Technology & Biotechnology*, *36*(6), 259–266.

Habashi, F., Awadalla, F. T., & Zailaf, M. (1986). The recovery of uranium and the lanthanides from phosphate rock. *Journal of Chemical Technology & Biotechnology*, *36*(6), 259–266.

He, Z., Zhang, Z., Yu, J., Zhou, F., Xu, Y., Xu, Z., … Chi, R. (2016). Kinetics of column leaching of rare earth and aluminum from weathered crust elution-deposited rare earth ore with ammonium salt solutions. *Hydrometallurgy*, *163*, 33–39.

Hedrick, J. B. (1994). *Rare Earths*. USGS Minerals Information publication.

Hogarth, D. D. (1988). Chemical Composition of Fluorapatite and Associated Minerals from Skarn Near Gatineau, Quebec. *Mineralogical Magazine*, *52*(366), 347–358.

Honaker, R., Groppo, J., Bhagavatula, A., Rezaee, M., & Zhang, W. (2016). Recovery of Rare Earth Minerals and Elements from Coal and Coal Byproducts, (July).

Honaker, Rick, Hower, J., Eble, C., Weisenfluh, J., Groppo, J., Rezaee, M., & Bhagavatula, A. (2015). *Laboratory and Bench-Scale Testing for Rare Earth Elements*.

Hower, J. C., Ruppert, L. F., & Eble, C. F. (1999). Lanthanide, yttrium, and zirconium anomalies in the Fire Clay coal bed, Eastern Kentucky. *International Journal of Coal Geology*, *39*(1–3), 141–153.

Hozumi, K. (1971). Chemistry of low-temperature oxygen plasma and its applications. *Kagaku-No- Ryoiki*, *25*, 713–723.

Hozumi, K. (1976). Low-Temperature Plasma Chemistry, 97–111.

Hozumi, K. (1977). Plasma ashing mechanism and application (japan). *Analytical Biology*.

Huminicki, D. M. C., & Rimstidt, J. D. (2009). Iron oxyhydroxide coating of pyrite for acid mine drainage control. *Applied Geochemistry*, *24*(9), 1626–1634.

Jha, M. K., Kumari, A., Panda, R., Rajesh Kumar, J., Yoo, K., & Lee, J. Y. (2016). Review on hydrometallurgical recovery of rare earth metals. *Hydrometallurgy*, *165*, 2–26.

Jordens, A., Cheng, Y. P., & Waters, K. E. (2013). A review of the beneficiation of rare earth element bearing minerals. *Minerals Engineering*, *41*, 97–114.

Kadoğlu, Y. Y., Karaca, S., & Bayrakçeken, S. (1995). Kinetics of pyrite oxidation in aqueous suspension by nitric acid. *Fuel Processing Technology*, *41*(3), 273–287.

Kanazawa, Y., & Kamitani, M. (2006). Rare earth minerals and resources in the world. *Journal of Alloys and Compounds*, *408*, 1339–1343.

Kenneth N. Han. (2002). *Fundementals of Aqueous Metallurgy*. Society for Mining,

Metallurgy, and Exploration

Kim, E., & Osseo-Asare, K. (2012). Aqueous stability of thorium and rare earth metals in monazite hydrometallurgy: Eh-pH diagrams for the systems Th-, Ce-, La-, Nd- (PO 4)-(SO 4)-H 2O at 25 ??c. *Hydrometallurgy*, *113–114*(March), 67–78.

Kim, R., Cho, H., Han, K., Kim, K., & Mun, M. (2016). Optimization of Acid Leaching of Rare-Earth Elements from Mongolian Apatite-Based Ore. *Minerals*, *6*(3), 63.

Kolker, A., Scott, C., Hower, J. C., Vazquez, J. A., Lopano, C. L., & Dai, S. (2017). Distribution of rare earth elements in coal combustion fly ash, determined by SHRIMP-RG ion microprobe. *International Journal of Coal Geology*, *184*, 1–10.

Komadel, P., & Madejová, J. (2013). Acid activation of clay minerals. *Developments in Clay Science*, *5*, 385–409.

Korose, C. P., & Elrick, S. D. (2010). Coal Geology of Illinois. *Keystone Coal Industry Manual. Coal Age, Jacksonville, Florida, Mining Media International*, 456–467.

Krishnamurth, N., & Gupta, C. K. (2005). *Extractive metallurgy of rare earths* (second).

Kuhn, J. K., Fiene, F., & Harvey, R. (1978). *Geochemical Evaluation and Characterization of A Pittsburgh No. 8 and A Rosebud Seam Coal*.

Kumari, A., Panda, R., Jha, M. K., Lee, J. Y., Kumar, J. R., & Kumar, V. (2015). Thermal treatment for the separation of phosphate and recovery of rare earth metals (REMs) from Korean monazite. *Journal of Industrial and Engineering Chemistry*, *21*, 696–703.

Levenspiel, O. (1999). *Chemical reaction engineering*. *Ind. Eng. Chem. Res* (Vol. 38).

Li, H., Guo, F., Zhang, Z., Li, D., & Wang, Z. (2006). A new hydrometallurgical process for extracting rare earths from apatite using solvent extraction with P350. *Journal of Alloys and Compounds*, *408*, 995–998.

Li, Mei, Zhang, X., Liu, Z., Hu, Y., Wang, M., Liu, J., & Yang, J. (2013). Kinetics of leaching fluoride from mixed rare earth concentrate with hydrochloric acid and aluminum chloride. *Hydrometallurgy*, *140*, 71–76.

Li, Minting, Wei, C., Qiu, S., Zhou, X., Li, C., & Deng, Z. (2010). Kinetics of vanadium dissolution from black shale in pressure acid leaching. *Hydrometallurgy*, *104*(2), 193–200.

Lin, R., Howard, B. H., Roth, E. A., Bank, T. L., Granite, E. J., & Soong, Y. (2017). Enrichment of rare earth elements from coal and coal by-products by physical separations. *Fuel*, *200*, 506–520.

Makanyire, T., Jha, A., & Sutcliffe, S. (2016). Kinetics of hydrochloric acid leaching of niobium from TiO2 residues. *International Journal of Mineral Processing*, *157*, 1–6.

Merritt, R. R. (1990). High temperature methods for processing monazite: I. Reaction with calcium chloride and calcium carbonate. *Journal of the Less Common Metals*, *166*(2), 197–210.

Moldoveanu, G. A., & Papangelakis, V. G. (2012). Recovery of rare earth elements adsorbed on clay minerals: I. Desorption mechanism. *Hydrometallurgy*, *117–118*, 71–78.

Moldoveanu, G. A., & Papangelakis, V. G. (2013). Leaching of rare earths elements from clay materials, 1–9.

Mouchos, E., Wall, F., & Williamson, B. J. (2016). Easily Leachable Rare Earth Element Phases in the Parnassus-Giona Bauxite Deposits , Greece, *XLV*(May).

Papangelakis, V. G., & Moldoveanu, G. (2014). Recovery of Rare Earth Elements From Clay Minerals. *1St European Rare Earth Resources Conference*, 191–202.

Peelman, S., Sun, Z. H. I., Sietsma, J., & Yang, Y. (2014). Leaching of Rare Earth Elements : Past and Present. *ERES2014: 1st European Rare Earth Resources Conference*, 446–456.

Peelman, S., Sun, Z. H. I., Sietsma, J., & Yang, Y. (2016). *Leaching of Rare Earth Elements*. *Rare Earths Industry*. Elsevier Inc.

Petrakova, O. V, Panov, A. V, Gorbachev, S. N., & Milshin, O. N. (2015). Improved efficiency of red mud process through scandium oxide recovery. *Proceedings of the Bauxite Residue Valorisation and Best Practices Conference*, *1*, 355–362.

Pourbaix. (1966). *Atlas of Electrochemical Equilibria in Aqueous Solution*. Pergamon, New York, USA.

Richaud, R., Herod, A. A., & Kandiyoti, R. (2004). Comparison of trace element contents in low-temperature and high-temperature ash from coals and biomass. *Fuel*, *83*(14-15 SPEC. ISS.), 2001–2012.

Riley, K. W., French, D. H., Farrell, O. P., Wood, R. A., & Huggins, F. E. (2012). Modes of occurrence of trace and minor elements in some Australian coals. *International Journal of Coal Geology*, *94*, 214–224.

Ruan, C., Jun, T., Zhongjun, L., & Cui, P. (2005). Existing state and partitioning of rare earth on weathered ores. *Journal of Rare Earths*, *23*(6), 756–759.

Sadri, F., Nazari, A. M., & Ghahreman, A. (2017). A review on the cracking, baking and leaching processes of rare earth element concentrates. *Journal of Rare Earths*, *35*(8), 739–752.

Salmi, T., Grenman, H., Warna, J., & Murzin, D. Y. (2013). New modelling approach to liquid-solid reaction kinetics: From ideal particles to real particles. *Chemical Engineering Research and Design*, *91*(10), 1876–1889.

San Cristóbal, A. G., Castelló, R., Martín Luengo, M. A., & Vizcayno, C. (2009). Acid activation of mechanically and thermally modified kaolins. *Materials Research Bulletin*, *44*(11), 2103–2111.

Seferinoglu, M., Paul, M., Sandström, Å., Köker, A., Toprak, S., & Paul, J. (2003). Acid leaching of coal and coal-ashes. *Fuel*, *82*(14), 1721–1734.

Seredin, V. V., & Dai, S. (2012). Coal deposits as potential alternative sources for lanthanides and yttrium. *International Journal of Coal Geology*, *94*, 67–93.

Sparks, D. L. (1986). Kinetics of ionic reactions in clay minerals and soils. *Advances in Agronomy*, *38*(C), 231–266.

Tessier, a, Campbell, P. G. C., & Bisson, M. (1979). Sequential Extraction Procedure for the Speciation of Particulate Trace Metals. *Analytical Chemistry*, *51*(7), 844–851.

Tian, J., Chi, R. A., & Yin, J. Q. (2010). Leaching process of rare earths from weathered crust elution-deposited rare earth ore. *Transactions of Nonferrous Metals Society of China*, *20*(5), 892–896.

Tiwari, M. K., Bajpai, S., Dewangan, U. K., & Tamrakar, R. K. (2015). Suitability of leaching test methods for fly ash and slag: a review. *Journal of Radiation Research and Applied Sciences*, *8*(July), 14.

Walters, A., & Lusty, P. (2011). Rare earth elements - Commodity Profile. *British Geological Survey*, (November), 54.

Wang, L., Long, Z., Huang, X., Yu, Y., Cui, D., & Zhang, G. (2010). Recovery of rare earths from wet-process phosphoric acid. *Hydrometallurgy*, *101*(1), 41–47.

Wang, Z., Guo, S., & Ye, C. (2016). Leaching of copper from metal powders mechanically separated from waste printed circuit boards in chloride media using hydrogen peroxide as oxidant. *Procedia Environmental Sciences*, *31*, 917–924.

Wu, G., Li, J., & Xu, Z. (2013). Triboelectrostatic separation for granular plastic waste recycling: A review. *Waste Management*, *33*(3), 585–597.

Xiao, Y., Chen, Y., Feng, Z., Huang, X., Huang, L., Long, Z., & Cui, D. (2015). Leaching characteristics of ion-adsorption type rare earths ore with magnesium sulfate. *Transactions of Nonferrous Metals Society of China (English Edition)*, *25*(11), 3784–3790.

Xiao, Y., Feng, Z., Huang, X., Huang, L., Chen, Y., Liu, X., … Zhiqi, L. (2016). Recovery of rare earth from the ion-adsorption type rare earths ore: II. Compound leaching. *Hydrometallurgy*, *163*(May), 83–90.

Xiao, Y., Feng, Z., Huang, X., Huang, L., Chen, Y., Wang, L., & Long, Z. (2015). Recovery of rare earths from weathered crust elution-deposited rare earth ore without ammonia-nitrogen pollution: I. leaching with magnesium sulfate. *Hydrometallurgy*, *153*, 58–65.

Xiao, Y., Liu, X., Feng, Z., Huang, X., Huang, L., Chen, Y., & Wu, W. (2015). Role of minerals properties on leaching process of weathered crust elution-deposited rare earth ore. *Journal of Rare Earths*, *33*(5), 545–552.

Yagi, S., & Kunii, D. (1955). 5th Symposium (International) on Combustion. *Chem. Eng.(Japan)*, *19*(500), 231.

Yamamura, T., Mehmood, M., Maekawa, H., & Sato, Y. (2004). Electrochemical Processing of Rare-Earth and Rare Metals by Using Molten Salts. *Chemistry for Sustainable Development*, *12*, 105–111.

Yang, X. J., Lin, A., Li, X. L., Wu, Y., Zhou, W., & Chen, Z. (2013). China's ion-adsorption rare earth resources, mining consequences and preservation. *Environmental Development*, *8*(1), 131–136.

Yu, J., Guo, Z., & Tang, H. (2013). Dephosphorization Treatment of High Phosphorus Oolitic Iron Ore by Hydrometallurgical Process and Leaching Kinetics. *ISIJ International*, *53*(12), 2056–2064.

Zdravkov, B. D., Čermák, J. J., Šefara, M., & Janků, J. (2007). Pore classification in the characterization of porous materials: A perspective. *Central European Journal of Chemistry*, *5*(2), 385–395.

Zhang, J., & Zhao, B. (2016). *Separation Hydrometallurgy of Rare Earth Elements*. *Springer*.

Zhang, P., Han, Z., Jia, J., Wei, C., Liu, Q., Wang, X., … Miao, S. (2017). Occurrence and Distribution of Gallium, Scandium, and Rare Earth Elements in Coal Gangue Collected from Junggar Basin, China. *International Journal of Coal Preparation and Utilization*, 1–14.

Zhang, Q. W., & Saito, F. (1998). Non-thermal process for extracting rare earths from bastnaesite by means of mechanochemical treatment. *Hydrometallurgy*, *47*(2–3), 231–241.

Zhang, W., Honaker, R. Q., & Groppo, J. G. (2017). Flotation of monazite in the presence of calcite part I: Calcium ion effects on the adsorption of hydroxamic acid. *Minerals Engineering*, *100*, 40–48.

Zhang, W., Rezaee, M., Bhagavatula, A., Li, Y., Groppo, J., & Honaker, R. (2015). A Review of the Occurrence and Promising Recovery Methods of Rare Earth Elements from Coal and Coal By-Products. *International Journal of Coal Preparation and Utilization*, *35*(6), 295–330.

Zhang, Wencai, Yang, X., & Honaker, R. Q. (2018a). Association characteristic study and preliminary recovery investigation of rare earth elements from Fire Clay seam coal middlings. *Fuel*, *215*, 551–560.

Zhang, Wencai, Yang, X., & Honaker, R. Q. (2018b). Association characteristic study and preliminary recovery investigation of rare earth elements from Fire Clay seam coal middlings. *Fuel*, *215*(November 2017), 551–560.

VITAE

EDUCATION

Southern Illinois University Carbondale, IL, U.S.

    M.S. in Mining Engineering, December 2014.

China University of Mining & Technology, China.

    B.E. in Mineral Processing Engineering, June 2011

AREA OF EXPERTISE

Coal preparation, Coal flotation, Physical beneficiation, Hydrometallurgy.

RESEARCH EXPERIENCE

- 01/2019-present, Postdoc Research Fellow, Department of Mining Engineering, University of Kentucky, Lexington, KY, USA
- 08/2015-01/2019, Research Assistant, Department of Mining Engineering, University of Kentucky, Lexington, KY, USA
- 05/2012-05/2015, Research Assistant, Department of Mining Engineering, Southern Illinois University, Carbondale, IL, USA.

SELECTED PROJECTS

- Design and development of rare earths recovery and production from coal sources. (2016-now)
  - ✓ Kinetics study of rare earth leaching and process rate control.
  - ✓ Flowsheet development including size reduction, froth flotation, leaching, solvent extraction, and precipitation to produce high purity rare earth oxide.
  - ✓ ¼ tph pilot plant continuous operation and optimization.
- Froth flotation reagent grading and performance improvement. (2015-2016)
  - ✓ Evaluated 9 different frothing reagents using column flotation in terms of air fraction rating, water entrainment, and separation efficiency.

- Fine particle drying technologies evaluation and optimization. (2013-2014)
  - ✓ Parametric study design and testing of reusable molecular sieve dewatering technology; Project Co-principal investigator; Reports writing and presenting.
- Coal fly ash utilization through geopolymer concrete and mineral extraction (2012-2014)
  - ✓ Developed a formula of mixture to create concrete cylinder that had uniaxial compressive strength of 6300 psi using 100% cement-free coal fly ash.

INDUSTRIAL EXPERIENCE

Summer Internship: *at Prairie State Generating Company, LLC., Marissa IL (2015)*
- Product quality enhancement (processing plant); Product quality online detection system calibration; Surface operation, material handling and maintenance.

Industrial testing:
- Belt conveying X-Ray sorter testing on run-of-mine coal at Walton, KY. (2015)
- Full size FGX air table dry coal separator evaluation; parametric study and optimization among seven operating factors. (2014)
- Automation system on coal spiral in IL Knight Hawk coal processing plant: operation debugging, and data base establishing for the automation programing. (2013)

Practical training: (Xuehu & Chengjiao coal processing plant, China)
- Involved in plant operation and equipment maintenance activities, etc. (Summer 2010 & 2011)

PUBLICATIONS

Peer-reviewed Journals

1. X. Yang, J. Werner, and R.Q. Honaker, 2018. "Leaching of Rare Earth Elements from an Illinois Basin Coal Source." *Journal of Rare Earths.* Volume 37, Issue 3, March 2019, Pages 312-321.

2. Honaker, R.Q., Zhang, W., and Yang, X. "Conception of an integrated flowsheet for rare earth elements recovery from coal coarse refuse," *Minerals Engineering.* Vol. 122. 233-240, 2018.

3. Zhang, W., Yang, X., and Honaker, R.Q. "Association characteristic study and preliminary recovery investigation of rare earth elements from Fire Clay seam coal middlings." *Fuel.* 215. 551-560, 2018.

Peer-reviewed Conference Proceedings

1. R. Honaker, X. Yang, A. Chandra, W. Zhang, J. Werner. Hydrometallurgical Extraction of Rare Earth Elements from Coal: Proceedings of the First Global Conference on Extractive Metallurgy. Extraction 2018. January 2018.

2. Akbari, H., Heller, T., Shin, S., Yang, X., Kolay, P., Kumar, S., and Mohanty, M.K. "Geopolymer-based concrete to reduce carbon footprint of the construction industry," *Mining Engineering,* Vol. 65, No. 12, pp .57-62, 2013.

Conference Presentations

1. X. Yang and R. Honaker (2018). "Leaching Kinetics of Rare Earth Elements from an Enriched Coal Source." *2018 SME Annual Conference.* Minneapolis, MN, 2018.

2. Yang X., Honaker, R.Q., and Han, K. "Hydrometallurgical Recovery of Rare Earth Elements from Coal Sources", *2017 SME Annual Conference,* Denver, CO 2017

3. Yang, X., Huang, Q., and Honaker, R.Q., 2017. "Frother Evaluation for Improved Recovery and Selectivity in Column Flotation", *2017 SME Annual Conference*, Denver, CO 2017

4. Yang, X., Mohanty, M.K., Luttrell, G.H., Bratton, B., McDaniel, B., and McDaniel, A. "Pilot-scale evaluation of an emerging drying technology for fine coal drying", *2014 SME Annual Conference*, Salt Lake City, Utah, February 2014.

5. X. Yang, H. Akbari, and M.K. Mohanty, 2013, "Climate change and carbon dioxide: A review", *2013 SME Annual Conference*, Denver, Colorado, February 26.

HONORS/AWARDS

- 2019 Outstanding Graduate Student Award. (2019)
- SME Mineral Processing Division (MPD) Scholarship Award. (2017)
- SME WAAIME Scholarship grand award. (2016-2018)
- 2012 P3 Program Awarded by the US Environmental Protection Agency (EPA). (2012)